UNIVERSITY OF LIVERPOOL

Expression and modulation of potassium channels in neuroblastoma

Thesis submitted in accordance with the requirements of the University of Liverpool for the degree of Master of Philosophy

By

Meraj Ondhia

July 2017

Abstract

Neuroblastoma is a paediatric cancer derived from the sympathoadrenal cell lineage. Most cases are diagnosed in children under the age of 5 and neuroblastoma is responsible for 15% of paediatric oncology deaths. Neuroblastoma tumours demonstrate remarkable clinical variability which reflects their significant biological heterogeneity. Currently, even with intensive multimodal treatment, patients with high-risk disease have a poor prognosis. Therefore, further understanding of the biology of neuroblastoma may contribute to developing novel therapeutic approaches. Potassium (K^+) channels are involved in the regulation of many biological processes associated with cancer; including cell proliferation, apoptosis, migration and angiogenesis. Overexpression of multiple K^+ channels has been demonstrated in a number of types of cancer. However, the role of K^+ channels in neuroblastoma has yet to be extensively evaluated.

In this study K^+ channel gene expression was assessed initially in primary neuroblastoma tumours and in two high-risk, human neuroblastoma-derived cell lines: BE2C and SKNAS. Quantitative PCR, western blotting and immunocytochemistry were used to assess K^+ channel expression in BE2C and SKNAS cells. KCNQ2/Kv7.2, a voltage-gated K^+ channel, was found to be highly expressed in the BE2C cell line and expression of KCNQ2/Kv7.2 was 101 fold greater in BE2C cells relative to SKNAS cells. Furthermore, functional assays demonstrated that XE991, a compound which inhibits KCNQ/Kv7 channels, reduced BE2C cell proliferation *in vitro*. In addition, XE991 was found to induce morphological changes in BE2C cells, akin to neuronal differentiation, *in vitro.* The effect of XE991 on BE2C cell proliferation *in vivo* was investigated using the chick embryo model, however no significant effect was detected.

We have established that K^+ channels are expressed by neuroblastoma cells and differential expression exists between two neuroblastoma cell lines. KCNQ2 expression may contribute to the biological heterogeneity observed in neuroblastoma cell lines and primary tumours. Furthermore, it is evident that modulation of KCNQ2/Kv7.2 has a role in BE2C cell behaviour *in vitro*.

Acknowledgements

There are many people I would like to thank for their encouragement and support throughout the course of this project. I entered the laboratory not knowing how to hold a pipette correctly and less than one year and many experiments later I have learnt many valuable lessons both inside and outside the laboratory. So for this incredible opportunity my deepest gratitude goes to my supervisors Dr John Quayle, Dr Diana Moss and Professor Paul Losty. Dr Quayle and Dr Moss have been excellent at guiding me throughout this year and their advice and encouragement has been fundamental to this project. Thank you for affording me the opportunity to work in your laboratories and for being ever-willing to answer my questions. I would like also like to thank Professor Paul Losty who has provided excellent advice and support throughout the year.

I must also thank Dr Tomoko Kamishima, her patient and excellent teaching style in the laboratory was pivotal for me to become confident with working in the laboratory independently.

I am hugely grateful for the help and guidance I have received from Dr Rabiu Inuwa and Rasha Swadi. In the laboratory they have gone above and beyond to assist me from the very first day and in the office they have provided warm friendship throughout the year. I wish them both the very best for the future. I would like to thank Dr Mingming Yang for his help and friendship. I would also like to acknowledge Dr Chris Law for his help in conducting FACS.

I would like to thank Alder Hey Children's Hospital for providing the funding to undertake this unique and invaluable opportunity.

Lastly and most importantly I would like to thank my parents and sister for their unconditional love and support.

List of abbreviations

A260	Absorbance at 260nm
A280	Absorbance at 280nm
AHSCT	Autologous haematopoietic stem cell transplant
ALK	Anaplastic lymphoma kinase
ASCL1	Achaete-scute homolog-1
ATP	Adenosine triphosphate
ATRX	Alpha thalassemia/mental retardation syndrome X-linked
BCA	Bicinchoninic acid
BMP	Bone morphogenetic protein
BSA	Bovine serum albumin
CAM	Chorioallantoic membrane
cDNA	Complementary deoxyribonucleic acid
CDK	Cyclin dependent kinase
CNS	Central nervous system
CO_2	Carbon dioxide
Cq	Cycle quantification
CT	Computed tomography
DAPI	4', 6-Diamindino-2-Phenylindole,Dihydrochloride
$DiBAC_4(3)$	Bis-(1,3-Dibutylbarbituric Acid) Trimethine Oxonol
DMEM	Dulbecco's modified Eagle's medium
DMSO	Dimethyl sulfoxide
E	Embryonic day
EDTA	Ethylenediaminetetraacetic acid
FACS	Fluorescence activated cell sorting
FBS	Fetal bovine serum
GEMM	Genetically engineered murine model
GFP	Green fluorescent protein
hERG	Human ether-a-go-go related gene
HBSS	Hanks balanced salt solution
HPRT1	Hypoxanthine phosphoribosyltransferase 1
HRP	Horseradish peroxidase
HVA	Homovanillic acid

ICC	Immunocytochemistry
IDRF	Image-defined risk factor
IHC	Immunohistochemistry
INPC	International Neuroblastoma Pathology Classification
INRG	International Neuroblastoma Risk Group
INRGSS	International Neuroblastoma Risk Group Staging System
INSS	International Neuroblastoma Staging System
K^+	Potassium ion
K2P	Two pore potassium channel
KCa	Calcium-activated potassium channel
KCN	Potassium channel
Ki67	Antigen identified by monoclonal antibody Ki67
Kir	Inward rectifying potassium channel
KLF4	Kruppel-Like Factor
Kv	Voltage-gated potassium channel
MDM2	Mouse double minute 2 homolog
MIBG	Metaiodobenzylguanidine
MRI	Magnetic resonance imaging
mRNA	Messenger ribonucleic acid
MTT	3-(4,5- dimethyl-2-thiazolyl)-2,5-diphenyl-2H-tetrazolium bromide
MYC	Myelocytomatosis viral related oncogene
NB84	Uncharacterised antigen in neuroblastoma cells
NCBI	National Centre for Biotechnology Information
NCC	Neural crest cell
NEAA	Non-essential amino acids
NRQ	Normalised relative quantification
NRT	No reverse transcriptase control
NSE	Neuron-specific enolase
NTC	No template control
PBS	Phosphate buffered saline
PFA	Paraformaldehyde
PHOX2A	Paired-like homeobox 2A
PHOX2B	Paired-like homeobox 2B
PNT	Peripheral neuroblastic tumour

PSS	Physiological saline solution
qPCR	Quantitative Polymerase Chain Reaction
RG	Reference gene
ROBO2	Roundabout, axon guidance receptor, homologue 2
RQ	Relative quantification
RT	Reverse transcriptase
SDS	Sodium dodecyl sulfate
SEM	Standard error of the mean
SSC	Sodium citrate buffer
STMN4	Stathmin-like 4
TBST	Tris-buffered saline with Tween 20
TG	Target gene
TrKA	Tropomyosin receptor kinase A
VMA	Vanillylmandelic acid
WB	Western blotting
XE-991	10,10-bis(4-pyridinylmethyl)-9(10H)-anthracenone

Table of contents

List of figures

List of tables

Chapter 1: Introduction

1.1 Neuroblastoma

1.1.1 Overview

Neuroblastoma is a malignant tumour derived from neural crest cells of the sympathetic nervous system and is most commonly diagnosed in childhood. Neuroblastoma is characterised by remarkable biological and histological heterogeneity. This is reflected by diverse clinical outcomes ranging from spontaneous regression without treatment to metastatic disease resistant to multimodal therapy [1].

1.1.2 Epidemiology, genetic predisposition and risk factors

Neuroblastoma is a rare tumour, nevertheless it is the most frequently diagnosed malignancy of infancy (<1 year of age). The median age at diagnosis is 18 months and 40% of cases are diagnosed in infants [1]. In children aged 0-14 the incidence of neuroblastoma is 9-12 per million and the mortality rate is 9.1 per million [2-4].

Familial cases of neuroblastoma account for 1-2% of cases and median age of diagnosis is 9 months [5]. Activating mutations of the ALK gene are detected in the majority of hereditary neuroblastomas [6]. Heterozygous germline mutations of PHOX2B are associated with a subset of familial neuroblastoma cases and often present in conjunction with other neural crest disorders, congenital hypoventilation syndrome and Hirschsprung's disease [7].

In contrast to most adult malignancies, where clear aetiological factors have been identified, the aetiology of paediatric cancers is largely unknown and this applies to neuroblastoma. The embryonal origin of tumour cells and young age at onset suggest pre- and perinatal exposures may be of significance. Several factors have been investigated including maternal smoking and alcohol consumption, prenatal hormone exposure, gestational weight and age, however no consistent associations have been demonstrated in large studies [8, 9].

1.1.3 The neural crest

The neural crest is a population of multipotent embryonic cells which give rise to a number of diverse cell lineages [10]. The cells from which neuroblastoma tumours arise, sympathetic ganglion neurons, are derivatives of neural crest cell (NCC) progenitors [11]. Embryonic NCC migration and maturation is mediated by a complex network of extrinsic signals; deregulation of which may predispose multipotent neural crest precursors to malignant transformation [10]. In addition, transgenic expression of genes involved in neural crest development e.g. MYCN, ALK, PHOX2B, recapitulates neuroblastoma in genetically engineered murine models, further supporting the prenatal origin of neuroblastoma [12, 13].

1.1.3.1 Development of sympathetic nervous system

The ectoderm differentiates into the neural plate and the non-neural ectoderm, the interface of these regions is the neural plate border [14]. Inductive influences from the ectoderm, neuroepithelium and mesoderm induce NCC formation at the neural plate borders [15, 16]. Prior to migration NCCs undergo complete or partial epithelial-to-mesenchymal transition (EMT), which confers enhanced migratory ability and decreased need for intercellular contact [17, 18]. Neural crest specifiers form a transcriptional network to promote degradation of the basement membrane and down-regulate cell adhesion molecules e.g. N-Cam, N-cadherin, cadherin 6B [19].

Pre-migratory neural crest cells express neural crest specifiers responsible for survival, migration and maintaining multipotency e.g. FOXD3 and SOX10 [20, 21]. MYCN influences NCC migration and expansion and is highly expressed in early migratory NCCs. Expression is reduced differentiating sympathetic neurons and absent in adult tissues [22].

After delaminating from the neural tube truncal NCCs take two migratory pathways; those destined to become melanocytes migrate dorsolaterally into the ectoderm. NCCs destined to colonise sympathetic ganglia, dorsal root ganglia and adrenal medullae migrate ventrolaterally [11, 23]. Migrating NCCs are exposed to multiple microenvironments and migration cues, which are essential in the control of the motility, directionality and specificity of cellular movements [24, 25]. Ephrin proteins, expressed in the posterior section of each sclerotome, bind to NCC surface Eph receptors, initiating a process which limits cell motility, thus controlling the specificity of cellular movements [26]. Sympathetic precursor NCCs expressing chemokine receptor type 4 (CXCR4) are drawn to the dorsal aorta and the region surrounding the gut by the chemotactic CXCR4 ligand, stromal cell-derived factor 1 (SDF-1) [27].

In the area of the dorsal aorta aggregated NCCs form sympathoadrenal progenitor cells prior to divergence into two cell lineages: sympathetic ganglion neurons and adrenal chromaffin cells [11]. Under instruction of bone morphogenetic proteins (BMPs), secreted by the cells of the wall of the dorsal aorta, NCCs destined to become sympathetic neurons acquire neuronal and catecholaminergic properties (**Figure 1.1)** [28]. BMPs initiate achaete-scute homolog 1 (ASCL1) production [29]. ASCL1 is the first marker of neuronal specification ASCL1 and promotes the expression of paired-like homeobox 2A (PHOX2A) and 2B (PHOX2B). These genes together drive the expression of enzymes necessary for catecholamine synthesis, tyrosine hydroxylase (TH) and dopamine ß-hydroxylase (DBH) [30]. PHOX2B also initiates terminal sympathoadrenal differentiation. Loss-of-function studies demonstrate that ASCL1 and PHOX2B null mice fail to properly develop autonomic ganglia [31]. Heart and neural crest derivatives expressed transcript 2

(HAND2) is expressed independently of ASCL1 and HAND2-null allele mice showed reduced number of sympathetic neurons and TH and DBH expression [32]

.

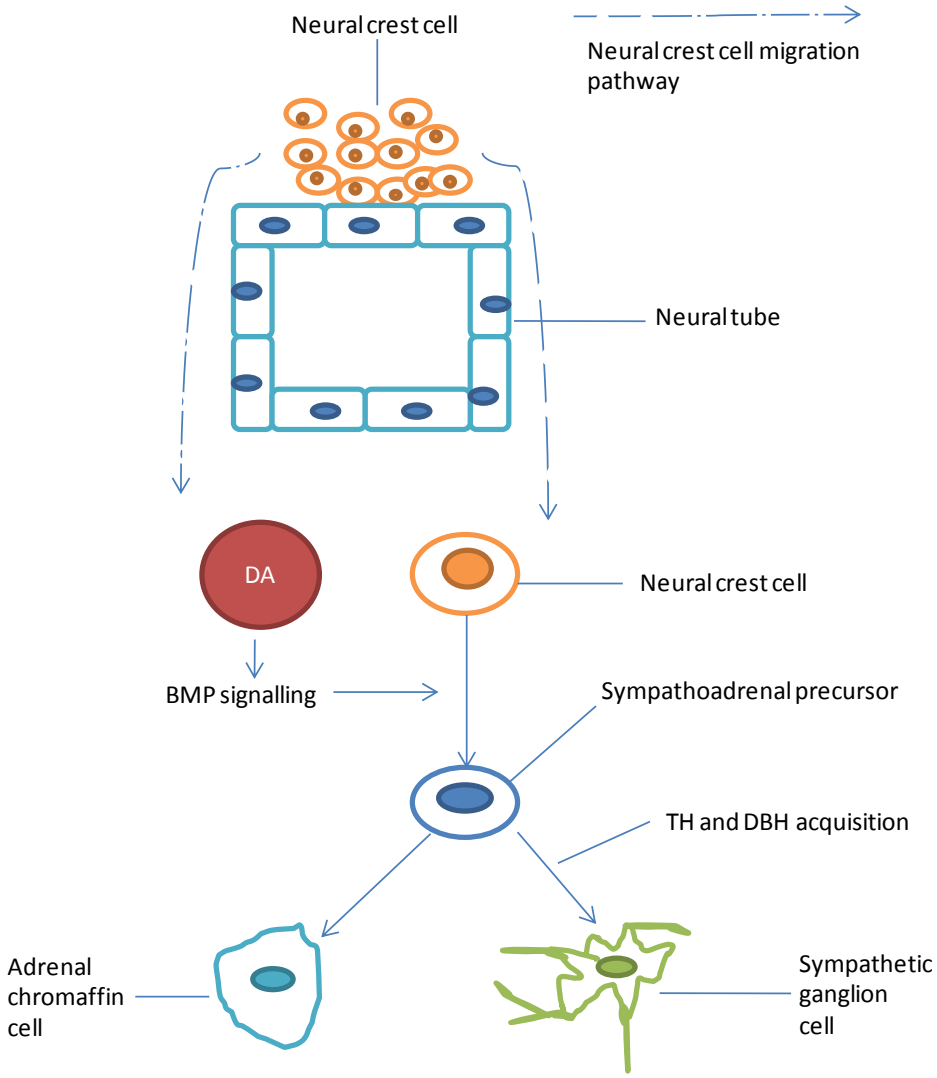

Figure 1.1: Neural crest cell migration and sympathoadrenal differentiation. Neural crest cells destined to become cells of the sympathoadrenal lineage delaminate from the neural plate borders and migrate to the region of the dorsal aorta (DA). Bone morphogenetic signalling (BMP) signalling initiates differentiation of the sympathoadrenal precursor and multiple transcription factors are involved in this process. At this stage cells committed to becoming sympathetic ganglia acquire the catecholaminergic enzymes, dopamine-ß hydroxylase (DBH) and tyrosine hydroxylase (TH).

1.1.4 Molecular biology

Advances in molecular biology research have substantially increased the understanding of the genetic events which drive the development and progression of neuroblastoma. In particular, DNA content, structural chromosomal changes and amplification of the MYCN gene play a significant role. The outcome of these alterations is a loss of balance between cell proliferation and cell death. Neuroblastoma tumours demonstrate significant clinical heterogeneity, this perhaps reflects the absence of a single genetic alteration common to all tumours [34].

1.1.4.1 DNA content

Virtually all cancers demonstrate aneuploidy, an abnormal number of chromosomes [35]. A diploid cell has 46 chromosomes, the majority of neuroblastoma tumour cells are either hyperdiploid (58-80 chromosomes) or near-diploid (35-57 chromosomes) [36]. Genetic models suggest more malignant tumours maintain near-diploid DNA content due to a fundamental defect in genomic stability, resulting in chromosomal rearrangements and unbalanced translocations. Importantly, tumours which have near- diploid DNA content tend confer a worse prognosis compared with hyperdiploid tumours. Ploidy is one of the genetic variables included in the INRG pretreatment classification schema [37]

1.1.4.2 Segmental chromosomal aberrations

Somatically acquired segmental chromosome aberrations (SCAs) with associated DNA copy number alterations occur almost always in high-risk neuroblastoma [34]. Deletion at the chromosomal region 1p36 is observed in 25-35% of cases [38]. Gain of 1-3 additional copies of chromosome 17q is the most common genetic aberration in neuroblastoma, occurring in 48-83% of cases. [39, 40]. Both chromosome 1p deletion and 17q gain are correlated with unfavourable prognostic features, including MYCN amplification and older age at diagnosis [40].

Allelic loss of chromosomal region 11q23 occurs in 15-20% of primary neuroblastoma tumours [41]. Chromosome 11q deletion is inversely associated with MYCN amplification, therefore is a powerful prognostic marker in non-MYCN amplified tumours and is included as prognostic criterion in the INRG pretreatment classification schema [40, 42].

1.1.4.3 The MYCN proto-oncogene

The MYCN proto-oncogene is located on chromosome 2p24. Amplification (increased number of copies) of this gene occurs in a subset of neuroblastoma tumours and confers a poor prognosis for patients [37]. MYCN amplification is detected by fluorescence or chromogenic in situ hybridisation and is most commonly seen as extra-chromosomal chromatin bodies (double minutes) or less

commonly as multiple copies of MYCN gene integrated as tandem repeats into one chromosome (homogenously staining region) [43].

MYCN encodes for the n-myc protein, which together with c-myc and l-myc belong to the myc family of basic helix-loop-helix (bHLH) proteins which function as transcription factors [44]. The n-myc oncoprotein possesses a leucine zipper motif which allows it to form dimers with multiple proteins including the Max/Mad network, a group of interacting factors which influence gene transcription. N-myc translocates to the nucleus and dimerises with the protein max, this dimer then binds to the E-box sequence (CANNTG) in DNA promoter to regulate gene transcription. Max also heterodimerises with the Mad family of proteins and mad-max heterodimers function as transcriptional repressors at E-box sites [45].

Amplification of the MYCN gene leads to overexpression and increased transcriptional activation/repression of over 200 genes; the overall effect of which is permissive to tumour development and survival. Upregulated genes are related to proliferation, drug resistance and angiogenesis, whereas downregulated genes include those involved in cell cycle, apoptosis and differentiation [46]. In genetically engineered murine models (GEMM) [47], MYCN overexpression alone is insufficient to recapitulate tumourigenesis; this requires additional genetic aberrations e.g. MYCN transgene amplification and MYCN-induced up-regulation of Sirtuin 1 and Sirtuin 2, both of which increase MYCN stability [48]. Consequently, a proportion of these mice spontaneously developed neuroblastoma tumours which display similar localisation, histology and chromosomal aberrations to human tumours [13].

MYCN amplification is observed in 16-35% of neuroblastoma cases [40, 49] and is firmly associated with advanced disease and poor prognosis regardless of stage of disease or age at diagnosis [37]. In children < 18 months, with metastatic disease and MYCN amplification 5-year overall survival is 34%, this is remarkably lower than in the same cohort lacking MYCN amplification (82%) [37].

Knockdown of MYCN expression in murine models of neuroblastoma demonstrated an increase in tumour apoptosis and cellular differentiation and suppression of cell growth [47]. Inhibition of MYCN is therefore an attractive therapeutic approach. However, the structure of MYCN largely prevents direct inhibition. Indirect mechanisms of inhibiting MYCN are being pursued, this includes inhibiting MYCN-dependent transcription e.g. BET-bromodomain inhibitors, histone deacetyltransferases inhibition, interfering with MYCN stabilisation e.g. aurora kinase inhibitors, MDM2 inhibition and inducing differentiation e.g. retinoic acid [46].

1.1.5 Neuroblastoma and the hallmarks of cancer

The previous section discussed a number of genetic aberrations that contribute to the development and biological heterogeneity of neuroblastoma tumours. The question remains as to how does each genetic aberration contribute to the development of neuroblastoma; a complex process which requires the evolution of a sympathetic neuroblast into a malignant tumour. This evolution is a highly multifaceted process which requires the acquisition of complex biological capabilities. Hanahan and Weinberg have described eight hallmark features of cancer and two enabling characteristics which a tumour acquires as it progresses [50]. These characteristics are discussed below in the context of neuroblastoma (**Figure 1.2**).

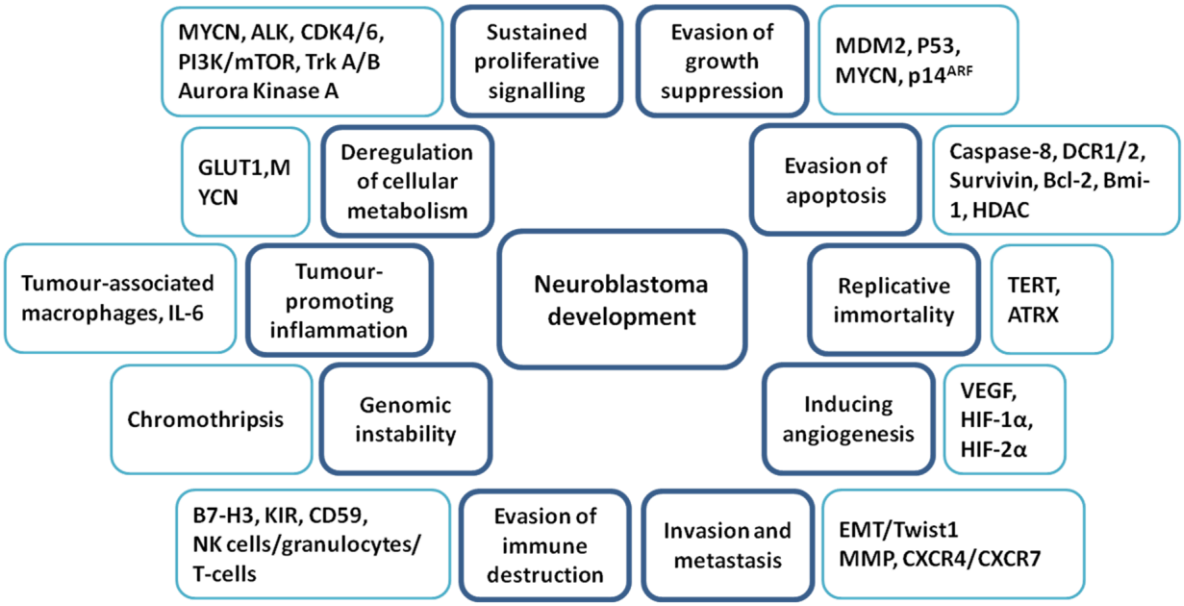

Figure 1.2: The hallmarks of cancer and neuroblastoma. Hanahan and Weinberg (2011) [50] have described hallmark and enabling characteristics which a cancer cell acquires during the complex process of tumourigenesis. These characteristics (dark blue boxes) are applicable to neuroblastoma tumours. There are multiple genes and genetic events which contribute to the acquisition each characteristic in neuroblastoma (light blue boxes).

1.1.5.1 Sustained proliferative signalling

Cell proliferation is necessary for growth and normal tissue function and is strictly coordinated to maintain normal architecture and function [50]. The process of cell proliferation can be resolved into the following sequence of events; binding of growth factor to specific receptor on cell membrane; activation of the growth factor receptor; signal transduction to the nucleus; activation of nuclear regulatory factors that regulate DNA transcription; entry into the cell cycle and cell division. A feature of all tumours is deregulation of cell proliferation and any of the aforementioned steps may

be corrupted; thereby endowing cells with the essential trait of maintaining proliferative signalling [51]. Mutated or over-expressed proto-oncogenes promote uncontrolled cell proliferation through several mechanisms and two oncogenes implicated in oncogenesis in neuroblastoma, MYCN and ALK, are discussed below.

Neuroblastoma growth is regulated by a multitude of cytokines and growth factors that interact with cell surface non-receptor and receptor tyrosine kinases (RTKs) [52]. Anaplastic lymphoma kinase (*ALK*) is an RTK expressed in the developing embryonal and neonatal brain [53]. Activating mutations of ALK lead to enhanced kinase function, ligand-independent activation and loss of auto-inhibition [54], resulting in the activation of a plethora of downstream signalling pathways which facilitate cellular processes required for oncogenesis including cell proliferation, growth and survival [53]. Oncogenic mutations of ALK are detected in the majority of hereditary neuroblastomas and 7-10% of sporadic cases of neuroblastoma; ALK therefore provides an attractive molecular target for therapy in neuroblastoma and inhibitors of ALK are currently in phase I/II clinical trials [6, 53].

A well-characterised function of MYCN is to promote proliferation and cell cycle progression. In the embryonic period this is critical for normal neuronal and brain development [44]. In neuroblastoma, MYCN amplification leads to a hazardous combination of activation of cell cycle drivers and suppression of anti-proliferative proteins. MYCN acts a powerful inhibitor of cell differentiation through negative regulation of tropomyosin related kinase A (TrkA) expression. Consequently cells become arrested in the proliferative stage and are unable to terminally differentiate into post-mitotic sympathetic neurons [55].

Cyclin-dependent kinase 4 (CDK4) is a direct transcriptional target of MYCN. CDK4 forms a complex with cyclin D2 which hyperphosphorylates the Rb: E2F1 complex; thus allowing E2F1 to initiate transcription of genes involved in cell cycle progression leading to uncontrolled proliferation [56, 57].

1.1.5.2 Evasion of growth suppression

Neoplastic cells must also overcome intrinsic cellular mechanisms that oppose uncontrolled cell proliferation. Tumour suppressor genes (TSGs) are a vital component of cellular anti-proliferative mechanisms through their role in inhibition of uncontrolled cell cycle progression, response to oncogene activation and DNA damage. *TP53* is an archetypal TSG and is mutated in a multitude of human cancers [58]. Multiple cellular stimuli including anoxia, DNA damage and inappropriate oncogenic signalling stimulate p53 activity which functions to repress unrestrained cell proliferation. The primordial response to DNA damage is activation of temporary cell cycle arrest (quiescence) to

allow DNA damage repair. If the DNA damage is irreparable p53 can induce cell cycle arrest (senescence) and cell death (apoptosis). [50, 51].

In neuroblastoma mutational inactivation of TP53 is highly uncommon (<2%) at diagnosis [59]. Alternative mechanisms of p53 inactivation in neuroblastoma have been proposed including cytoplasmic sequestration, increased mouse double minute 2 homolog (MDM2) activity and inactivation of the p14ARF gene. MDM2 is a known oncoprotein that destabilises/sequesters p53 thereby limiting its activity and p14ARF protects p53 from MDM2 mediated degradation [60, 61]

The retinoblastoma (RB) gene, the prototypical tumour suppressor gene, represses proliferation by controlling the G1-S checkpoint of the cell cycle [50]. In heritable cases of retinoblastoma affected children possess a germline mutation of the RB gene, a subsequent somatic mutation leads to biallelic inactivation [62]. In the 1970s Knudson and Strong demonstrated a heritable component to neuroblastoma, therefore in a similar manner to the RB gene it would have been expected that a neuroblastoma tumour suppressor gene would have been discovered; however such a gene remains elusive [63].

Chromosome 1p and 11q deletion and their association with high-risk neuroblastoma suggests a putative location for a TSG and several candidates have been identified, but their contribution to tumourigenesis and prognostic significance remains to be identified [64]. Furthermore, genome-wide association studies (GWAS) have been undertaken to detect DNA polymorphisms linked to oncogene activation or loss of tumour suppression [34]. Resultantly, multiple genetics associations with neuroblastoma have been identified e.g. BARD1, ATRX, LIN28B, but each association has a relatively modest effect size. It is evident multiple polymorphisms cooperate to contribute to tumourigenesis [65].

1.1.5.3 Evasion of apoptosis

In addition to uninhibited proliferation tumour cells must resist powerful mechanisms of cell death. Apoptotic cell death is primarily executed through the extrinsic or intrinsic pathways which ultimately results in the activation of a proteolytic cascade of caspases leading to cell death. In neuroblastoma multiple genetic aberrations occur to protect tumour cells from apoptosis [50, 66].

The intrinsic (mitochondrial) pathway of apoptosis is triggered by various stimuli and leads to permeabilisation of the mitochondrial membrane which allows the release of initiators of apoptotic pathways e.g. cytochrome c. The Bcl-2 family of proteins play a pivotal role in the regulation mitochondrial apoptotic pathways and elevated expression of the anti-apoptotic members of the Bcl-2 family (Bcl-2, Mcl-1 and Bcl-xL) has been observed in both neuroblastoma primary tumours and

cells lines [67-69]. Caspase-8 is a key regulator of apoptosis induction through the extrinsic pathway. Hypermethylation of a regulatory region in the CASP8 gene has been identified to account for its loss of expression in neuroblastoma tumours [70, 71].

Somewhat paradoxically MYCN, through transcriptional activation of p53, is a powerful inducer of apoptosis [59]. This perhaps underpins the mechanism as to why MYCN amplified tumours initially demonstrate sensitivity to chemotherapy, as p53-mediated apoptotic pathways are functional. However, as chemotherapy tends to induce mutations in p53, this results in a loss of anti-apoptotic function, leading to relapse and chemoresistance [46]. Whether MYCN promotes a net tumourigenic effect is reliant upon on the cooperation of anti-apoptotic proteins e.g. Bcl-2.

1.1.5.4 Replicative immortality

Telomeres are specialised structures present at the ends of chromosomes. During each cell division there is progressive shortening of telomeres at the end of chromosomes. Short telomeres are recognised by the cell's DNA repair machinery e.g. p53 and RB which induce cell cycle arrest and senescence. Senescence describes an irreversible entrance into a non-proliferative but viable state. In circumstances where p53 or RB are inactivated e.g. cancer cells, the cells utilise the non-homologous joining pathway in an attempt to save the cell. This inappropriate repair results in massive genomic instability and leads to mitotic catastrophe; characterised by significant apoptosis. Germline cells and stem cells both express telomerase; a specialised reverse transcriptase able to extend telomeres and is virtually absent from somatic cells. However if a cell manages to reactivate telomerase during the period of genomic instability then cell death is avoidable. Cancer cells achieve immortality through upregulation of telomerase thus maintaining telomere length. [50, 51].

In neuroblastoma telomerase activity is upregulated and correlates with advanced disease and poor prognosis. In stage 4S disease lack of telomerase activity is linked with spontaneous regression. [72]. Whole genome sequencing has found *TERT* (encoding telomerase) promoter rearrangements, in approximately 25% of patients, leading to enhancer hijacking and activation. TERT is also a direct transcriptional target of MYCN [73].

Alternative lengthening of telomeres (ALT) is a non-telomerase mechanism of telomerase lengthening and occurs in approximately 10% of human cancers [74]. *ATRX* is an RNA helicase involved in chromatin remodelling, telomere maintenance and suppressor of ALT [75]. ATRX loss of function mutations occur in 9-10% of sporadic neuroblastomas suggesting a role for ATRX mutations in maintaining replicative immortality [65].

1.1.5.5 Angiogenesis

Even with the growth advantages described previously tumours cannot enlarge beyond 1-2 mm in diameter unless they are vascularised to allow delivery of oxygen and nutrients and evacuate waste products. Neoangiogenesis, the generation of new vessels develop from existing capillaries involves a complex cascade of cellular events controlled by the balance of pro-angiogenic e.g. vascular endothelial growth factor (VEGF) and inhibitory factors e.g. thrombospondin-1 (TSP-1). During tumour development an angiogenic switch is activated and involves increased production of angiogenic factors and/or loss of angiogenic inhibitors by tumour and stromal cells, leading to neoangiogenesis. However, tumour vasculature is abnormal; vessels are leaky, dilated and haphazardly arranged [50, 51].

Neuroblastoma is characterised by prominent angiogenesis [76]. Increased tumour vascularity and microvascular proliferation is correlated with unfavourable prognostic features including MYCN amplification. Aggressive tumours are associated with high expression of VEGF and other markers of active angiogenesis e.g. platelet-derived growth factor A [77]. Highly aggressive tumours which are stroma-poor demonstrate significant angiogenesis. Schwann cells, which are more abundant in stroma-rich tumours, exert anti-angiogenic function through secretion of numerous angiogenic inhibitors e.g. secreted protein acidic and rich in cysteine (SPARC). In one study, expression of SPARC was found to be inversely correlated with the degree of malignant progression [78].

1.1.5.6 Invasion and metastasis

Metastasis is the primary reason for the resultant mortality in cancer and the invasion-metastasis cascade is a complex process involving a series of sequential steps to allow spread of a primary tumour. These steps consist of local invasion, intravasation into blood vessels and lymphatics, transit through the vasculature, extravasation form the vessels, colonisation growth of micrometastases into macroscopic tumours [50, 51].

Matrix metalloproteinases (MMP) e.g. MMP-9 play an important role in regulation of tumour cell adhesion and migration. An association between overexpression of MMP2 and MMP9 has been observed in advanced neuroblastoma [79]. Epithelial-mesenchymal transition (EMT) occurs during normal neural crest development and is also an important mechanism for both the initiation of tumour invasion and subsequent metastasis [80]. Synergistically acting transcription factors e.g. Snail, Slug and Twist promote EMT by suppressing the expression of E-cadherin thus potentiating cell invasion. TWIST-1 has been shown to be highly expressed in a subset of metastatic tumours [81].

1.1.5.7 Deregulation of tumour metabolism

Neuroblastoma tumours require abnormally high amounts of glucose and other macromolecules to enable continual unchecked proliferation. It is well established these needs are met through alterations in key metabolic pathways [50]. In the presence of oxygen, cancer cells shift their glucose metabolism away from oxidative phosphorylation to glycolysis; this is termed the Warburg effect and has been demonstrated in neuroblastoma by the use of positron emission technology to visualise the avid uptake of fluorodeoxyglucose [82]. MYCN has been implicated in altered tumour metabolism through activation of genes involved in glycolysis, glutamine metabolism, fatty acid metabolism and mitochondrial function [83].

1.1.5.8 Evading immune destruction

Most tumours, including neuroblastoma, arise in immunocompetent hosts. Malignant cells therefore require a strategy to avoid recognition and destruction by the host immune system. Neuroblastoma cells display downregulation of human leucocyte antigen (HLA) class 1 and adhesion molecules thereby impairing cell recognition by cytotoxic T cells and NK cells. [84, 85]. In addition, MYCN amplification down regulates HLA 1 expression [86]. Tumour-associated macrophages (discussed in **section 1.1.5.10**) are also recruited to suppress lymphocyte activity [87].

Neuroblastoma cells express high levels of cell surface gangliosides which are important in migration and adhesion. Neuroblastoma-derived gangliosides (GD) inhibit the functional activity of T, NK and dendritic cells and contribute to tumour induced bone marrow suppression [88]. Monoclonal-antibody (MAb) mediated targeting of the oncofetal differentiation antigen GD2 increases neuroblastoma susceptibility to antibody-dependent cell-mediated cytotoxicity [33].

1.1.5.9 Genomic instability

Eight hallmark features of malignancy have been discussed and it is evident that numerous alterations in the genomes of neoplastic cells are responsible for acquisition of all of the hallmarks. In addition, two enabling characteristics have been described. This refers to an increased tendency of alterations in the genome during the life cycle of cells and is a major enabling characteristic for tumourigenesis [50]. Remarkable maintenance systems minimise genomic instability and mutations in the genes that control these processes confer tumour cells with increased susceptibility to genomic instability [89]. During tumour progression cells divide continuously and mutant clones of tumour which are genomically heterogeneous will arise. Those clones with favourable genomic characteristics will survive and propagate, allowing continual tumour progression [90].

How do these clones acquire the necessary genomic alterations to facilitate tumour progression? The longstanding debate in the theory of clonal expansion is whether malignant clones evolve

gradually through a series of sequential genetic alterations or a single, catastrophic event [90]. Chromothripsis is an example of a catastrophic event and describes local shedding of a chromosome and random reassembly, thus leading to structural aberrations. In one study chromothripsis was identified in approximately 18% of high-stage neuroblastomas resulting in structural aberrations in genes involved in neuroblastoma pathogenesis [65].

1.1.5.10 Tumour-promoting inflammation

Tumour-promoting inflammation is the second enabling characteristic of tumour development. It is well established that tumours are densely infiltrated by leucocytes of both the innate and adaptive components of the immune system [91]. In neuroblastoma, $CD68^{+}$ tumour-associated macrophages (TAM) and other myeloid-derived cells produce immunosuppressive and tumour growth-promoting mediators e.g. interleukins (IL). IL-6 induces a signal transducer and activator of transcription 3 (STAT3) mediated transcriptional programme which enhances cell proliferation, further recruitment of suppressive myeloid cells and direct suppression of T cells and natural killer cells [92].

1.1.6 Histopathologic classification

Peripheral neuroblastic tumours (PNTs) are a family of tumours arising from primitive sympathetic precursors cell derived from the neural crest [93]. The International Neuroblastoma Pathology Classification (INPC) defines four morphologic categories of neuroblastic tumours: neuroblastoma, ganglioneuroblastoma intermixed, ganglioneuroblastoma nodular and ganglioneuroma [94] **(Figure 1.3)**. This classification represents a spectrum of maturation ranging from tumours composed predominately of undifferentiated neuroblasts to those consisting fully differentiated neurons surrounded by dense Schwannian stroma.

PNTs are composed of a mixture of neuroblasts- with various degrees of differentiation- and Schwann cells, in various proportions. The relative abundance of each is highly significant for prognosis. [93]. Undifferentiated neuroblasts are small, immature blue round cells, which contain dense hyperchromatic nuclei, scant cytoplasm and demonstrate high mitotic activity. In contrast differentiated neuroblasts have a large round nucleus with a prominent nucleolus, abundant cytoplasm and cytoplasmic Nissl bodies (granular body composed of endoplasmic reticulum). Schwann-cells constitute the fibrous stroma of PNTs. The origin and function of Schwann cells in neuroblastic tumours is unclear. An initial hypothesis proposed that Schwann cells were part of the malignant process as they shared the same genomic aberrations as their neuroblast counterparts. However, it has also been postulated that Schwannian stromal cells secrete anti-proliferative factors crucial to neuronal differentiation.

Neuroblastoma tumours are primarily composed of nests of undifferentiated, poorly differentiated or differentiating neuroblasts and by definition, less than 50% Schwannian stroma 95]. As one of the small, blue cell tumours of infancy and childhood, neuroblastomas must be distinguished from other tumours in this group including the Ewing sarcoma family of tumours, rhabdomyosarcoma, nephroblastoma and desmoplastic small round cell tumour [96]. Histologically, neuroblastoma may be distinguished by the presence of eosinophilic neuritic processes (neuropil) and Homer-Wright pseudorosettes (a collection of neuroblasts surrounding areas of neuropil).

Ganglioneuroblastomas are composed of neuroblasts that are undifferentiated and those that are transitioning towards differentiation. Ganglioneuroblastomas are further divided into intermixed and nodular subtypes depending on neuroblastic and Schwannian stroma development. Ganglioneuroblastomas, the nodular subtype in particular, demonstrate malignant potential, although this is far lower than for neuroblastoma [97].

Ganglioneuromas are the most histologically mature PNT and consist entirely of maturing/mature ganglion cells surrounded by Schwannian stroma. Ganglioneuromas tend occur in older patients and are six-to-ten times less common than neuroblastoma [97]. They often present as an asymptomatic mass discovered on routine radiographic study or causes a local mass effect [98, 99]. Neuroblastoma and ganglioneuroblastoma tumours may both undergo spontaneous maturation to more mature tumours, the mechanism by which and how often this occurs is unclear at present [99].

The prognostic significance of tumour histology was traditionally determined by the Shimada classification. This was modified to create the International Neuroblastoma Pathology Classification (INPC). The INPC is an age-linked classification based on the presence or absence of Schwannian stroma, degree of neuroblastic differentiation and the mitosis-karyorrhexis index (MKI). Based on this classification tumours are divided into favourable and unfavourable histology subgroups **(Figure 1.3)** [94, 95].

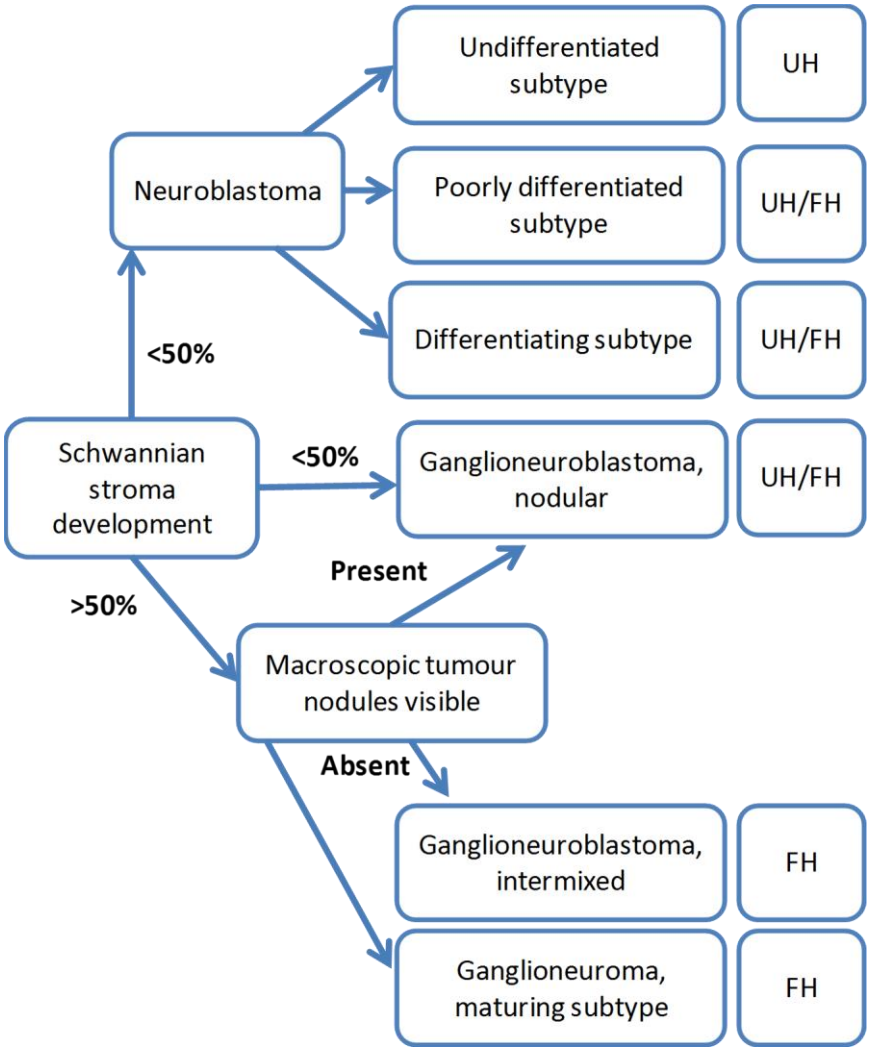

Figure 1.3: Histopathologic classification of peripheral neuroblastic tumours Simplified diagram of the International Neuroblastoma Pathology Classification demonstrating the histological subtypes of peripheral neuroblastic tumours. This classification is based on the abundance of Schwannian stroma and the presence/absence of neuroblastic tumour nodules and classifies tumours into unfavourable (UH) and favourable (FH) histological subgroups. Favourable tumours demonstrate increased Schwannian stroma development.

1.1.7 Diagnosis and screening

Confirmation of a diagnosis of neuroblastoma requires a combination of laboratory tests, multi-modality imaging and pathology studies.

1.1.7.1 Laboratory findings

Several serum markers, including ferritin, neuron specific enolase (NSE), lactate dehydrogenase (LDH), although non-specific for neuroblastoma, demonstrate elevated levels and are predictive of poor outcome [100, 101].

Neuroblastoma tumours have the capacity for secretion of catecholamine products, the metabolites of which, vanillylmandelic acid (VMA) and homovanillic acid (HVA), are detectable in the urine of 90% of patients. The relative amounts of catecholamine metabolites in the urine is related to the degree of cellular maturation, increased dopamine levels or low HVA/VMA ratio is associated with a poorly differentiated tumour and indicative of poor prognosis [102]. In addition, urinary levels of these two catabolites can be used as markers of tumour progression or relapse [5].

1.1.7.2 Radiographic imaging

Initial imaging is performed according to the presenting features e.g. in children presenting with an abdominal mass the initial investigation is ultrasonography [103]. Further local assessment is then performed by cross-sectional imaging by magnetic resonance imaging (MRI) or computed tomography (CT) to determine the extent of the primary tumour, organ of origin, vascular encasement, lymph node involvement and identify metastatic disease [104].

MRI is the most commonly used imaging modality and offers the advantage of better tissue discrimination compared with CT scanning, allowing superior determination of the organ of origin and regional invasion [103-105]. In addition, the lack of exposure to ionising radiation is highly favourable in infants and children [103]. MRI is also the preferred modality for investigating intraspinal extension of tumours [105]. Contrast-enhanced CT is an additional imaging modality. At CT imaging most tumours are heterogeneous, demonstrate calcifications and may show focal areas of necrosis or haemorrhage [104]. Scintigraphic imaging allows identification of the primary tumour and sites of metastases. Meta-iodobenzylguanidine (MIBG) is structurally similar to noradrenaline and neuroblastoma cells express the noradrenaline transporter which allows uptake and storage of MIBG. 90% of neuroblastoma tumours selectively concentrate MIBG and this allows an anatomical assessment of tumour site and metastases [106]. MIBG is taken up by all catecholamine-producing tumours including ganglioneuroma, ganglioneuroblastoma, phaeochromocytoma and carcinoid tumours, therefore it is does not allow discrimination between these tumours. In addition, approximately 10% of neuroblastomas do not concentration MIBG, thus a negative scan may be inconclusive [97]. MIBG scanning is the imaging study of choice in evaluating the extent of cortical bone and bone marrow involvement. 18F-Fluorodeoxyglucose positron emission scanning exploits tumour cell glucose dependence to maintain aerobic glycolysis and is a valuable imaging modality in the assessment of MIBG-negative tumours [107].

1.1.7.3 Biopsy

Adequate tumour tissue sampling is paramount for diagnosis, risk stratification and treatment assignment. Previously, open surgical biopsy was the preferred approach to obtaining tissue

samples, however minimally invasive methods e.g. core needle biopsy are more commonly employed now. Tissue samples are obtained by core needle biopsy from multiple different regions of the tumour. Multiple cores are essential as significant biological and histological heterogeneity may exist within a single tumour [5, 108]. Tumour tissue is also utilised for molecular and genetic studies e.g. fluorescence in situ hybridisation to detect MYCN amplification [40]. Whole genome sequencing approaches are rapidly becoming more time and cost efficient and allow the identification of gene amplifications, chromosomal aberrations, homozygous deletions and other mutations simultaneously [34].

1.1.7.4 Bone marrow evaluation

Bone marrow infiltration is evaluated in all cases of neuroblastoma for accurate staging [103]. This is performed by bilateral bone marrow aspirates and biopsies, usually taken at the time of diagnosis. In addition, immunohistochemical staining for anti-ganglioside GD2, NSE and ferritin is also performed to reduce the number of false-negative cases [109].

1.1.7.5 Screening

Identification of neuroblastoma in infants, even with metastatic disease, leads to marginally improved survival [110]. This rationale led to extensive screening studies being conducted using urinary catecholamine analysis. Screening was found to substantially improve the detection rate, however tumours identified by screening were mostly clinically and biologically favourable. Ultimately, screening programmes do not reduce the prevalence of advanced disease or overall mortality and have been abandoned [111].

1.1.8 Neuroblastoma presentation

The presenting features of neuroblastoma are determined by the anatomical location of the primary tumour, extent of disease progression, tumour dissemination and the occurrence of paraneoplastic phenomena. Although significant overlap exists three main clinical scenarios are recognised and are discussed below [103].

1.1.8.1 Localised tumours

Approximately 40% of patients present with localised disease and the widespread distribution of sympathetic ganglia and paraganglia reflects the multiple sites at which primary tumours may develop **(Figure 1.4)** [103]. The most common site of primary tumours is the adrenal medulla (47.7%), followed by abdominal/retroperitoneal ganglia (23.8%), thoracic ganglia (15.1%), pelvic ganglia (3.0%), cervical ganglia (2.7%) and other sites (7.9%) [112]. The site of the primary tumour also has prognostic implications e.g. thoracic primary tumours are associated with favourable

prognostic features e.g. younger age at diagnosis, non-MYCN amplified and hyperdiploid tumours. [112]. Unusual sites of primary disease have also been described including the lung, kidney, stomach and thymus [97].

Approximately 70% of neuroblastoma tumours arise in the abdominal cavity. Adrenal medulla and abdominal ganglia tumours may present with abdominal pain and distension, anorexia, vomiting and a palpable abdominal mass detected on clinical examination is a frequent manifestation. In addition, abdominal and pelvic ganglia tumours may cause compression of adjacent structures leading to constipation or urinary retention [5].

Cervical or upper thoracic ganglia tumours may disrupt sympathetic neural pathways leading to Horner's syndrome, the features of which include ptosis, enophthalmos, miosis and anhidrosis [113]. Intrathoracic neuroblastomas arise in the mediastinum; posterior mediastinal widening caused by a tumour mass may be detected incidentally by imaging studies obtained for other indications. Occasionally, large thoracic tumours can compress adjacent structures e.g. superior vena cava, oesophagus, trachea [114].

Paraspinal tumours in any body region may extend through neural foramina causing nerve root or spinal cord compression and occurs in 5-15% of patients [115]. The clinical manifestations of intraspinal extension are motor weakness, sensory deficit, back pain and sphincter dysfunction. Malignant spinal cord compression represents an oncological emergency and requires urgent intervention to avoid long-term neurological sequeale [116].

1.8.1.2 Metastatic disease

Approximately 50% of patients present with evidence of haematogenous or lymphatic dissemination [117]. Children with metastatic disease tend to have extensive tumour burden and are severely unwell at presentation displaying constitutional symptoms such as fever, irritability, weight loss [1]. The most common sites of metastasis are bone marrow (30%), cortical bone (22%), lymph nodes (15%) and liver (12%) [37]. Widespread cortical bone and marrow infiltration may cause bone pain, limping and bone marrow suppression. An unusual site of metastasis is the retro-orbital venous plexus, causing periorbital ecchymoses (raccoon eyes) and proptosis (protrusion of the eyeball) [1].

1.8.1.3 Paraneoplastic syndromes

Two major paraneoplastic syndromes are encountered in neuroblastoma and are associated with localised tumours and favourable tumour biology. Opsoclonus-myoclonus syndrome (OMS), also called dancing eyes syndrome, occurs in 2-4% of patients with neuroblastoma and is characterised by opsoclonus (rapid, involuntary eye movements), myoclonus (involuntary twitching of a muscle or

group of muscles) and cerebellar ataxia. The associated tumour is often small, localised and well-differentiated; therefore the survival rate is highly favourable. The presence of anti-neuronal antibodies in patients with neuroblastoma associated OMS and favourable response to immunosuppressive therapy strongly supports an autoimmune aetiology [118, 119]. Refractory diarrhoea associated with failure to thrive and metabolic disorders are observed in approximately 4% of patients and results from hypersecretion of vasoactive intestinal peptide (VIP) by differentiated tumours e.g. ganglioneuroblastomas. Surgical resection of the primary tumour usually leads to resolution of symptoms [120].

1.1.8.4 Stage 4S/MS

An intriguing presentation of neuroblastoma is stage 4S, also referred to as stage MS in the INRG staging system. The hallmark of stage 4S/MS is the possibility of spontaneous tumour regression and favourable prognosis, even in the presence of significant tumour burden [121]. Stage 4S/MS is characterised by metastatic disease in children less than 18 months, with metastases confined to the liver, skin and/or bone marrow. Skin metastases are detected as palpable, subcutaneous nodules resembling a blueberry muffin appearance [122]. Extensive liver metastases cause severe hepatomegaly leading to massive abdominal distension, respiratory distress and bowel and renal impairment secondary to obstruction [5]. Several mechanisms to explain the phenomena of spontaneous regression are suggested including neurotrophin deprivation, immunomodulation, loss of telomerase activity [99].

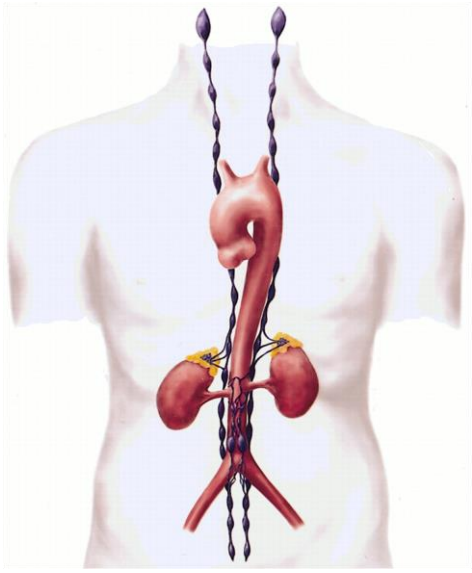

Figure 1.4: Anatomic distribution of sympathetic ganglia. The sympathetic chain ganglia, also called paravertebral ganglia, are paired structures in the cervical, thoracic, abdominal and pelvic regions. The medulla of the adrenal gland is also considered a ganglion of the sympathetic nervous system. Neuroblastoma tumours may originate in any of these structures. Reproduced from Lonergan et al. (2002) [97] with permission.

1.1.9 Disease staging

The International Neuroblastoma Risk Group (INRG) is a global collaboration formed in 2004 and has developed the INRG staging system (INRGSS) and INRG risk classification system. The traditional method of tumour staging, the International Neuroblastoma Staging System (INSS), was based on the surgeon's judgement of resectability at the time of diagnosis, therefore was a subjective assessment [123]. In order to facilitate the comparison of clinical trials conducted across the world the INRG assessed the clinical data of 8 800 patients to devise a parallel staging system (**Table 1.1**) and pre-treatment classification schema **(Figure 1.5)** [37].

Localised tumours are classified based on the presence of imaging-defined risk factors (IDRFs); surgical risk factors identified by radiographic imaging which increase the difficulty of tumour excision and are largely based on the number of body compartments occupied by the tumour and the relationship of the tumour with adjacent structures and vasculature [124].

International Neuroblastoma Risk Group staging system (INRGSS)

L1	Radiological risk factors absent: Localised tumour confined to one body compartment and not involving vital structures, as defined by the list of image-defined risk factors
L2	Local-regional tumour with presence of one or more image-defined risk factors
M	Distant metastatic disease (except stage MS)
MS	Metastatic disease in children younger than 18 months, with metastases confined to the skin, liver and/or bone marrow.

Table 1.1: International Neuroblastoma Risk Group staging system (INRGSS)

1.1.10 Risk stratification

Several neuroblastoma research groups cross the world have developed models of disease risk stratification. The most important prognostic features are age, stage and MYCN status. These parameters help to define multiple patterns of disease. Low risk tumours arise in the first months of life and are localised; provided there is no MYCN amplification these patients have excellent survival with minimal treatment. Conversely, an unfavourable outcome is expected in children with tumours which possess MYCN amplification at any age or metastatic tumours and age > 18 months on diagnosis. The International Neuroblastoma Risk Group (INRG) has developed a pretreatment classification schema in order to develop a model of risk stratification to facilitate the delivery of risk-adapted treatments **(Figure 1.5)** [37].

INRG stage	Age (months)	Histologic category	Grade of tumour differentiation	MYCN	11q aberration	DNA content	Pre-treatment risk group
L1/L2		GN maturing: GNB intermixed					Very low
				NA			Very low
				Amp			High
L2	< 18	Any, expect GN maturing or GNB intermixed		NA		No	Low
						Yes	Intermediate
	≥ 18	GNB nodular; neuroblastoma	Differentiating	NA	No		Low
			Poorly differentiated or undifferentiated		Yes		Intermediate
				Amp			High
M	< 18			NA		Hyper-diploid	Low
	< 12			NA		Diploid	Intermediate
	12 to < 18			NA		Diploid	Intermediate
	< 18			Amp			High
	≥ 18						High
MS	< 18			NA	No		Very low
					Yes		High
				Amp			High

Pre-treatment risk group	Proportion of patients (%)	5-year event-free survival (%)
Very low	28.2	> 85
Low	26.8	> 75 to ≤ 85
Intermediate	9.0	≥ 50 to ≤ 75
High	36.1	< 50

Figure 1.5: The International Neuroblastoma Risk Group Consensus Pretreatment Classification schema and prognosis based on pre-treatment risk. GN, ganglioneuroma; GNB, ganglioneuroblastoma; NA, non-amplified; Amp, amplified [37].

1.1.11 Principles of management

The management of neuroblastoma includes an array of modalities. Localised tumours and recurrences respond well to surgical resection. However, most children with neuroblastoma have locally advanced or metastatic disease at presentation and will require intensive multimodal therapy including chemotherapy, radiotherapy, autologous haematopoietic stem cell transplantation, differentiation therapy and immunotherapy. In selected cases careful observation only may be the appropriate course of action [1, 103]. These modalities are combined on the basis of clinical and biological factors in the individual patient and the consequent risk-group assignment [37]. The principles of each treatment option and multimodal therapy in the context of risk stratification are discussed below.

1.1.11.1 Surgery

Radiographic imaging is an essential component of the pre-surgical assessment and identifies the presence of image-defined risk factors (IDRFs) which enables staging [124].

Surgery has an important role both at the time of diagnosis and during treatment. Surgical resection of tumours aims to achieve complete resection with minimal residual viable tumour tissue. Tumour size, the extent of vascular encasement and the exact location are important considerations in selecting the surgical approach [123, 125]. Options available for most abdominal tumours include upper transverse, bilateral subcostal and midline transperitoneal incisions. A transthoracic extension can be added to any incision for excision of tumours with thoracoabdominal extension [125].

INRG Stage L1 **(Table 1.1)** tumours are confined to the organ of origin e.g. adrenal gland and can be removed macroscopically. Stage L2 **(Table 1.1)** tumours have spread beyond the tumour of origin and are often encasing surrounding vasculature e.g. abdominal tumours and aorta/inferior vena cava. The tumour must be carefully exposed to determine the relationship between the tumour and adjacent structures. Vascular encasement and compression of the renal vessels, splenic vein, inferior vena cava, aorta, coeliac artery and superior mesenteric artery may occur and if identified tumour dissection must be performed to free the vessels [125]. Once the vessels are freed, different segments of the tumour are removed piecemeal. Exploration of loco-regional nodes should also be undertaken at the time of resection [123]. The infiltrative nature of neuroblastoma tumours means microscopic negative margins are difficult to obtain, thus the aim is gross total resection [1].

Minimally invasive surgery has gained popularity in paediatric oncological surgery. Multiple study groups have found thoracoscopic/laparoscopic surgery is a safe option for the resection of selected

cases of neuroblastoma without IDRFs, however open surgery should be preferred if complete tumour resection is uncertain or vascular control is considered difficult [126].

Intraoperative and postoperative complications are not uncommon due to the extensive surgery often necessary. Surgical complications vary dependent on the site and extent of the primary tumour and include haemorrhage, injury to a vascular structure and visceral damage [5]. Injury to viscera occurs in 5% of cases and occasionally this will lead to removal of the affected organ e.g. renal infarction requiring nephrectomy [125]. Postoperative complications include bowel obstruction (1-5%) and wound infections or dehiscence [123].

1.1.11.2 Chemotherapy

Chemotherapy is the main modality of treatment for patients with metastatic and locally advanced disease and is indicated in low-risk patients with symptomatic involvement of vital organs [5]. A combination of agents is used to overcome drug resistance to individual agents. Most regimens involve the use of different combinations of anthracyclines, platinum based compounds, etoposide, microtubule inactivating agents and alkylating agents. For high-risk patients chemotherapy is delivered in three phases: induction of remission, consolidation of remission and eradication of minimal residual disease [103].

1.1.11.3 Radiotherapy

Neuroblastoma tumours are highly sensitive to radiotherapy and total body irradiation (TBI). TBI has been shown to decrease relapse and increase event-free survival in high-risk neuroblastoma [127]. However, its use in very young children is controversial due to the risk of long term adverse effects e.g. secondary malignancy [1].

1.1.12 Risk-based multimodal therapy

1.1.12.1 Very-low risk and low-risk neuroblastoma

Very-low and low-risk neuroblastomas (localised tumours with favourable histology and biological characteristics and stage MS) account for almost half of all newly diagnosed cases of neuroblastoma [37]. The aim of treatment is to balance maintaining excellent patient survival whilst delivering minimal therapy. Infants <1 year with adrenal masses <5 cm presumed to be neuroblastoma can be observed without obtaining histological confirmation or surgical resection [103]. Observation includes physical examination, urinary catecholamine levels and imaging. This approach avoids the potential complications of surgery such as vital organ damage in infants [103]. For patients >1 year of age with localised disease that is amenable to resection the tumour should be resected. In the absence of MYCN amplification, any residual disease following surgical resection of the tumour is not

considered a risk factor for relapse, further treatment is not required and overall survival is almost 100% [128]. For children with low-risk disease (INRG stage L2 without biological risk factors) the management strategy depends on the manifestation of symptoms. If present, limited chemotherapy is indicated. Complete resection of the primary tumour or radiotherapy is not indicated [123].

1.1.12.2 Intermediate-risk neuroblastoma

Intermediate-risk neuroblastoma refers to non-MYCN amplified stage L2 tumours and metastatic tumours in children <18 months with diploid DNA content **(Table 1.1)**. Children in this group are treated with two to eight cycles of chemotherapy followed by surgical resection of the residual tumour where possible [103, 123]. In patients with an unfavourable genomic profile e.g. 11q deletion a more intensive treatment regimen which includes radiotherapy. Based on these approaches, the estimated overall survival of infants with metastatic disease is >90%, however for children >18 months with stage L2 tumours overall survival is 70% [129].

1.1.12.3 High-risk neuroblastoma

This classification includes all patients with MYCN-amplified tumours, this subgroup accounts for 20-25% of high-risk cases. The majority of patients with high-risk disease are >18 months and have metastatic disease [37]. The current approach for high-risk neuroblastoma involves intensive induction chemotherapy to reduce tumour burden and metastases, followed by surgery to remove the primary tumour and subsequent myeloablative chemotherapy supported with AHSCT. This is followed by maintenance therapy for minimal residual disease with anti-GD2 monoclonal antibody, cytokine immunotherapy and differentiating therapy **(Figure 1.6).**

Induction chemotherapy involves a combination of four-to-six agents, commonly carboplatin, cisplatin, cyclophosphamide, doxorubicin, vincristine and etoposide. Stem cell harvest is also performed during induction therapy for later autologous transplant. Local control of tumour spread is attempted by means of surgical resection of the primary tumour. However, in patients with advanced disease total resection is often difficult due to frequent tumour encasement of surrounding vasculature.

Consolidation therapy aims to eradicate remaining tumour cells with the use of cytotoxic agents and radiotherapy at myeloablative doses. This eliminates tumour infiltration from the bone marrow, but also depletes normal bone marrow reserves, thus is followed by AHSCT. Addition of myeloablative therapy with AHSCT was a major step in improving event-free survival in high-risk patients [130].

Around 50% of high-risk patients develop early or late relapse, often from minimal residual disease (MRD) in the bone or bone marrow [131]. 13-*cis*-retinoic acid induces cell growth arrest and

differentiation of tumour cells and has become the standard for treating MRD. 13-*cis*-retinoic acid administered after consolidation therapy was found to improve event-free survival, however overall survival was not increased. GD2 is a surface glycosphingolipid abundant on the surface of neuroblastoma cells and can be targeted by an anti-GD2 monoclonal antibody (MAb). Anti-GD2 MAb activates both granulocyte and natural killer cell-mediated lysis of tumour cells [33]. Granulocyte-macrophage colony-stimulating factor (GM-CSF) increases bone marrow production of neutrophils and eosinophils, thus potentiating the immune response. A seminal randomised trial showed significant improvement in event-free survival in high-risk patients receiving combination therapy consisting of 13-*cis*-retinoic acid, anti-GD2 antibody, GM-CSF and interleukin-2 compared with patients receiving 13-*cis*-retinoic acid alone [132]. This regime is now the standard of care in most centres for maintenance therapy in high-risk cases [5, 103] **(Figure 1.6)**.

1.1.12.4 Acute and long-term sequelae of treatment

Most patients treated for high-risk neuroblastoma experience therapy-associated acute toxicity including pain, mucositis, vomiting and increased risk of infection [103]. In addition, a large study of neuroblastoma survivors found an eight-fold increase in the incidence of chronic disease compared with sibling cohorts. Furthermore, survivors have an increased relative risk of mortality and developing a secondary malignancy including thyroid, renal and soft tissue cancers and acute myeloid leukaemia [127].

1.1.12.5 Relapsed neuroblastoma

Relapse after induction and consolidation therapy is associated with a very poor outcome and survival beyond 3 years without further recurrence or death is rarely and salvage treatment involves chemotherapy and targeted radiotherapy [5, 103].

1.1.12.6. Targeted therapies

Most children diagnosed with high-risk neuroblastoma do not respond to or relapse after conventional therapy, despite significant advances and multimodal therapy [1]. The identification of somatic gene mutations and greater understanding of signalling pathways in neuroblastoma has provided strong rationale for developing targeted therapies. Multiple agents which target aberrant signalling pathways are undergoing phase I/II testing including aurora kinase inhibitors, BET bromodomain inhibitors and ALK inhibitors [103, 133]. The success of anti-GD2 targeted therapy has created significant interest in developing additional immunomodulating therapies [33, 133].

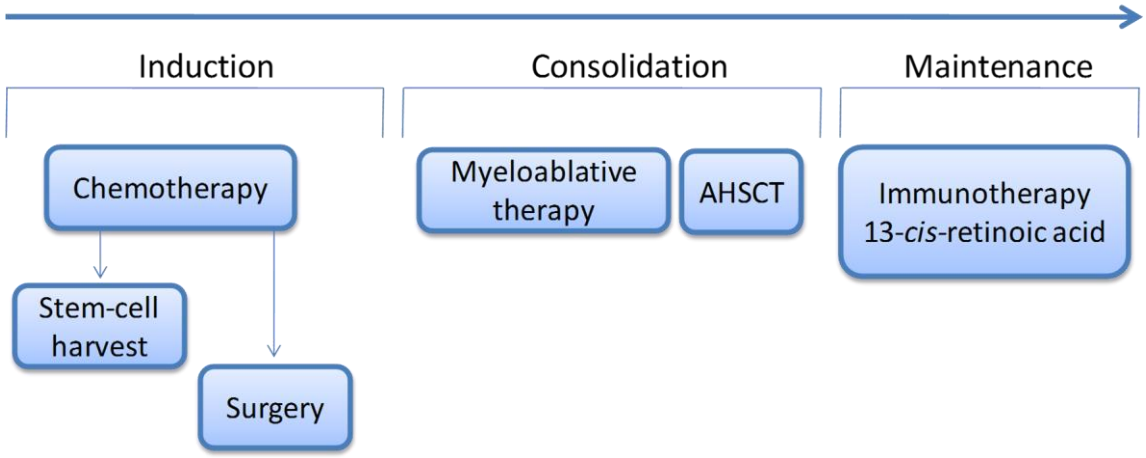

Figure 1.6: A visual summary of the current standard of therapy for the management of high-risk neuroblastoma. Treatment occurs in three blocks: induction, consolidation and maintenance. Induction therapy involves cycles of chemotherapy to reduce primary tumour burden and metastases; stem-cell harvest is performed for later transplantation and surgical resection of the primary tumour is undertaken towards the end of induction therapy. Consolidation therapy aims to eradicate and residual disease from bone marrow by myeloablation followed by stem cell transplant. Maintenance therapy is aimed at minimal residual disease and a combination of immunotherapy and differentiation therapy. AHSCT, autologous haematopoietic stem cell transplant [103].

1.1.13 *In vivo* models of neuroblastoma

Developing novel chemotherapeutic agents against paediatric cancers including neuroblastoma poses a significant problem due to the relatively low number of patients available for clinical trials. Animal models are vital to further our understanding of the biology of neuroblastoma and in the development and investigation of compouds which may have anti-tumour efficacy [134, 135].

A significant advancement in neuroblastoma research was the development of genetically engineered murine models (GEMM). The murine genome may be manipulated to influence the expression of specific genes and Weiss et al. [13] have developed the TH-MYCN murine model. Mice belonging to this transgenic strain overexpress the MYCN oncogene and sporadically develop neuroblastoma tumours in a similar pattern to humans. This discovery has facilitated research of MYCN amplified tumours and *in vivo* investigation of novel therapeutic agents. A strength of GEMMs is that tumours, likewise in humans, arise in immunocompetent hosts; this is favourable as the immune response plays a significant role in both tumour development and response to therapeutic agent [13, 47]. However, despite the strengths of GEMMs, tumours developed in mice are not of human origin, this limits the clinical translation of results obtained in GEMMs.

Xenografts are an alternative animal model of cancer whereby human tissue is transplanted into an immunodeficient animal, most often mice. Cells may be implanted subcutaneously or orthotopically, whereby cells are transplanted directly into the organ in which the tumour originates e.g. the adrenal gland in neuroblastoma. Thus, key strengths of xenograft models are that tumours are derived from human tissue and chemotherapeutic compounds can be screened for anti-tumour efficacy *in vivo* [135]. Unlike GEMMs xenografts models require the host animal to be genetically manipulated in order to be immunodeficient.

Biomedical research has long employed the chick embryo as an *in vivo* model, for example the Rous sarcoma virus (RSV) was identified in the chick embryo in 1911 [136]. The chick embryo displays molecular, cellular and anatomical homogeneity with human embryos which makes it a suitable model in which to recapitulate human disease [135-137]. In biomedical research, the chorioallantoic membrane (CAM), an extra-embryonic membrane responsible for calcium transport, gas exchange and water and electrolyte homeostasis, is of particular interest. Owing to its highly vascular nature, the CAM has been utilised as a model to study angiogenesis. However, there is increasing recognition of the CAM system as a xenograft model of cancer and the efficacy of this model has been successfully demonstrated in previous studies [137-139]. Multiple tumour cell lines have been effectively cultured on the CAM and xenograft tumours display the characteristics of *in vivo* tumours including solid tumour development, angiogenesis and metastasis [137-140]. This is achievable due to the natural immunodeficiency of the chick embryo which allows the CAM to accept tumour cells without mounting an immune response. Following tumour development the efficacy of chemotherapeutic compounds may be assessed by delivery *in ovo.* Tumours may subsequently be excised and characterised e.g. the anti-proliferative effect of a compound may be assessed by determining the Ki67 index [141, 142]. Compared to murine models the CAM system offers several advantages. As previously mentioned the immunodeficient nature of the chick allows xenotransplantation of any cell-line without genetic manipulation of the chick embryo, the vascular nature of the CAM supports rapid development of the primary tumour and the CAM system represents an intermediate between cultured cells and animals hence does not raise any legal or ethical issues [140-142].

1.2 Potassium (K^+) channels

1.2.1 Overview

Cells are enveloped by the plasma membrane, comprised by a fluid mosaic of proteins embedded in a phospholipid bilayer. Bipolar phospholipids e.g. phosphatidylcholine are the most abundant lipid in the membrane and are termed amphipathic i.e. they possess both a polar, hydrophilic head group and two uncharged hydrophobic tails; these moieties confer lipid molecules with the ability to form spontaneous bilayers in aqueous environments. The hydrophilic heads face the intra- and extra-cellular water and the hydrophobic tails form the core of the bilayer [143]. The plasma membrane serves as a semi-permeable barrier that regulates the passage of solutes. The hydrophobic nature of the bilayer allows hydrophobic and small polar molecules to passively diffuse across the membrane e.g. O_2 and H_2O. The membrane acts a barrier to large polar or charged molecules e.g. glucose and ions. The passage of ions is achieved by integral membrane proteins that form channels, pumps and transporters. Potassium (from here on in will be referred to as K^+) channels are ubiquitously expressed in almost all living organisms and mediate the flux of K^+ across the plasma membrane. Conductance of K^+ is vital for many cellular processes in both excitable and non-excitable cells. In excitable cells, they contribute to resting membrane potential and repolarise the plasma membrane after action potential firing. Moreover, K^+ channels have important physiological roles in excitable and non-excitable cells including regulation of osmolarity, Ca^{2+} signalling, lymphocyte activation, cell migration, differentiation, proliferation and apoptosis [144, 145].

The K^+ channel gene family is the largest and most diverse of the ion channel families. The human genome contains 79 genes encoding potassium channel α-subunits which can be further divided into 4 superfamilies based on structure and function and each superfamily has distinct and defining features [146-148] **(Figure 1.7)**. Nevertheless, the archetypal structure of all K^+ channels is consistent across each superfamily. 4 α-subunits associate in radial symmetry to form multimeric channels, either as homomers with identical α-subunits or as heteromers with α-subunits from the same subfamily. Hydrophobic segments of each α-subunit, the transmembrane domain (TMD), span the membrane. Each subunit contains a pore forming domain and the multimeric structure forms a pore (P) through which K^+ permeation occurs. Each channel has an N-terminus and C-terminus which is normally intracellular.

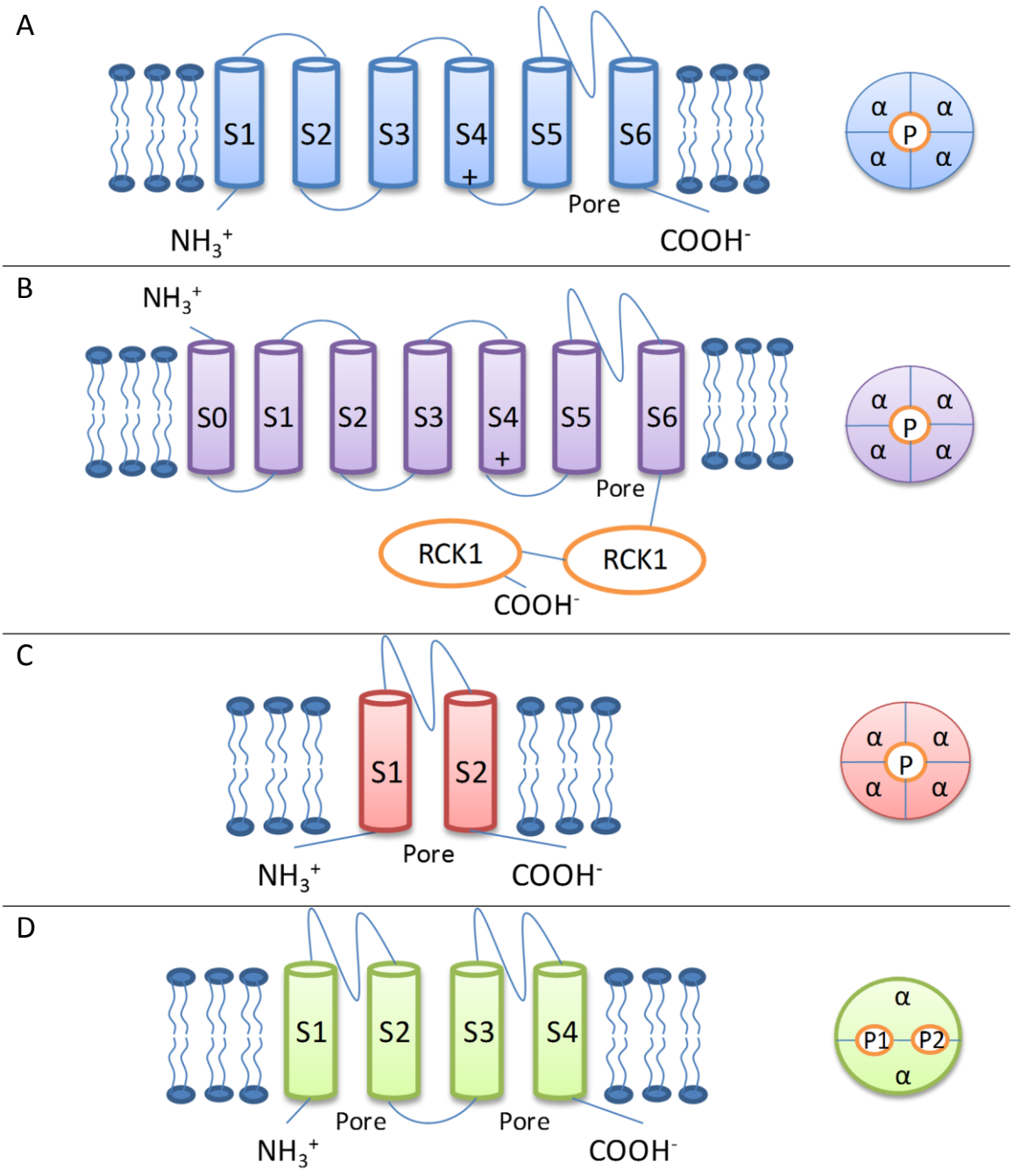

Figure 1.7: Representative structure of the transmembrane topology of potassium (K^+) channel subunits and channel assembly. (A) Voltage-gated K^+ channels (Kv) subunits comprise six transmembrane domains (TMD) and one pore domain. (B) Large conductance calcium-activated K^+ channels subunits comprise seven TMDs and one pore domain. Two regulators of K^+ conductance (RCK) domains are in the C-terminus, RCK2 is the putative Ca^{2+} binding site. (C) Inward rectifying K^+ channel subunits (Kir) comprise two TMDs and one pore domain. (D) 2 pore K^+ channel subunits (K2P) comprise four TMDs and two pore domains. Subunits are arranged circumferentially around the central pore as homomers/heteromers [147].

1.2.2. Properties of K^+ channels

K^+ channels are an example of passive transport system which demonstrates three salient properties: selectivity, conductivity and gating, each property is briefly discussed below.

1.2.2.1 Selectivity

X-ray crystallography studies of KcsA have contributed significantly to our understanding of the architecture and chemistry of K^+ channels [149, 150]. KcsA is K^+ channel which has 4 subunits, each of which contains 2 transmembrane domains and was isolated from *Streptomyces lividans* [149]. Despite its relatively simple topology, KcsA closely resembles eukaryotic K^+ channels in terms of ion permeation and selectivity [149]. The pore region of the channel is lined by a highly conserved sequence of amino acids (TXXTXGYG) which forms the selectivity filter. In solution ions strongly interact with water and acquire a hydration shell. As each K^+ ion passes through the narrow pore it is stripped of its hydration shell. To compensate for the energetic cost of dehydration, carbonyl oxygen atoms on the amino acid residues take the place of water oxygen atoms, therefore this arrangement of oxygen atoms mimics hydration. This mechanism explains why K^+ channels are highly selective for K^+ relative to sodium ions (Na^+). Na^+ (0.95Å radius) is a smaller ion than K^+ (1.33Å radius), therefore would only be able to interact with oxygens on one side of the channel which is energetically less favourable [148, 150].

1.2.2.2. Conductivity

Flow of K^+ is driven by the electrochemical gradient and K^+ channels are able to achieve highly selective and high conductive rates, around 10^7 ions $channel^{-1}$ $second^{-1}$ [151]. K^+ ions are conducted in single file and multiple ions are able occupy the selectivity filter. Resultantly the positively charged ions will repel each other; this electrostatic repulsion is one feature which permits rapid conduction [152].

1.2.2.3. Gating

Channels have multiple conformational states including activation, deactivation and inactivation [152]. Gating is the process by which the channel moves between conformation states of the channel as it opens and closes. In the closed state the channel is impermeable to ions; a stimulus then evokes a conformational change leading to the channel opening (activation). Following activation some channels can shift to another conformation, inactivation, during which the channel is not closed but refractory to further activation and non-conducting. Deactivation is the process of channel going from the open to closed conformation [147].

1.2.3. Voltage-gated K^+ channels

The first voltage-gated K^+ channel (VGKC) to be cloned was the shaker gene in Drosophila melanogaster (fruit fly). The legs of shaker gene mutant Drosophila display aberrant movements under anaesthesia [153]. In humans 40 genes encode for VGKC α-subunits across 10 gene subfamilies and each gene has a corresponding protein name denoted as Kv*x*. The 10 subfamilies are: KCNA (Kv1), KCNB (Kv2), KCNC (Kv3), KCND (Kv4), KCNF (Kv5), KCNG (Kv6), KCNH (Kv10/11/12), KCNQ (Kv7), KCNS (Kv8), KCNV (Kv9). Within each subfamily there are multiple members denoted by a number e.g. KCNQ2 encodes for Kv7.2. Kv5, 6, 8 and 9 subunits are unable to form functional homomers and can only co-assemble with Kv2 subunits [146, 147].

Each α-subunit of the VGKC contains six transmembrane domains (S1-6). Co-assembly of helices S5-S6 of each subunit forms central pore domain. Helices S1-S4 comprise the voltage sensing domain and surrounds the central pore domain. The VSD and central pore domain are linked by the S4-S5 linker [153]. In addition, some Kv channels can associate with ß-subunits (also called auxiliary subunits) which can alter the channel structure and biophysical properties e.g. members of the KCNE subfamily may associate with Kv7.1/Kv11.1 cardiac channels [154].

1.2.3.1. How do VGKCs activate and inactivate?

Structural studies are in consensus that the voltage sensing domain (VSD) consists of 4 helices (S1-4), specifically the S4 helix has upto 8 positively charged arginine or lysine residues which represent the VSD [155]. What remains unclear is the mechanism by which the VSD translocates the charge across the membrane when membrane potential changes and several models of voltage sensing have been proposed. Each model is in agreement that positive residues on the S4 helix carry out translocation of the charge, the S4 helix can adopt different conformations and that negative residues in other helices balance the positive residues [156]. To elucidate the mechanism by which the VSD and central pore domain are electromechanically coupled Mackinnon and colleagues have studied mammalian Kv1.2. They found motion of the S4 helices are transmitted to the activation gate via the S4-S5 linker [157]. Voltage-gated K^+ channels demonstrate two mechanisms of inactivation, N-type and C-type. N-type inactivation is a fast process which occurs in some Kv channels. The first ~30 amino acid residues at the N-terminus on the cytosolic aspect of the channel enter the pore to inhibit ion conductance [158]. Support for this mechanism comes from Fan et al. who demonstrated that a mutated Shaker channel lacking the N-terminus demonstrates lack of inactivation Electrostatic interaction occurs between the inactivation ball on the N-terminus and the T1–S1 linker region of Kv1.4 channel. C-type inactivation occurs in many voltage-gated K^+ channels and results from conformational changes of the selectivity filter [159]

1.2.4 Calcium activated potassium channels

The calcium activated superfamily of K^+ channels (KCa) has 6 members which are distinguished by conductance; big conductance, KCNMA1 (KCa1.1, BK); small conductance KCNN1 (KCa2.1, SK1), KCNN2 (KCa2.2, SK2), KCNN3 (KCa2.3, SK3); intermediate conductance, KCNN4 (KCa3.1, IK1) and KCNU1 (KCa5.1) [160]. All KCa channels are tetrameric and each α-subunit has 6 transmembrane segments, except for the BK channel which has unique structural and functional features. The α-subunits of BK channel each contain 7 transmembrane domains. In addition to the canonical 6 TMDs there is an initial TMD termed S0, preceding S1. As a result the N-terminus is extracellular. BK channels are activated by increased intracellular Ca^{2+}, membrane depolarisation or both synergistically; segments S0-S4 from the VSD and S5-S6 form the pore-forming domain. In addition, the BK channel has 4 ß-subunits, encoded by KCNMB1-4, which modify the biophysical and pharmacological properties of the channel. The C-terminus has 2 putative regulators of K^+ conductance (RCK) domains, RCK1 and RCK2, which is the likely site of Ca^{2+} binding [147].

The KCa superfamily plays a key role in excitable and non-excitable cells. In neurons KCa channels contribute to action potential repolarisation, regulation of membrane potential, neuronal firing rates, and neurotransmitter release [161]. KCa channels are also present in the vasculature where they contribute to vascular tone and endothelial synthesis of vasoactive modulators [162]. SK and IK channels share identical topology to VGKCs are gated solely by intracellular Ca^{2+} and display lower single-channel conductance compared with BK channels [147].

1.2.5 Inwardly rectifying potassium channels

Inward rectifier channels (Kir) are a unique subfamily of potassium channels; they are activated at membrane potential negative to equilibrium potential of K^+ and allow inward flow of K^+. The α-subunits are encoded by genes denoted KCNJ*x* [163]. The primary structure comprises 2 transmembrane segments and a single pore domain and subunits may co-assemble as homotetramers or heterotetramers. 15 genes encoding α-subunits have been identified and are divided into 7 subfamilies (Kir1.x – Kir7.x) and further divided into 4 functional subgroups: classical, G protein-gated, ATP-sensitive and K^+ transport [164].

Kir channels demonstrate multiple gating mechanisms. During membrane depolarisation Mg^{2+} and polyamines physically block outward K^+ conductance, on hyperpolarisation this block is released and allows K^+ influx, thus the name inward rectifier. Other factors which regulate Kir channels include phosophatidylinosital-4,5-bisphosphate (PIP_2), ATP and G-proteins [146, 147].

Kir channels are widely distributed across the body including cardiac myocytes, neurons and pancreatic ß-cells and have wide-ranging physiological functions [147]. For example, K_{ATP}-channels are formed by Kir6.x subunits which co-assemble with sulphonylurea receptor (SUR) proteins to form a functional channel that is inhibited by increase in the intracellular ATP/ADP ratio. This is the basis of insulin release in pancreatic ß-cells; raised intracellular glucose levels leads to K_{ATP} channel inhibition leads to membrane depolarisation, Ca^{2+} influx through voltage-gated calcium channels and insulin exocytosis [165]. Mutations of Kir channel encoding genes have been implicated in many human diseases, primarily of the nervous, endocrine and cardiac systems. For example loss of function mutations in KCNJ2, the gene encoding Kir2.1 α-subunits, leads to Andersen's syndrome which predisposes those affected to potentially fatal ventricular arrhythmias [166].

1.2.6 Two pore potassium channels

The α-subunits of two pore potassium channels (K2P) channels are composed of 4 transmembrane segments and 2 pores domains. A unique feature of K2P channels is they are formed from homo- or hetero- dimers of α-subunits [147]. The mammalian K2P superfamily has 15 members; encoding genes are denoted as KCNKx, with x corresponding to the order of discovery [167]. K2P family members display significant biophysical differences e.g. TASK-1 is constitutively open at rest and functions as an open rectifier, whereas TREK-1 is an outward rectifier which requires an activating stimulus. Furthermore, K2P channels are regulated by physical e.g. membrane stretch and chemical stimuli e.g. extra-cellular protons, lipids, volatile anaesthetics and may be divided into further subgroups based on their regulators [168]. K2P channels activate over a range of voltages, may be constitutively open at rest and have a role in regulation of resting membrane potential [169]. The role of K2P channels in disease is less well established compared with other K^+ channel superfamilies and few gene mutations leading to channel dysfunction have been identified.

1.2.7 K^+ channelopathies

Channelopathies are diseases that develop due to mutations in ion channel encoding genes [170]. K^+ channel are expressed ubiquitously throughout the body. Consistent with the widespread distribution of K^+ channels, mutations in genes encoding K^+ channels lead to dysfunction across a number of organ systems. Most often mutations lead to a loss of channel function, however gain of function mutations have also been identified [147, 170]. The list of channelopathies is rapidly expanding due to advances in the understanding of the role of ion channels in both physiological and pathophysiological processes. **Table 1.2** outlines the distribution and associated channelopathies of specific K^+ channels.

Disease	Gene	Effect on function
Episodic ataxia, type 1	KCNA1	LoF
Spinocerebellar ataxia type 13	KCNC3	LoF
Brugada syndrome, type 6	KCND3	LoF
Benign familial neonatal seizures	KCNQ2, KCNQ3	LoF
Deafness, autosomal dominant, type 2A	KCNQ4	LoF
Generalised epilepsy with paroxysmal dyskinesia	KCNMA1	LoF
Early infantile encephalopathy type 14	KCNT1	LoF
Nocturnal frontal lobe epilepsy type 5	KCNT1	LoF
Familial atrial fibrillation	KCNQ1, KCNE2, KCNA5, KCNJ2,	LoF/GoF
Long QT syndrome	KCNQ1, KCNH2, KCNE1, KCNE2, KCNJ2, KCNJ5	LoF
Short QT syndrome	KCNH2, KCNQ1, KCNJ2	GoF
Bartter's syndrome type 2	KCNJ1	LoF
Familial hyperaldosteronism type 3	KCNJ5	LoF
EAST syndrome	KCNJ10, KCNJ16	LoF
Transient neonatal diabetes mellitus, type 3	KCNJ11	GoF
Familial hyperinsulinaemic hypoglycaemia type 2	KCNJ11	LoF
Type 2 Diabetes Mellitus	KCNJ15	LoF
Thyrotoxic periodic paralysis	KCNJ18	LoF

Table 1.2: Mutations in K^+ channel encoding genes lead to diseases of the nervous, cardiovascular urinary and endocrine systems. LoF, loss of function; GoF, gain of function.

1.3 Kv7 channels

1.3.1. Overview

KCNQ genes encode members of the Kv7 subfamily of voltage gated K^+ channels and 5 members of this subfamily- Kv7.1-5, have been identified [171]. Kv7.1 (KCNQ1) is primarily expressed in cardiac tissue, vascular smooth muscle cells and epithelial cells. Kv7.2-Kv7.5 (KCNQ2-5) channels are predominantly expressed in the peripheral and central nervous system including sympathetic, hippocampal and cerebellar neurons [172, 173].

1.3.2. Structure

Kv7 channel subunits have 6 transmembrane domains (TMD) and a single P-loop that forms the selectivity filter of the pore. The P-loop contains the signature sequence TxxTxGYG [174]. All Kv7 subunits, except Kv7.1 which has 4, have 6 positively charged amino acid residues in the S4 TMD which forms the voltage sensing domain. Kv7 subunits display 30-65% structural homology and have a highly homologous region on their intracellular C-terminus, termed the A'-domain. The length of C-terminus is very variable, whereas the length and amino acid sequence of the N-terminus is relatively constant between the 5 subtypes [174, 175]. Kv7.1 subunits do no coassemble with other Kv7 subunits and form homomeric channels. Conversely, Kv7.3 is poorly expressed as a homomer, but can form heteromers with all other subunits except Kv7.1. Kv7.2, Kv7.4 and Kv7.5 subunits can form functional homomers [174]. In addition, Kv7 channel function may be influenced by accessory ß-subunits. For example, KCNE1 encodes a regulatory subunit (minK) which assembles with Kv7.1 subunits in cardiac tissue; forming the I_{Ks} channel which is responsible for the delayed rectifier current of the cardiac action potential [176].

1.3.3. Kv7.2 and the M-current

Generally expression of homomeric Kv7 channels produces outwardly rectifying voltage K^+ currents that activate positive to -60 mV and display little or no inactivation. There are particular characteristics associated with each current whether expressed as a homomer or heteromer. KCNQ2 encodes Kv7.2 subunits and heterologous expression of Kv7.2 subunits in a range of mammalian cells has demonstrated homomeric Kv7.2 channels conduct selective currents activated by depolarisation at membrane potential around -50 mV, exhibit slow activation and deactivation and lack inactivation [172, 174].

The M-current (I_{KM}), a voltage-gated K^+ current, is widely distributed in the mammalian peripheral and central nervous system [177]. I_{KM} is a non-inactivating, voltage-dependent K^+ current that activates at -60 mV. I_{KM} activates slowly at subthreshold potentials and does not inactivate,

therefore generates a steady outward current [172]. Activation of G-protein coupled receptors e.g. muscarinic receptors, hence the name, can suppress I_{KM} by triggering phospholipase-Cß activation, leading to decreased PIP2 availability which suppresses channel function [178]. The molecular identity of the channel underlying the M-current was later identified to be coassembled Kv7.2 and Kv7.3 subunits. Heterologous expression studies demonstrate that the biophysical properties and pharmacological sensitivities of the Kv7.2/Kv7.3 heteromers recapitulate I_{KM} [179]. When defined by biophysical properties all Kv7 homomers are capable of forming M-like current. However, in most native neurons functional M-channels are formed either by Kv7.2/7.3 heteromers or Kv7.2 homomers [180]. Kv7.3/Kv7.5 heteromers have also been found to contribute to M-current [181].

The physiological function of I_{KM} has been characterised. As activation of I_{KM} is relatively slow it does not contribute to repolarisation of action potentials. Rather I_{KM} serves to act as a brake for repetitive action potential discharges and has an important role in controlling neuronal excitability [182]. In sympathetic neurons activation of the M-channel during the initial stages of an action potential serves to suppress later action potentials and abbreviate the duration and frequency spikes induced by sustained depolarisation. The M-current may be enhanced with the Kv7 activator, retigabine, thus hyperpolarising the neuron membrane potential and inhibiting spike generation. Whereas M-channel blockade with XE991 produces a prolonged spike discharge i.e. induces tonic firing. The M-current is believed to abbreviate action potential generation by the following mechanism. Following initial depolarisation of membrane potential there is increased membrane conductance and enhanced current passed by the M-channel, thereby causing membrane potential hyperpolarisation and raising the threshold for further action potential generation [172, 182].

1.3.4. Kv7 pharmacology

Kv7 channels have a unique pharmacology significant potential for therapeutic benefit. A number of compounds have been developed with varying selectivity [183].

1.3.4.1. Activators

Flupirtine and retigabine are the best characterised Kv7 activators and activate Kv7.2-5 channels. The main action of retigabine is to shift the current-voltage curve to the left, so that channels open at more hyperpolarised membrane potentials. Consequently, there is an increased outward K^+ current and suppression of neuronal firing. A hallmark feature of multiple conditions including epilepsy is neuronal excitability, therefore Kv7 activation may have anticonvulsant activity [184]. ML213 is a relatively novel activator which is selective for Kv7.2 (EC_{50}= 230 nM) and Kv7.4 (EC_{50}= 510 nM) channels [185].

1.3.4.2. Blockers

Linopirdine was the first selective I_{KM} blocker and was introduced as a cognition enhancer for potential application in Alzheimer's disease, however in trials it was large ineffective due to relatively low I_{KM} blocking potency, therefore requiring high doses which inadvertently caused cholinergic hyperstimulation effects e.g. tremors [186]. To overcome this limitation, XE991, a more potent inhibitor of the M-current was developed. The order potency of XE991 for homomeric Kv7 channels is Kv7.2 (IC_{50}= 0.7 μM), Kv7.1 (IC_{50}= 0.8 μM), Kv7.5 (IC_{50}= 50 μM) and Kv7.3 (IC_{50}= 65 μM). XE991 potency on the Kv7.2/Kv7.3 heteromultimer channel is similar to Kv7.2 homomultimers (IC_{50}= 0.6 μM) [174, 183]. Another challenge of blocking Kv7 channels is maintaining specificity. Although with lower potency, linopirdine and XE991 can also block Kv7.1 channels in cardiac tissue. This is problematic due to the risk of inducing long QT syndrome and potentially fatal ventricular arrhythmias. XE991 is less potent on the I_{Ks} current which contributes to cardiac repolarisation compared with Kv7.1 homomeric channels alone (IC_{50}= 11 μM vs. 0.8 μM) [174].

1.3.5 Human disease of Kv7 dysfunction

4 of the 5 members of the Kv7 subfamily have been implicated in human disease. Indeed KCNQ1, KCNQ2 and KCNQ3 were first identified by positional cloning in families affected by heritable disease [187, 188]. The gene products of KCNQ2 and KCNQ3, Kv7.2 and Kv7.3 are expressed in most brain regions including the cortex, cerebellum, basal ganglia and hippocampus. Mutations in KCNQ2 and KCNQ3 cause benign familial neonatal seizures (BFNS), a rare, autosomal dominant epilepsy syndrome which causes frequent, unprovoked partial or generalised clonic seizures in the first days of life [189]. The consequence of mutations is loss of channel function and reduced K^+ current. Given the physiological role of Kv7.2/Kv7.3 is to reduced neuronal excitability, a hallmark

pathophysiological feature of epilepsy, it is understandable that KCNQ2 and KCNQ3 mutations may lead to BFNS [190]. Inherited mutations of the Kv7.1 encoding gene (KCNQ1) and its regulatory subunit (KCNE1) may cause disruption of channel assembly and altered channel kinetics. This leads to impaired cardiac repolarisation and may lead to Long QT syndrome (LQTS) which predisposes affected individuals to potentially fatal ventricular arrhythmias [191]. Expression of KCNQ4 is localised to the inner ear and certain brainstem nuclei. KCNQ4 mutations are associated with non-syndromic sensorineural deafness type 2 (DFNA2). The progressive nature of DFNA2 suggests that KCNQ4 currents are not essential for hearing, but reduced currents may contribute to a degenerative process [192].

1.4 K^+ channels and cancer

1.4.1. Overview

Many K^+ channels demonstrate deregulated expression in human cancer and channels belonging to all four K^+ channel superfamilies have been implicated [145]. Many cancer cell-lines and primary tumours demonstrate overexpression of K^+ channels compared with the equivalent native cells from which they originate. However, the question exists whether overexpression initiates tumourigenesis, facilitates tumour progression or has no functional significance [193]. K^+ channels are implicated in multiple oncological processes including cell proliferation, apoptosis, cell migration, metastasis and angiogenesis [144, 145]. The role of K^+ channels in cell proliferation and apoptosis are further discussed below.

1.4.2 Cell proliferation

Uncontrolled cell proliferation is a defining feature of cancer [50] and many studies report that K^+ channels are essential for neoplastic cell proliferation. A permissive role for K^+ channel expression in multiple cancers is supported by numerous reports that pharmacological inhibition or genetic suppression of K^+ channels inhibits growth in multiple cancer types and that overexpression of specific K^+ channels in heterologous systems promotes tumourigenesis [194, 195]. Several mechanisms have been proposed that may explain the role of K^+ channels in tumour cell proliferation and are discussed below.

1.4.2.1. Regulation of membrane potential

A significant factor that regulates the cell cycle is membrane potential, as progression of the cell cycle is accompanied by rhythmic membrane potential oscillations [193]. K^+ channels are critical determinants of cell membrane potential; this ability to regulate membrane potential is thought to be vital for passage through the cell cycle. At the G1-S transition point of the cell cycle an increase in K^+ current leads to a relatively hyperpolarised membrane potential **(Figure 1.8)**. Since tumour cells have a relatively depolarised membrane potential it is plausible that such cells need to up-regulate K^+ channel expression to produce the hyperpolarisation necessary to transition from G1 to S phase [193, 196, 197].

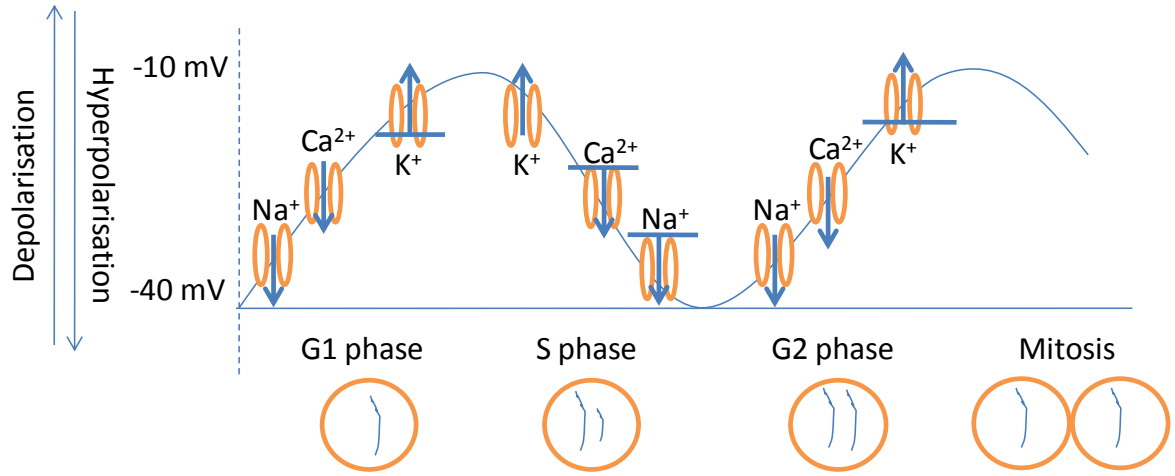

Figure 1.8: Membrane potential oscillations during the cell cycle. A transient hyperpolarisation at the G1-S transition point, mediated by increased K^+ channel activity, has been observed in multiple cancer cell lines. This is followed by reduced K^+ currents and transient membrane potential is depolarised as the cell approaches mitosis [198].

1.4.2.2. Control of cell volume

Another mechanism linking K+ channel conductance to cell proliferation is regulation of cell volume [144]. Throughout the cell cycle regulation of osmolarity allows accurate control of cell volume. Ion channels, mainly K^+ and Cl^-, are important regulators of osmolarity by governing ion flow. At the G2-M transition point of the cell cycle, the outward movement of K+ and Cl- is accompanied by cytoplasmic water efflux thus reducing cell volume; this is necessary for pre-mitotic condensation (PMC) and promotes successful mitotic entry [200]. A subset of medulloblastoma tumours demonstrates EAG2 overexpression. EAG2 enriches at the plasma membrane during G2 and mitosis and promotes K^+ efflux for pre-mitotic condensation, with the elevated K^+ current driving volume reduction prior to mitosis. Further to this, genetic suppression of EAG2 leads to perturbation of cell volume which activates tumour suppression pathways [200]

1.4.2.3 Involvement in signalling pathways

The canonical function of all K^+ channels is K^+ permeation, however all channels have a cytoplasmic domain which may engage in protein-protein interactions [144, 145]. It is plausible that K^+ channels can influence oncological process independent of their capacity to enable K^+ permeation. Kv1.3 has been shown to interact with other proteins involved in cell proliferation and apoptosis including ß1-integrin and p56 [201, 202]. In addition, the human ether-a-go-go related (hERG) channel can form macromolecular complex with VEGF receptor-1 and ß1 integrin which confers a pro-migratory phenotype in human leukaemia cells [203].

1.4.3 Apoptosis

Voltage-gated K^+ channels have emerged as important regulators of programmed cell death in normal and neoplastic cell types and tissues. Apoptotic volume decrease (AVD) is a hallmark event of incipient apoptosis and is largely attributable to K^+ efflux [145, 204]. This decrease in cytoplasmic K+ concentration during AVD appears to promote the hallmark events of apoptosis including mitochondrial depolarisation, cytochrome *c* release from mitochondria and caspase activation [204]. Kv1.3 (encoded by KCNA3) has been extensively studied in the context of apoptosis. This particular channel is expressed at the inner membrane of the mitochondria where it is directly inhibited by the pro-apoptotic protein BAX which leads to cytochrome *c* release and initiation of apoptosis [205]. Pharmacological inhibition of mitochondrial Kv1.3 can induce apoptosis in macrophages and melanoma cell lines [206, 207].

1.4.4 Therapeutic potential

Aberrant expression of potassium channels is a frequent observation in tumours and influences multiple oncological processes [144, 145, 208]. In many cases, overexpression of K^+ channels is associated with accelerated disease progression and a poorer patient outcome. Beyond purely scientific interest this is also relevant for clinical practice. Agents that target K+ channels potentially offer a novel therapeutic approach in the management of cancer. Indeed, there are many approved K^+ channel modulators currently used in clinical practice to treat a spectrum of disorders including diabetes, epilepsy and cardiac arrhythmias. Many of the major K^+ channels involved in the pathophysiology of cancer have existing pharmacological modulators, for example two potent blockers of hERG channel, astemizole and imipramine, are licensed for other indications and have been shown to abolish hERG currents and decrease tumour cell proliferation *in vitro* and *in vivo* [209]. However, a challenge of hERG blockade is undesirable cardiovascular side effects which limit their clinical applicability. Despite the increasing evidence to support the role of K^+ channels in cancer the development of cancer treatment using K^+ channel-targeting compounds is at a very early stage.

1.4.5 The role of K^+ channels in neuroblastoma

There are relatively few studies addressing the role of K^+ channels specifically in neuroblastoma cells. Early studies have demonstrated a link between neuroblastoma cell proliferation and K^+ channels. Tamoxifen and quercetin inhibited the proliferation of mouse neuroblastoma NG108-15 cells and in both instances it was demonstrated that this effect was somewhat mediated by K^+ channel blockade [210, 211].

The ether-a-go-go (EAG) Kv channel subfamily consists of 8 members (encoded by KCNH1-8), the human ether-a-go-go related (hERG) channel is an extensively studied member of this family [171]. Despite having the typical structure of a depolarisation activated Kv channel, hERG currents have unique biophysical features, principally a strongly voltage-dependent inward rectifying current. In cardiac myocytes the hERG channel passes the rapid component of the delayed rectified K^+ current (I_{Kr}) which plays a significant role in cardiac repolarisation [212].

The hERG channel has been widely implicated in the regulation of cell proliferation and apoptosis in cancer and during normal development [213]. In embryonic stages hERG currents are observed in neural crest-derived neurons which are replaced in mature neurons by inward rectifier currents [214]. Induction of differentiation in neuroblastoma derived SH-SY5Y cells, by long term exposure to retinoic acid, induces expression of an inward rectifier K^+ current, without loss of hERG1 expression. This persistence of expression suggests that hERG channels confer a selective advantage to neuroblastoma cells [215].

Arcangeli et al. demonstrated in unsynchronised SH-SY5Y neuroblastoma cells that membrane potential varies considerably from cell-to-cell. These variations correlate with cell-to-cell differences in the activation of inward rectifier currents and were not apparent after synchronising the cells in G1. This provided evidence to suggest inward rectifier currents may contribute to cell cycle progression. However, the identity of the channels that carried the inward current was unknown [216]. Crociani et al. later demonstrated that SH-SY5Y neuroblastoma cells express the *N*-truncated hERG1b variant alongside the full-length hERG1 protein, and heteromeric channels comprised of these subunits was the molecular correlate of the inward rectifier current. The hERG subunit expressed was cell-cycle dependent; hERG1 was up-regulated during the G1 phase and hERG1b was up-regulated during the S phase [217]. Another hERG variant, hERGuso, is expressed both at the mRNA and protein level in SH-SY5Y cells despite being absent from normal cells [218].

Building on earlier studies which demonstrate hERG expression in neuroblastoma cells more recent studies have aimed to characterise the effect of modulation of hERG activity on neuroblastoma cell behaviour in vitro and *in vivo*. Pharmacological inhibition and genetic knockdown of hERG had a significant anti-proliferative effect on SH-SY5Y cells in vitro and suppressed cell cycle progression by arresting cells in G0/G1 phases of the cell cycle. Furthermore, the *in vivo* activity of hERG blockade and knockdown was studied in SH-SY5Y xenografted mice, which found both methods inhibited

tumour growth [219, 220]. These studies have demonstrated a positive role of the hERG channel in neuroblastoma tumour progression which warrants further investigation.

Pardo et al. showed that EAG1, which encodes for Kv10.1, is normally expressed in the adult central nervous system and is expressed by a variety of cancer cell lines including neuroblastoma derived SH-SY5Y cells. Genetic knockdown of EAG1 reduced cell proliferation and implantation of CHO cells overexpressing EAG1 subcutaneously in immunodeficient mice led to enhanced tumour growth compared with controls injected with Kv1.4-expressing CHO cells. Therefore, over-expression of EAG1 appears to be advantageous for tumour growth *in vivo* [195].

Beyond the EAG family of Kv channels there have been surprisingly few studies assessing the role of K^+ channels in neuroblastoma. Curci et al. found that both activation and inhibition of the large-conductance Ca^{2+} activated K^+ channel promoted cell proliferation in SH-SY5Y cells [221]. Leung et al. reported that non-specific blockade of Kv channels in mouse neuroblastoma N2A cells inhibited cAMP stimulated neurite outgrowth, a common measure of neuroblastoma cell differentiation, was correlated with inhibition of Kv currents in these cells. In addition, gene knockdown of Kv1.1, Kv1.4 and Kv2.1 also inhibited cAMP stimulated neuritogenesis which suggests Kv channel-mediated K efflux contributes to neuritogenesis [222]. Tau is a microtubule-assembly factor that promotes tubulin polymerisation and stabilisation of microtubules. There is evidence to suggest tau-mediated alteration of Kv channels influences neuroblastoma cell proliferation. Expression of multiple Kv channels (Kv2.1, Kv4.1, Kv5.1, Kv7.4 Kv9.2 and Kv12.1) was identified in human SK-N-SH and mouse N2A neuroblastoma cell lines. In SK-N-SH and N2A cells overexpression of tau increased cell proliferation and induced downregulation in mRNA levels of Kv channels [223, 224]. The relevance of these results for human neuroblastoma are unclear, however the authors noted that tau overexpression is associated with resistance of some chemotherapeutic agents which bind microtubules e.g. taxanes therefore Kv channel expression may be associated with chemotherapy resistance.

1.5 Aims

Neuroblastoma is a highly biologically heterogeneous cancer and is often resistant to multi-modality treatment [1, 5, 103]. Further understanding of biological aspects of neuroblastoma may contribute to the development of novel therapeutic compounds. Many studies have identified a key role for K^+ channels in tumour initiation and progression and have demonstrated application of K^+ channel modulating compounds affects the cellular functions e.g. proliferation of many types of tumour cells [144, 145]. Given their surface localisation and well characterised pharmacology, K^+ channels may be a promising therapeutic target in neuroblastoma.

This thesis aims to investigate the role of K^+ channels in neuroblastoma and the specific aims were:

- To investigate the expression of K^+ channels in primary neuroblastoma tumours.
- To determine the expression and function of specific K^+ channels in neuroblastoma cell lines.
- To assess the effect of modulating specific K^+ channels on neuroblastoma cell viability, proliferation and differentiation *in vitro*.
- To assess the effect of K^+ channel modulation in xenograft tumours using the chick embryo model, an *in vivo* model of neuroblastoma tumour development and progression.

The methods used to achieve these aims are discussed in chapter two. Study results are collated in chapter three, followed by discussion and conclusion in chapter four.

Chapter 2: Materials and methods

2.1 Materials

2.1.1 Cell lines

Multiple neuroblastoma cell lines have been established from primary and metastatic tumours. Two neuroblastoma cell lines, SK-N-BE(2)-C and SK-N-AS, were cultured. SK-N-BE-(2)-C (will be referred to as BE2C from here on in) is a subclone of SK-N-BE(2), a cell line established from a bone marrow biopsy taken from a 2 year old child with disseminated neuroblastoma after repeated courses of chemotherapy and radiotherapy. BE2C cells possess multiple genetic aberrations: MYCN amplification, chromosome 1p deletion and chromosome 17 translocation. SK-N-AS (will be referred to as SKNAS from here on in) was established from a bone marrow biopsy from a 6 year old child with disseminated neuroblastoma and possesses a single copy of MYCN, chromosome 1p deletion and 11q deletion. These cell lines were chosen as they are characteristic of two types of clinically high risk neuroblastoma tumours: MYCN amplified and chromosome 11q deletion. Both cell lines were cultured in Dulbecco's modified eagle media supplemented with 10% fetal bovine serum (FBS), 1% non-essential amino acids (NEAA) and 1% penicillin streptomycin. Cells labelled with green fluorescent protein (GFP) and without labelling were used.

2.1.2 Antibodies

Primary Antibody	Species	Application-Dilution	Clonality	Source	Catalogue #
Anti-ß-tubulin	Mouse	WB- 1:300	MC	Sigma Aldrich	T4026
Anti-Kv7.2	Rabbit	WB- 1:1000	PC	Chemicon	AB5595
Anti- Kv7.2	Rabbit	WB- 1:400	PC	Alomone	APC-050
Anti-Kv7.2	Rabbit	WB- 1:250 ICC- 1:200, 1:400	PC	Abcam	Ab22897
Anti-Ki67	Rabbit	ICC- 1:100	MC	Abcam	Ab15580
Anti-Ki67	Mouse	IHC- 1:200	MC	Leica Biosystems	KI67-MM1-L-CE
IgG1 Negative control	Mouse	IHC- 1:250	MC	Dako	X0931
NB84	Mouse	ICC- 1:200	MC	Leica-Biosystems	NCL-NB84

Table 2.1: Details of primary antibodies used. WB, Western Blot; IC, immunocytochemistry; IHC, immunohistochemistry; MC, monoclonal; PC, polyclonal

Secondary Antibody	Host species	Application-Dilution	Conjugate	Source	Catalogue #
Anti-mouse IgG	Goat	IF- 1:500	Alexa 488	Thermo Fisher Scientfic	A11029
Anti-mouse IgG	Goat	WB- 1:10 000	HRP	Fitzgerald Industries International	43C-CB1569-FIT
Anti-mouse IgG	Goat	IHC- 1:500	HRP	Dako	DM822
Anti-rabbit IgG	Goat	IF- 1:500	Alexa 594	Thermo Fisher Scientific	A-11037
Anti-rabbit IgG	Goat	IF- 1:500	Alexa 488	Thermo Fisher Scientfic	A11034
Anti-rabbit IgG	Goat	WB- 1:5000	HRP	Sigma-Aldrich	A0545

Table 2.2: Seconday antibodies used. WB, Western Blot; IF, immunofuorescence; IHC, immunohistochemistry; HRP, horseradish peroxidase

2.1.3 Fluorescent probes

Probe	Source	Catalogue #
Bis-(1,3-Dibutylbarbituric Acid) Trimethine Oxonol ($DiBAC_4(3)$)	Thermo Fisher Scientific	B-438
4',6-diamidino-2-phenylindole (DAPI)	Thermo Fisher Scientific	D3571
Hoechst 33342 , trihydrochloride, trihydrate	Thermo Fisher Scientific	H3570

Table 2.3: Fluorescent probes used

2.1.4 Therapeutic compounds

XE991 (Cat no. 2000, Tocris Biosciences), ML213 (Cat no. 4519, Tocris Biosciences) and Palbociclib (PZ0199, Sigma-Aldrich, UK.) were used in this study.

2.2 Bioinformatics

R2 Genomic Analysis and Visualisation Platform is a publically available database (http://r2.amc.nl) and was utilised to assess gene expression in primary neuroblastoma tumours. R2 is a bioinformatic platform which contains datasets from gene expression microarrays for many pathological conditions and normal tissues. Each dataset utilised microarray analysis to evaluate gene expression. Briefly, total RNA was extracted from frozen neuroblastoma tumours which contained >95% neuroblastoma cells and labelled cRNA was hybridized to a microarray e.g. Affymetrix Human genome U133 Plus 2.0. The mRNA levels were determined using a normalisation algorithm e.g. MAS5.0.

R2 holds expression profiles for ≥2000 primary neuroblastoma tumours across multiple datasets. In addition to gene expression, datasets also document clinical and genetic details of tumour sample, e.g. age of patient, clinical stage, MYCN status. Furthermore, multiple modes of analysis were possible in R2, including gene expression in a single and multiple datasets. **Figure 2.1** illustrates the method for selecting a dataset and inputting a gene of interest which was common to each mode of analysis.

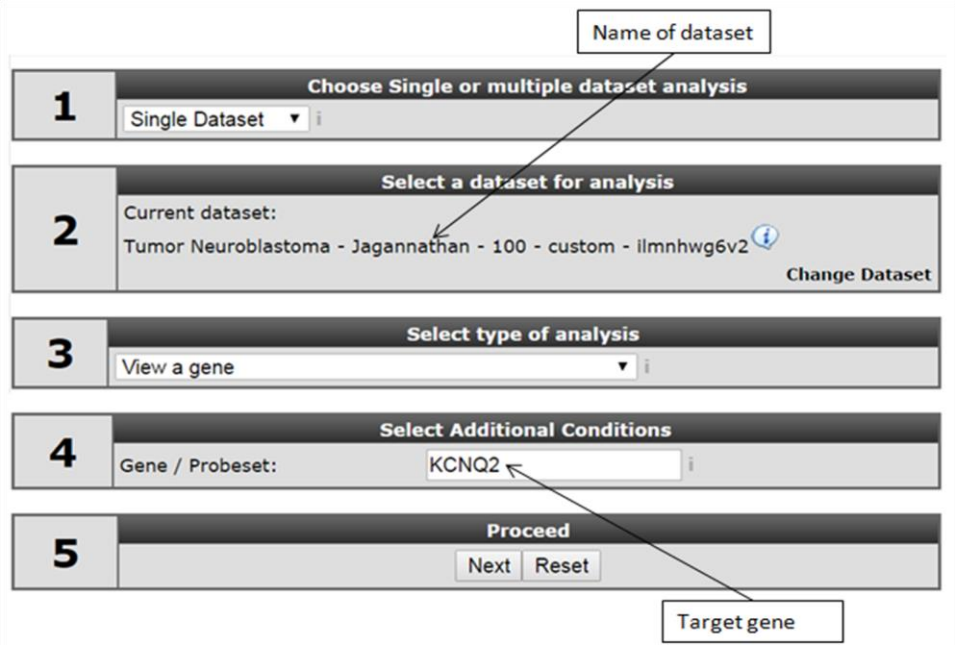

Figure 2.1: Method of inputting gene for evaluation in a single dataset in the R2 Genomic Analysis and Visualisation Platform.

2.3 Cell Culture

2.3.1 Routine subculturing

All cell culture work was carried out in a laminar flow cabinet. Cells were cultured in 75 cm^2 flasks (Corning, UK) containing 12 ml of culture media and were incubated in a humidified environment at 37^oC and 5% CO_2. Cultured cells were passaged once 80-90% confluency was reached. During passaging existing media was removed and cells were washed with 10 ml of Hanks Balanced Salt Solution without Calcium and Magnesium (HBSS) (H9394, Sigma-Aldrich, UK). 0.05% trypsin/EGTA was then added to the flask and incubated for 4-5 minutes at 37^oC and 5% CO_2. Following trypsinisation 10 ml of culture media containing 10% FBS was added to the detached cells to inactivate trypsin and create a cell suspension which was transferred to a 30 ml sterile universal bottle (Starlab, UK). Cells were disaggregated by pipetting vertically using a 1ml pipette, seeded at a concentration of 1-3 x 10^6 cells per flask and then incubated at 37^oC in a humidified environment containing 5% CO_2. Cell lines were tested and found free of mycoplasma contamination.

2.3.2 Culturing cells with therapeutic compounds

For all experiments in which the effect of therapeutic compounds was investigated in vitro the following method was used. Cells were seeded at an appropriate density and incubated at 37^oC/5% CO_2. Drug solutions were prepared by diluting stock solution in cell culture media. After 24 hours of incubation, media was discarded and replaced with the same volume of media solution containing the compound. Control samples were cultured with cell culture media supplemented with DMSO at the same concentration.

2.3.3 Recovery of cryopreserved cells

Frozen cells were stored in 2 ml cryogenic vials in liquid nitrogen. When required, vials of frozen cells were removed from liquid nitrogen and thawed on ice. Cells were resuspended by adding 20 ml of media drop wise and centrifuged at 1 000 rpm for 10 minutes. After centrifugation the supernatant was discarded and the cell pellet resuspended in 7 ml culture media containing 10% FBS. Cells were seeded in 25 cm^2 flasks and transferred into 75 cm^2 flasks once 80-90% confluent.

2.4 Quantitative PCR (qPCR)

The Polymerase Chain Reaction (PCR) allows amplification of small amounts of DNA. SYBR green is a fluorescent dye which specifically binds to double-stranded DNA and fluoresces only when bound to dsDNA. This property can be used to determine gene expression. At the end of each round of amplification the quantity of dsDNA increases and detection of fluorescent intensity increases. During the exponential phase of the reaction, fluorescence is directly proportional to amplification, thus allowing measurement of copy number. The cycle at which fluorescence exceeds the pre-determined threshold value is termed the Cycle of quantification (Cq) value.

2.4.1 RNA extraction

RNA extraction was completed using the RNeasy Mini Kit (Cat no. 74104, QIAGEN). Measures to prevent RNA degradation included working on a dedicated work bench, decontamination of all surfaces and pipettes using RNAzap cleaning agent (R2020, Sigma-Aldrich) and keeping samples on ice throughout.

Cells were cultured and harvested as described for subculturing **(Section 2.3.1)**. Cell suspension was centrifuged at 1 000 rpm for 10 minutes, the supernatant was discarded and the pellet gently disrupted by tapping the tube. RNA was extracted using spin-column based isolation and utilised 3 buffers: RLT, RW1 and RPE. To inactivate RNases, 1% ß-Mercaptoethanol was added to buffer RLT. 350µl of buffer RLT was added to lyse cells. A 19G needle and 1 ml syringe was used to draw the solution up and down in order to disrupt and homogenise the cells. An equal volume of 70% ethanol was added and the resulting solution transferred to an RNeasy Spin Column and centrifuged at 800 x g for 15 seconds. The flow through was discarded and 700 µl of buffer RW1 was added and centrifuged at 800 x g for 15 seconds. 500 µl of buffer RPE was added and centrifuged 800 x g for 15 seconds. The RNeasy Spin Column was transferred to a fresh collection tube and 40µl of RNAase free water was applied to the column membrane and centrifuged at 8000 x g for 60 seconds. RNA concentration (ng/µl) and quality (A260/280) were recorded using a NanoDrop spectrophotometer (Thermo Scientific, USA) and RNA was stored in aliquots at -80oC.

2.4.2 cDNA synthesis

The GoScript Reverse Transcription System (A5000, Promega, UK) was used to synthesise cDNA from RNA. The volume of RNA used was dependent on the concentration. Synthesis of cDNA involved two steps: annealing and reverse transcription. RNA samples were mixed with oligodT primers (0.5 µg/reaction) and heated to 72^{o}C to allow annealing of primers. The reagents and their respective volumes used in reverse transcription are detailed in **Table 2.4**. For the no reverse transcriptase controls nuclease-free water was added instead of reverse transcriptase. Reaction mixes were

placed in a thermocycler with the following settings: 25°C 5 minutes, 42°C for 60 minutes and 70°C for 15 minutes. The resulting cDNA was stored in aliquots at -20oC.

cDNA reaction mix reagents	Volume per reaction
GoScript Reaction Buffer	4 µl
$MgCl_2$	2 µl
PCR Nucleotide Mix (NdTP)	1 µl
Reverse Transcriptase	1 µl
RNAsin Ribonuclease Inhibitor	0.5 µl
Nuclease Free Water	6.5 µl
RNA + OligodT primers	5 µl
Final reaction mix	**20 µl**

Table 2.4: Reagents and corresponding volumes used during reverse transcription according to the manufacturer's protocol. $MgCl_2$, Magnesium Chloride.

2.4.3 Reference gene selection

Reference genes (RG) were selected to allow normalised relative quantification of genes of interest to be calculated. Two genes, ubiquitin C (UBC) and hypoxanthine phosphoribosyltransferase 1 (HPRT1) known to be stably expressed in neuroblastoma cell lines were selected [225].

2.4.4 Target gene selection

2.4.4.1 K+ channel genes

Based on the results of bioinformatic database evaluation 5 K^+ channel genes were selected: KCNQ2, KCNMA1, KCNH2, KCNB1 and KCNG1.

2.4.4.2 Differentiation genes

Kruppel-Like Factor (KLF4), Stathmin-like 4 (STMN4) Roundabout, axon guidance receptor, homologue 2 (ROBO2) were selected to quantitatively assess the effect on differentiation of therapeutic compounds [226].

2.4.5. Primers

All primer sequences were obtained from published papers and origene.com. NCBI Primer Blast was used to assess parameters including primer and product length, GC content and annealing temperature. Primer sequences were located in the FASTA mRNA sequence to ensure only primers spanning exon-exon boundaries were selected. Primer sequences were ordered from Eurofins Genomics (Germany) and Sigma-Aldrich (UK). Primers were in the form of lyophilised powder and were resuspended using nuclease-free water (ThermoFisher Scientific, UK) in 10 µM aliquots and stored at -20^{o}C. **Table 2.5** below details all primer pairs used.

Gene	Forward sequence (5'-3')	Reverse Sequence
UBC	ATTTGGGTCGCGGTTCTTG	TGCCTTGACATTCTCGATGGT
HPRT1	TGACACTGGCAAAACAATGCA	GGTCCTTTTCACCAGCAAGCT
KCNQ2	TCATCGGTGTCTCCTTCTTCGC	GAGAGGTTGGTGGCGTAGAATC
KCNMA1	CTCTCTCGGTTGGCAGACTTGT	TATCTCTCCAGTGCCTTCGTGG
KCNH2	GCTTGCTCAACTCCACCTC	TTTGGGGAATCTTGC
KCNG1	TCAACCTCTCCGTCAGCACCTT	TGAATGAGCCGCAGGAGGAACT
KCNB1	GAGGAGTTCGATAACACGTGCTG	GCAATGGTGGAGAGGACGATGA
KLF4	CGCCGCTCCATTACCAAGAGC	CGGTCGCATTTTTGGCACTG
STMN4	CCTAGCAGAGAAACGGGAACA	GGCGTGCTTGTCCTTCTCTT
ROBO2	GATGTGGTGAAGCAACCAGC	TGGCAGCACATCTCCACG

Table 2.5: Forward and reverse primer sequences for all primer pairs used in qPCR experiments.

2.4.5.1 Primer Efficiency

Primer efficiency was determined for KCNQ2, KNCMA1, KCNH2, KCNG1 and KCNB1. For each set of primers a standard curve was constructed to calculate the gene-specific PCR efficiencies from a 2-fold dilution series of cDNA template for each primer pair. The dilution series was made from cDNA samples obtained from BE2C cells and diluted in by a factor of 2 over 5 dilution factors. Real-time PCR was performed in triplicates as described below. Primer efficiency for UBC, HPRT1, STMN4, KLF4 and ROBO2 had been previously determined (Grace Mather, University of Liverpool).

2.4.6 Quantitative PCR (qPCR)

The first step of qPCR was preparation of reaction supermixes. **Table 2.6** details the reaction mix containing cDNA template.

Reagent (Concentration)	cDNA template positive
iTaq Universal SYBR Green Supermix (1x)	7.5 µl
Forward Primer (10µM)	0.75 µl
Reverse Primer (10µM)	0.75 µl
Distilled Water	4 µl
cDNA +RT	2 µl
Total volume/well	**15 µl**

Table 2.6: Reagents of the reaction supermix for all qPCR experiments

2.4.6.1 Controls

For all experiments a no template control (NTC) was included to monitor genomic DNA contamination and primer-dimer formation. A no reverse transcriptase control (NRT) was also included whenever a new preparation of RNA was used, to monitor genomic DNA contamination.

2.4.6.2 Plate layout

Reaction supermixes were prepared in triplicates and 15µl of reaction supermix was carefully pipetted into a single well of a 96-well hard-shell PCR plate (HSS9641, BioRad, UK). The plate was covered by a clear seal (MSB1001, BioRad, UK) and centrifuged briefly in a microplate centrifuge. An example plate design can be seen below **(Figure 2.2)**.

1	2	3	4	5	6
RG NTC	RG NRT	RG cDNA	TG NTC	TG NRT	TG cDNA
RG NTC	RG NRT	RG cDNA	TG NTC	TG NRT	TG cDNA
RG NTC	RG NRT	RG cDNA	TG NTC	TG NRT	TG cDNA

Figure 2.2: Example plate layout for one reference and one target gene. RG, reference gene; TG, target gene; NTC, no template control; NRT, no reverse transcriptase control

The plate was transferred to a CFX connect thermocycler (BioRad, UK), which was used for all experiments. The thermocycler employed precise temperature control and rapid temperature changes for optimal cDNA amplification. **Figure 2.3** outlines the cycling control for PCR amplification.

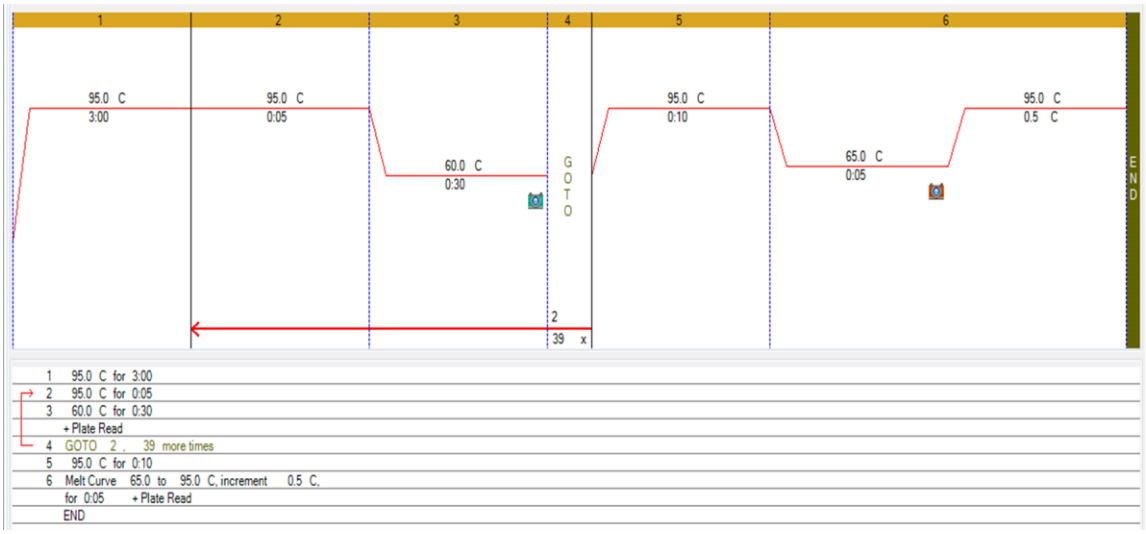

Figure 2.3: Cycling protocol for quantitative PCR amplification. The polymerase heat activation step of 95°C for 3 minutes was followed by 40 cycles of 95°C for 5 seconds (denaturation) and 60°C for 30 seconds (annealing and extension). After 40 cycles, the temperature increased 0.5°C every 5 seconds from 65°C to 95°C to generate melt curves.

2.4.7 Statistical analysis of qPCR data

Data was viewed using Bio-Rad CFX Manager 3.1 software. Amplification plots and melt curves were inspected to detect obvious anomalies. Fold change in target gene expression in untreated and treated cells was calculated relative to a control sample. Results were normalised to the expression of reference genes (HPRT1 and UBC), compensating for differences in starting quantity of cDNA and reaction kinetics.

The mean Cq value for 3 technical replicates from a single biological replicate was calculated, followed by the mean Cq value for 3 independent biological replicates. A commonly used method of calculating relative gene expression using qPCR data is the $2^{-\Delta\Delta Cq}$ method; however this is based on the assumption that primer efficiency is 100% i.e. every PCR cycle the copy number doubles exactly. However, primer efficiency is often not 100%, therefore an efficiency based method of analysis was employed and equations used are outlined below.

$$RQ = \frac{1}{E^{Cq}}$$

$$NRQ = \frac{RQ(Target\ gene)}{RQ(Reference\ gene)}$$

$$Relative\ expression\ ratio = \frac{\overline{\overline{NRQ}}(Treatment)}{\overline{\overline{NRQ}}(Control)}$$

E, primer efficiency; RQ, relative quantification; NRQ, normalised relative quantification

To conduct statistical analysis NRQ data requires logarithmic transformation as qPCR data are non-linear. This brings NRQ values back to the Cq scale and allows application of standard parametric tests [227].

2.5 Western blotting

2.5.1 Cell lysate preparation

BE2C and SKNAS cells were grown as a monolayer in 100 mm Petri dishes (Sarstedt, UK). To prepare cell lysate, the Petri dish was placed on ice and culture media was removed and cells washed once with ice cold Dulbecco's Phosphate Buffered Saline (DPBS) without Ca^{2+} and Mg^{2+} (14190144, Thermo Fisher Scientific, UK). Lysis buffer (100 mM Tris-Base, 25 mM NaCl, 300 µM EDTA, 300 µM EGTA, 0.05% Triton-X100, pH 7.6) containing 1% protease inhibitor cocktail (P8430, Sigma, UK) was added to the Petri dish for 5 minutes and cells were dislodged by scraping. The resulting lysate was collected and centrifuged at 13 000 rpm for 10 minutes at 4^{o}C. The supernatant was collected and pellet was discarded. The supernatant was mixed with an equal volume of 2x sample buffer (S3401, Sigma Aldrich, UK), and heated for 10 minutes at 98^{o}C. The protein extract was stored at -20^{o}C.

2.5.2 Determination of protein concentration

The protein concentration in each lysate was determined by the Pierce Bicinchoninic Acid (BCA) Protein Assay Kit. BCA working reagent (WR) was prepared by combining BCA reagents A (sodium, carbonate, sodium bicarbonate, bicinchoninc acid and sodium tartrate in sodium hydroxide) and B (4% cupric sulphate) in a 50:1 ratio. 5 concentrations (5-250 µg/mL) of Bovine Serum Albumin (BSA) were prepared by serial dilution in lysis buffer. Sample lysates were diluted 20-fold in lysis buffer. 25 µl of each standard and unknown sample was added to separate wells in a 96 well microplate. 25 µl of lysis buffer was also added to wells to generate blank readings. 200 µl of WR was then added to each well and mixed thoroughly on a plate shaker for 30 seconds. The plate was then incubated at 37^{o}C for 30 minutes. After cooling to room temperature absorbance was read at 562 nm using a Flexstation Microplate Reader (Molecular Devices) and accompanying software, SoftMax Pro (Molecular Devices). Absorbance values were corrected for absorbance in blank wells. Protein concentration in the samples was determined by reference to a standard curve consisting of known concentrations of BSA.

2.5.3 SDS-PAGE Electrophoresis

The short plate and spacer plate were cleaned with 70% ethanol and placed into the casting frame. Resolving gel (375 mM Tris Base pH 8.8, 6% glycerol, 0.1% SDS, 10% Acrylamide (BioRad 161-0158, Bio-Rad Laboratories, USA), 0.05% Ammonium Persulphate (APS) (A-9164, Sigma Aldrich, UK), 0.1%

tetramethylethylenediamine (TEMED) (T-9821, Sigma Aldrich, UK) was added between the plates and isopropanol was overlaid to prevent desiccation of the gel. Isopropanol was removed and stacking gel (50 mM Tris Base pH 6.8, 0.1% SDS, 4% Acrylamide, 0.08% APS, 0.17% TEMED) was added above the resolving gel; a well-forming comb was inserted into the stacking gel and left to polymerise. Next, the plates were clamped and combs were removed. 7 µl of rainbow molecular weight marker (RPN800E, G.E. Healthcare, UK) was added to the first well and 25 µl of lysate were loaded and the clamping frame was placed into an electrophoresis cell (Mini-Protean Tetra System, Bio-Rad Laboratories, USA) filled with running buffer (25 mM Tris Base, 192 mM Glycine, 0.1% SDS). The gel was run at 160 V for 1 hour (PowerPac Basic, Bio-Rad Laboratories, USA).

2.5.4 Western blotting

Separated proteins were transferred from the polyacrylamide gel onto a nitrocellulose membrane. A 'sandwich' was assembled, in a gel holder cassette, consisting of gauze, Whatman #3 filter paper (G.E. Healthcare, UK), the polyacrylamide gel and nitrocellulose membrane. To prevent drying of the gel, each component was soaked in transfer buffer (25 mM Tris Base, 192 mM Glycine, 20% Methanol). An ice pack was placed in the cell and the cell placed in ice tray to keep cool during transfer.

The cassette was then placed into the electrophoresis cell and filled with transfer buffer. 100 V was applied for 1 hour for electrophoretic transfer. Following transfer the nitrocellulose membrane was washed twice in Tris-buffered saline with Tween (TBST, 20 mM Tris Base, 137 mM NaCl, 0.1% TWEEN 20, pH 7.6). The membrane was stained with Ponceau S Solution (P7170, Sigma Aldrich, UK) to confirm successful transfer. The membrane was then washed in TBST to remove staining and then blocked by incubation with 10% non-fat milk (Marvel, UK) in TBST for 1 hour.

Next the primary antibody was diluted to required dilution using 10% non-fat milk in TBST and the membrane was incubated with 1 ml of the primary antibody overnight at 4^{o}C. The following day the membrane was washed in TBST 3 times for 10 minutes with agitation. The secondary antibody, conjugated with horseradish peroxidase, was diluted in 10% non-fat milk in TBST and incubated with the membrane for 90 minutes with agitation at room temperature. The membrane was again washed in TBST 3 times for 10 minutes. All membrane incubations were carried out at room temperature on a rocking platform (Rocker 25, Labnet International Inc., USA).

2.5.5 Developing

Presence of HRP-conjugated secondary antibodies was visualised by the enhanced chemiluminescence (ECL) method. The membrane was covered in ECL reagents (G.E. Healthcare, UK)

and light was captured using auto-radiographic film (Amersham Hyperfilm, G.E. Healthcare, UK) in a hyper-cassette. Exposure time was dependent on the strength of the signal and varied between 1-10 minutes. The film was processed using Kodak GBX fixer and developer solutions. Protein bands were sized against a pre-stained rainbow ladder.

2.5.6 Stripping and re-blotting

Stripping of the antibodies from the blot was performed to allow re-blotting of the membrane with a house-keeping protein to check for equal loading among wells. Nitrocellulose membrane were rehydrated with TBST and then washed in stripping solution (100 mM ß-Mercaptoethanol, 2% SDS, 62.5 mM Tris base, pH 6.7) 2 times for 10 minutes at room temperature. Membranes were then rinsed in TBST and blocked using 10% non-fat milk in TBST for 1 hour. The rest of the procedure was as previously described for western blotting.

2.5.7 Densitometric analysis

ImageJ software was utilised to semi-quantify protein intensity. Films were scanned and the image converted to greyscale. The rectangular selection tool was used to a draw around each band of interest and a profile plot was created for each band. A straight line was drawn to enclose the area of the peak to eliminate background signal. Using the wand tracing tool the area of each peak was determined. The size and intensity of the band correlates with area of the peak in a profile plot **(Figure 2.4)**.

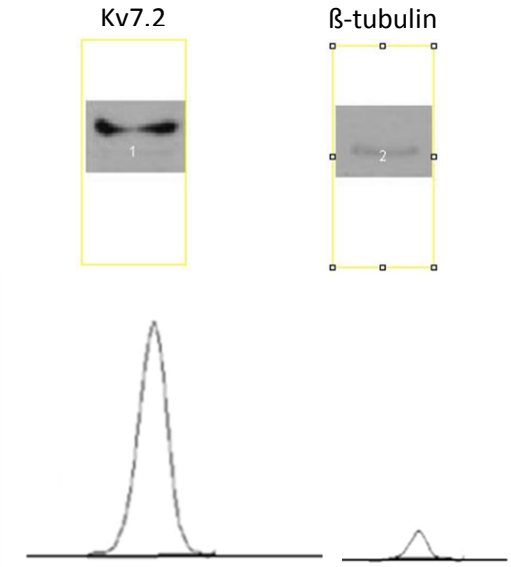

Figure 2.4: Example of conducting densitometric analysis of bands. Rectangular boxes were drawn around bands. Profile plots represent the density of the contents of the rectangle. The taller and broader peak for Kv7.2 reflects the greater intensity of the band.

2.6 Immunocytochemistry

Immunocytochemistry is a complementary technique to western blotting and is used to obtain information of the cellular location of the protein of interest.

2.6.1 Cell seeding

BE2C and SKNAS cells without GFP labelling were harvested and counted as previously described. 1 x 10^4 cells were seeded on size 1 13 mm cover slips and incubated at 37^{o}C for 18-24 hours to allow cell adhesion.

2.6.2 Fixing, quenching and permeabilising of cells

Culture medium was removed, cells were washed in DPBS, fixed with 2% PFA in PBS x1 pH 7.4 for 10 minutes and quenched with 100 mM glycine pH 7.4 for 10 minutes. Cover slips were incubated in permeabilising solution (0.27 mM KCl, 0.15 mM KH_2PO_4, 13.7 mM NaCl, 0.8mM Na_2HPO_4, 0.1% Triton-X100, pH 7.4) and then washed in PBS (2.7 mM KCl, 1.5 mM KH_2PO_4, 137 mM NaCl, 8 mM Na_2HPO_4, pH 7.2) 3 times for 5 minutes. Cover slips were then incubated in blocking solution (150 mM NaCl, 15 mM Sodium Citrate (SSC), 2% goat serum, 1% bovine serum albumin, 0.05% Triton-X100, pH 7.2) for 30 minutes at room temperature.

2.6.3 Antibody labelling and counterstaining

The primary antibody was diluted in blocking solution and 200 µl of diluted primary antibody was applied to each cover slip and incubated overnight at 4^{o}C. The following day, the primary antibody was removed and cover slips were washed in antibody washing solution (150 mM NaCl, 15 mM SSC, 0.05% Triton-X100) for 10 minutes 3 times. The secondary antibody and DAPI were diluted in blocking solution, applied to each cover slip and incubated at room temperature, protected from light for 1 hour. Cover slips were washed 3 times for 10 minutes in washing solution. 2% PFA was applied to each cover slip to post-fix for 5 minutes and then washed in washing solution 3 times to remove the fixative and washed twice in distilled H2O to remove salt. Cover slips were allowed to air dry, protected from light and mounted onto slide glass using fluorescent mounting medium (Dako, UK) and stored at 4^{o}C.

2.6.4 Confocal microscopy

A Leica confocal microscope was used to view slides using a 63x oil immersion objective. Data capture and extraction were carried out using Leica Confocal Software. Alexa Fluor 488 was excited at 488 nm using an argon-ion laser and emission light was detected at 500-550 nm.

2.7 DiBAC$_4$(3) fluorescence experiments

2.7.1 Cell seeding

BE2C and SKNAS cells were cultured, harvested and counted as previously described. Cells were seeded in wells in a 96 well microplate and incubated in a humidified environment at 37^{o}C and 5% CO2 for 24 hours for all experiments. The number of cells seeded and number of replicates varied dependent on the cell line and experiment.

2.7.2 Solutions

Experiments were conducted in Physiological Saline Solution (PSS) and High K^+ Solution. PSS contained: 137 mM NaCl, 5.6 mM KCl, 1 mM $MgCl_2$, 2 mM $CaCl_2$, 0.42 mM Na_2HPO_4 (anhydrous), 0.44 mM Na_2HPO_4 (hydrated), 10 mM 4-(2-hydroxyethyl)-1-piperazineethanesulfonic acid (HEPES), 4.17 mM NaHCO3, pH 7.4. High K^+ solution contained: 145 mM KCl, 1 mM $MgCl_2$, 0.42 mM Na_2HPO_4 (anhydrous), 0.44 mM Na_2HPO_4 (hydrated), 10 mM HEPES, 4.17 mM NaHCO3, pH 7.4.

2.7.3 DiBAC$_4$(3) experiments

When conducting experiments using DiBAC$_4$(3) the method for cell seeding, working solution preparation, loading with DiBAC$_4$(3) PSS and fluorescence detection was identical for all experiments and was as follows. On the day of experiments 0.18% glucose was added to PSS, then 2 mM DiBAC$_4$(3) stock solution was diluted in this solution to obtain a 1 µM working solution. Culture medium was removed from each well and replaced with 1 µM DiBAC$_4$(3) PSS and incubated at 37^{o}C/5% CO2 for 15 minutes. Following this, plates were transferred to a FlexStation Microplate Reader (Molecular Devices) where fluorescence was measured at 520 nm in response to an excitation wavelength of 485nm.

Using the aforementioned design, three different experiments were conducted: (1) characterising DiBAC4(3) fluorescence in BE2C and SKNAS cells, (2) response to high K^+ solution and (3) response to Kv7 channel modulation.

2.7.3.1 Characterising DiBAC$_4$(3) fluorescence in BE2C and SKNAS cells

Cells were seeded in a 96 well microplate at four densities: 1 x 10^5, 5 x 10^4, 2 x 10^4 and 1 x 10^4 cells per well. On the day of the experiment, culture medium was removed and cells were pre-incubated in 100 µL of 1 µM DiBAC$_4$(3) PSS for 15 minutes at 37^{o}C/5% CO_2. A reading of fluorescence was taken, then the microplate was removed from the plate reader and 100 µL DiBAC$_4$(3) PSS was added to all wells containing cells. DiBAC$_4$(3) PSS was also added to empty wells to determine background fluorescence. After incubation for 10 minutes at room temperature, a repeat reading of fluorescence was taken.

2.7.3.2 Response to high K^+ solution in BE2C cells

2 mM DiBAC4(3) stock solution was diluted in high K^+ solution to obtain a 1 µM DiBAC4(3) solution with a high K^+ concentration (145 mM). BE2C cells were incubated with 1 µM $DiBAC_4(3)$ PSS for 15 minutes and a continuous, baseline reading of fluorescence was measured for 120 seconds. At this time point DiBAC4(3) high K^+ solution was added to each well and a continuous reading of fluorescence was taken for a further 600 seconds. The ratio of fluorescent intensity (F/F0) was determined by dividing fluorescence at a given time (F) by fluorescence prior to adding $DiBAC_4(3)$ high K^+ solution (F0).

2.7.3.3 Response to Kv7 modulation

Kv7 channel modulating compounds (XE991 and ML213) were dissolved in 1 µM $DiBAC_4(3)$ PSS to obtain a 10 µM drug solution. XE991 and ML213 stock solutions were both prepared using DMSO, therefore a control solution was prepared by adding DMSO to $DiBAC_4(3)$ PSS. On the day of the experiment cells were incubated with $DiBAC_4(3)$ PSS at 37°C/5% CO_2 for 15 minutes. Following this, fluorescence was measured, the microplate was removed from the plate reader and 100 µl of DiBAC4(3) plus Kv7 drug solution or DMSO was added to each well and incubated at room temperature for 10 minutes. A second fluorescence reading was then taken. The change in relative fluorescence units (RFU) before and after addition of DMSO/compounds was determined.

2.8 Functional assays

2.8.1 Cell viability assay

2.8.1.1 Cell seeding

BE2C and SKNAS cells were harvested and counted as described previously **(Section 2.3.1)**. 1 x 10^4 cells were seeded per well in a 96 well microplate and incubated overnight at 37^{o}C to allow cell adhesion. 3 'blank' wells were prepared containing only cell culture medium. Drug solutions were prepared by diluting stock solution in culture medium. 18-24 hours after seeding cells the existing media was removed and replaced with media containing drug or DMSO. Following an incubation period of 72 hours, 10 µl of MTT solution (5mg/ml) was added to each well, for a final concentration of 0.45 mg/ml. The microplate was wrapped in foil to prevent light exposure and incubated for 4 hours at 37^{o}C. 100 µl 5% SDS 0.01 M HCl was added to each well and incubated at 37^{o}C overnight.

2.8.1.2 Absorbance detection

Spectrophotometric absorbance was detected at 570 nm using FLUOstar Omega microplate reader (Molecular Devices, UK). Absorbance values were adjusted by subtracting the 'blank' reading (MTT and media only). Absorbance values from treated wells were compared with control wells (i.e. cells treated with DMSO) to determine the effect of the treatment on the number of viable cells. Each experiment was performed in triplicates and repeated ≥3 times.

2.8.2 Cell proliferation analysis

2.8.2.1 Cell seeding and incubation with therapeutic compounds

Cells were seeded on size 1 13 mm glass cover slips as described previously **(Section 2.6)**. After 24 hours culture media was removed and replaced with drug solution or media containing DMSO.

2.8.2.2 Fixing, quenching and permeabilisation of cells

After a 72 hour incubation period cover slips were removed from the 24 well plate and placed into a staining tray. Cells were fixed with 4% PFA for 10 minutes and quenched with 200 mM Glycine pH 7.4 for 10 minutes. For blocking and permeabilisation cover slips were incubated in blocking solution (1% BSA, 0.5% Triton-X in 0.12 M phosphate pH 7.4) for 1 hour at room temperature.

2.8.2.3 Antibody labelling and counterstaining

Mouse anti-Ki67 primary antibody was diluted in blocking solution, applied to each cover slip and incubated overnight at 4^{o}C. A control cover slip was prepared by omitting the primary antibody. Following overnight incubation the primary antibody was removed and covers slips were washed 3 times in HBSS. The secondary antibody and DAPI were diluted in blocking solution and applied to

each cover slip. After 1 hour incubation at room temperature the cover slip was washed twice in HBBS and once in distilled H2O. Cover slips were allowed to air dry, protected from light and mounted onto slide glass using fluorescence mounting medium (Dako, UK). Slides were stored at 4°C and protected from light.

2.8.2.4 Quantifying Ki67 proliferative index

Quantification of cell proliferation was carried out by manual counting. Slides were observed under a Leica fluorescent microscope using a x40 oil immersion objective. The number of Ki67 positive cells (red) in each field were counted and expressed as percentage of the total number of DAPI stained cells (blue) in the same field. For each cover slip a minimum of four fields were examined and 100-200 cells were counted in each field. To eliminate bias, counting was performed blind; this was achieved by covering the identity of the cover slip and assigning cardinal numbers to each slide and checking the identity of the cover slip only after counting. Each experiment was conducted independently 3 times.

2.8.3 Fluorescence activated cell sorting (FACS)

2.8.3.1 Cell preparation

GFP-labelled BE2C cells were seeded in 25 cm^2 flasks and incubated for 18-24 hours to allow cell adhesion. Drugs were dissolved in culture media and existing media was replaced with drug solution after 24 hours.

2.8.3.2 Sample preparation for FACS

Cells were harvested and counted after 24 hours, as previously described. For each FACS sample to be analysed 1 x 10^6 cells in culture media were placed in polystyrene FACS tubes (Falcon, UK). Tubes were centrifuged at 1750 x g for 5 minutes in a tabletop centrifuge (Hermle Z400-K, Labnet International) and the supernatant was removed. The pellet was resuspended in 4% PFA for 5 minutes at room temperature, followed by permeabilisation in 4% PFA, 0.05% Triton X100 for 5 minutes at room temperature. 900 µl of PBS was added to form a 1ml cell suspension and centrifuged as above. The pellet was resuspended in 500 µl blocking solution (0.5% BSA, 0.1% Triton X100 0.12 M Phosphate), incubated for 30 minutes at room temperature and centrifuged as before. The pellet was incubated with 1 ml of 2.5 µg/ml of Hoechst 33342 in blocking solution (H3570, ThermoFisher Scientific, UK) for 30 minutes at room temperature.

2.8.3.3 Analysis

Samples were analysed on the FACS Canto II Flow Cytometer (BD Biosciences, USA) and for each

sample a population of 10 000 cells were measured. All data analysis was completed using Cytobank online software (www.cytobank.org) and results visualised as a scatter plot or histogram.

2.9 The chick embryo model

2.9.1 Growing tumours on the chorioallantoic membrane

2.9.1.1 Incubation of eggs

A batch of 24 fertilised white leghorn chicken eggs (Tom Barron Hatcheries, Preston UK) were incubated (Multihatch Mark II, Brinsea, UK) at 38°C and 40% relative humidity. The first day of egg incubation was embryonic day 0 (E0).

2.9.1.2 Fenestration

At E3 each egg was removed from the incubator and cleaned with 70% ethanol. To detach the embryo and surrounding vessels from the inner surface of the shell, an egg piercer was used to punch a small hole in the base of egg and a 19G gauge needle attached to a 5ml syringe was used to remove ~4ml of albumen. The puncture site was sealed using adhesive tape. To access the embryo and overlying membranes a rectangular window (20 mm x 10 mm) was created in the shell using a Power Craft PKW-160N Combitool, the window was sealed using adhesive tape and the eggs were re-incubated.

2.9.1.3 Topical implantation of cells

At E7 windowed eggs were removed from the incubator and assessed for survival. Cultured GFP-labelled BE2C cells were harvested and counted as described previously. Harvested cells were centrifuged at 1000 rpm for 10 minutes and the pellet was placed in a separate Eppendorf tube. Eggs were removed individually from the incubator and the surface of the chorioallantoic membrane (CAM) was lightly traumatised using a small piece of sterilised lens tissue. 5 µl of 0.05% trypsin was applied to the surface of the CAM and 2 x 10^6 cells were implanted.

2.9.1.4 Drug delivery

At E11 survival was assessed and eggs were viewed under fluorescence using a Leica M165 FC fully apochromatic corrected stereo microscope to assess for tumour formation. Surviving embryos with tumour formation were selected for drug injection. The volume of each egg is ~45 ml and had to be accounted for when delivering drug solutions. XE991 was dissolved in PBS at 100 mM, to obtain a treatment concentration of 40 µM 200 µL of drug solution was injected into the allantois using a 19G needle and 1 ml syringe.

2.9.1.5 Dissection

At E14 eggs were removed from the incubator individually and unviable embryos were removed. The shell surrounding the window was removed to maximise view. Brightfield and fluorescent images were captured using a Leica DFC425 C camera connected to the microscope. Tumours grown on the

CAM were removed using size 5 dissection tweezers and dissection scissors. Dissected tumours were washed in HBSS before being placed into 4% PFA for 1 hour. To prepare for paraffin embedding the tumours were dehydrated through a series of ethanol dilutions; tumours were placed in 70% ethanol for 1 hour and then stored at 4^{O}C in 100% ethanol.

E0

E3

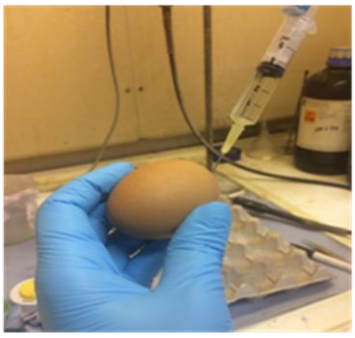

E7

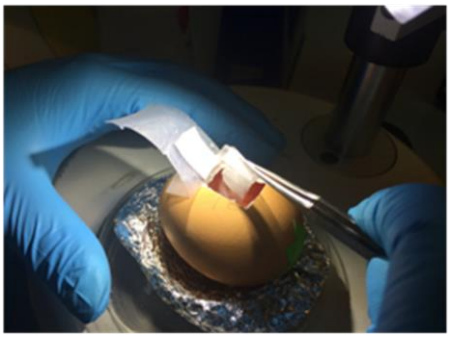

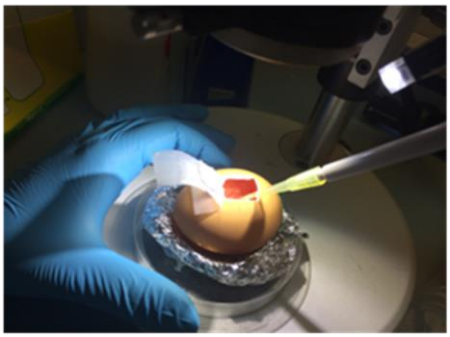

E11

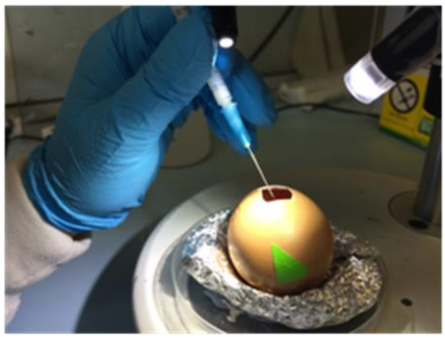

Figure 2.5: Visual display of steps in chick embryo experiment. E0: fertilised white leghorn eggs were incubated in Multihatch Mark II. E3: albumen removal, windowing with power tool, resealing window the adhesive tape. E7: light traumatisation of CAM surface with sterile lens tissue improves tumour formation followed by topical implantation of BE2C cells onto surface of CAM. E11: Injection of drug solution into allantois.

2.9.2 Tumour processing

Embedding tumours in paraffin allows long term preservation and storage. Tumours were removed from 100% ethanol and placed in the following sequence of solutions; isopropanol twice with agitation for 15 minutes; 50:50 isopropanol: paraffin at 60^{o}C for 1 hour with agitation every 15 minutes; 100% liquid paraffin at 60^{o}C for 1 hour; fresh 100% liquid paraffin incubated overnight at 60^{o}C. The following day tumours were placed in a metal mould and hot paraffin wax was poured into the mould using a Thermo Shandon Histocentre 3 (ThermoFisher, UK) and a plastic cassette was overlain. The paraffin was allowed to cool and set and plastic cassettes were subsequently stored at 4^{o}C.

2.9.3 Histological preparation

Formalin-fixed, paraffin embedded (FFPE) tissue blocks were cooled on ice prior to sectioning. Samples were cut into 4 µM sections using a Shandon Finese 325 microtome and S35 microtome blade (JDA-0100-00A, Feather). These sections were then transferred to the surface of a pre-heated water bath (40^{o}C) and then collected onto slide glass. 4-6 sections were cut from each block using this method. Slides were subsequently stored at 4^{o}C until required for immunohistochemical staining.

2.9.4 Antigen retrieval and deparaffinisation

Slides were placed in a slide rack compatible with the Dako PT Link (Dako, UK); this machine allowed the steps of deparaffinisation, rehydration and heat induced antigen retrieval to be combined. The slide rack was inserted into pre-heated high pH retrieval solution (Tris/EDTA, pH 9.0) for deparaffinisation. High-pH (buffer, pH 9.0) antigen retrieval was performed at 96^{o}C for 20 minutes. Slide racks were allowed to cool in the PT Link, after which slides were rinsed with FLEX wash buffer (50 mM Tris-base, 150 mM NaCl, 0.05% Tween 20, pH 7.6) to remove excess paraffin.

2.9.5 Immunohistochemistry (IHC)

Slide racks were transferred to the automated Dako autostainer system. IHC was performed using FLEX EnVisionTM reagents (Dako, UK). All steps were carried out at room temperature. Endogenous peroxidase was blocked by incubating slides with Peroxidase-Blocking Reagent (phosphate buffer containing hydrogen peroxide, 15mM NaN3) (DM821) for 5 minutes. Primary antibodies were diluted in antibody diluent (K8006) and slides were incubated with primary antibodies for 30 minutes, followed by incubation a goat anti-mouse secondary antibody conjugated with horseradish peroxidase (DM822) for 20 minutes. Positive staining was visualised with the chromogen, 3,3'-Diaminobenzidine (DAB), prepared by adding 1 µl of stock solution to 1 ml of substrate buffer

(DM823). Slides were washed with FLEX wash buffer (50 mM Tris-base, 150 mM NaCl, 0.05% Tween 20, pH 7.6) between each incubation.

2.9.6 Counterstaining and mounting

The principle of counterstaining is to improve the visibility of the structure of interest by staining the surrounding tissue with a contrasting colour. To counterstain, slides were immersed in haematoxylin solution for 20 seconds, washed with running tap water, cleared in 0.5% acid alcohol and incubated in Scott's tap water blueing agent for 30 seconds. Slides then underwent dehydration in a series of alcohol and xylene incubations before mounting with DPX mountant (Sigma, UK) on 22 x 50mm cover slips (630-2210, Menzel Gläser, UK). Tissue known to express the protein of interest was included as a positive control. Negative control involved the use of isotype specific control.

2.9.7 Quantifying Ki67 proliferative index

Slides were viewed under bright field microscopy and manual counting of histological sections allowed the quantification of Ki67 proliferative index. For each section ≥4 fields were assessed and 100-200 cells were counted per field. Ki67 positive nuclei are stained in brown by the immunohistochemistry technique. Negative nuclei are counterstained in blue by haematoxylin. The percentage of the brown-stained nuclei of the total number of cells determined the Ki67 index. Haematoxylin staining of nuclei allowed identification of both chick tissue and tumour nuclei. Chick tissue cells could be identified as they had a small nucleus whereas tumour tissue cells had a relatively larger nucleus.

2.10 Statistical analysis of data

Data are expressed as mean ± standard of the mean (SEM) of different treatments/experimental conditions. A non-paired Student's *t*-test was used for statistical comparison of the mean of two datasets. Statistical comparisons of the mean of two or more datasets was performed using one-way analysis of variance (ANOVA). Following ANOVA, a post-hoc Tukey test was applied. A value of $p<0.05$ was considered statistically significant. Statistical significance indicated as * $p< 0.05$, ** $p<0.01$ and *** $p<0.001$. SigmaPlot 13.0 (Systat Software, San Jose, USA) was used for statistical analysis and to present results graphically.

Chapter 3: Results

3.1 K^+ channel gene expression in primary neuroblastoma tumours

R2 Genomic Analysis and Visualisation Platform was utilised to evaluate K^+ channel gene expression in normal tissue and primary neuroblastoma tumours. **Figure 3.1** is an example of a single gene search within a dataset. KCNQ2 expression in a single dataset is demonstrated. Each data point represents the value of KCNQ2 gene expression plotted against individual patient samples. Additional parameters given are age, gender, disease stage, MYCN status, ploidy, disease risk, Shimada pathological classification and tissue type. The ranges of values of KCNQ2 expression in this dataset was 6.49 – 12.80 and the median value of expression was 11.1.

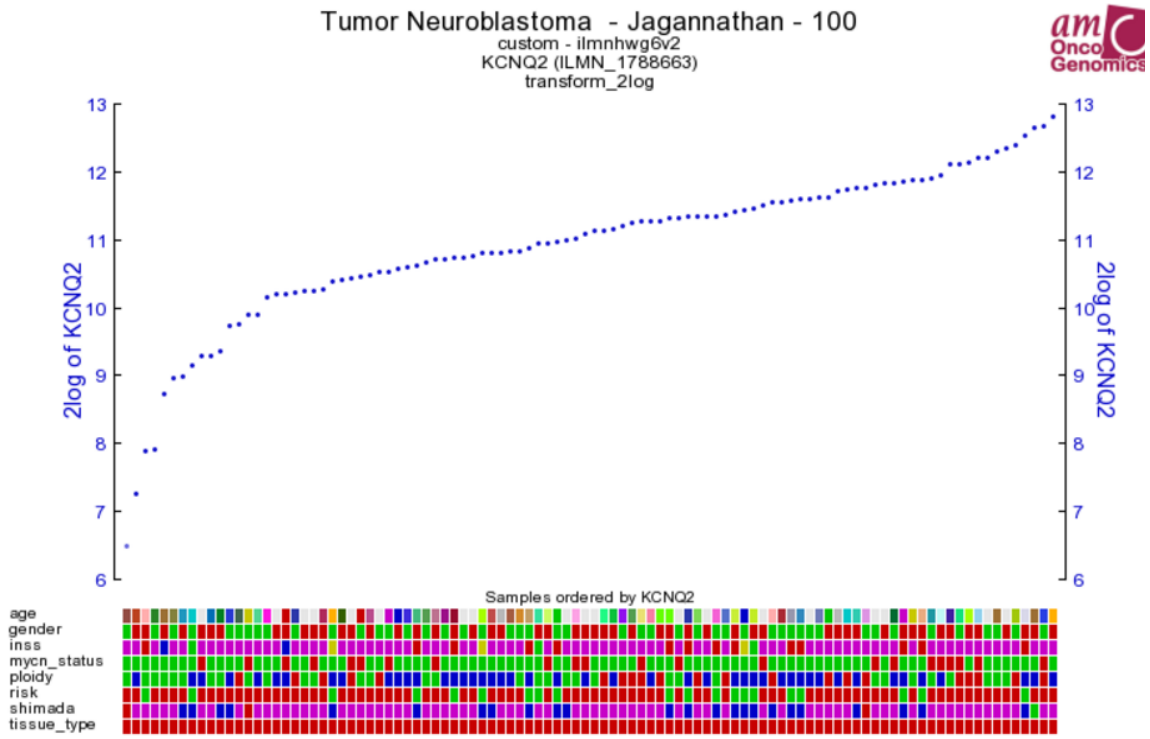

Figure 3.1: Gene expression dot plot for KCNQ2 in a dataset of 100 neuroblastoma tumours. Each data point represents the value of expression for a single tumour sample. Clinical and genetic parameters are also displayed. Graph generated using the R2 Genomic Analysis and Visualisation Platform.

The expression of all K^+ channel genes was evaluated in a single primary neuroblastoma dataset (Jagannathan, n=100 tumours). Within the dataset each patient sample had a value of gene expression and the median value of gene expression across all samples was determined. In the example above the ranges of values of KCNQ2 expression was 6.49 – 12.80 and the median value of expression was 11.1. This process was repeated for all 79 K^+ channel genes.

The reproducibility of results obtained in the first dataset search was tested by applying the same method to search 3 more primary neuroblastoma tumour datasets: Kocak, n= 649; SEQC, n= 498 and Asgharzardeh, n= 249. In total the median value of expression for 79 K^+ channel genes was therefore determined in 4 datasets (n= 1496). The next aim was to determine which K^+ channel genes demonstrated the highest level of expression. This was carried out by comparing K^+ channel gene expression across the 4 selected datasets. The microarray platform and normalisation method employed by each dataset was variable, therefore the scale employed to express the value of gene expression varied and raw values of expression were not comparable. To account for this during analysis each gene was ranked based on its median value of expression within a single dataset i.e. the most highly expressed gene was ranked as 1, the second as 2 and continuing to the gene with the lowest value of expression. Subsequently, to determine the mostly highly expressed gene, the median ranking of each gene across all 4 datasets was determined. For example, the ranking for KCNQ2 in 4 datasets was 1, 1, 1 and 3, therefore the median ranking of KCNQ2 across 4 datasets was 1. Of the 10 highest ranked genes 7 belonged to the family of voltage-gated K^+ channels. 5 genes were consistently highly ranked across all 4 datasets: KCNQ2, KCNG1, KCNB1, KCNMA1 and KCNH2 **(Figure 3.2)**.

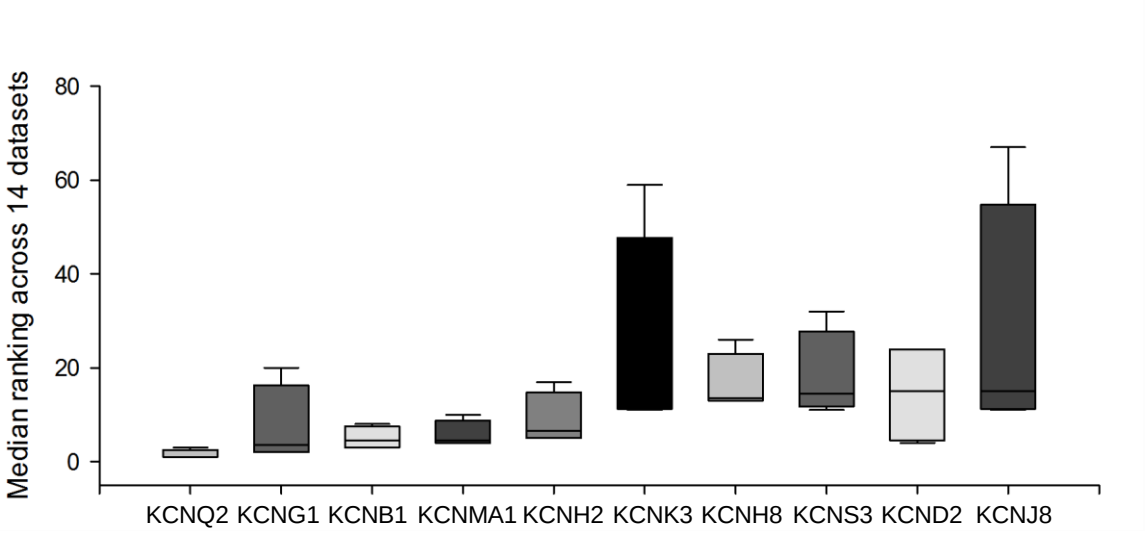

Figure 3.2: Evaluation of K^+ channel gene expression in 4 primary neuroblastoma datasets. Box plot representation of the median rank of the 10 most highly expressed K^+ channel genes across 4 primary neuroblastoma tumours datasets. Box- 25th and 75th percentiles; bars= minimum and maximum values.

The results from the evaluation of 4 datasets indicated that K^+ channel genes belonging to the voltage-gated and calcium-activated families demonstrate greatest expression in primary neuroblastoma tumours. To validate these findings these channels were assessed in a further 10 primary neuroblastoma datasets and this yielded similar results. Across 14 datasets KCNQ2, KCNH2, KCNB1, KCNMA1 and KCNG1 were still the 5 highest ranked genes **(Figure 3.3)**. The median rank of KCNQ2 was still 1 and its lowest rank in any given dataset was 5. This provided robust evidence that KCNQ2 is the most highly expressed K^+ channel gene in primary neuroblastoma tumours.

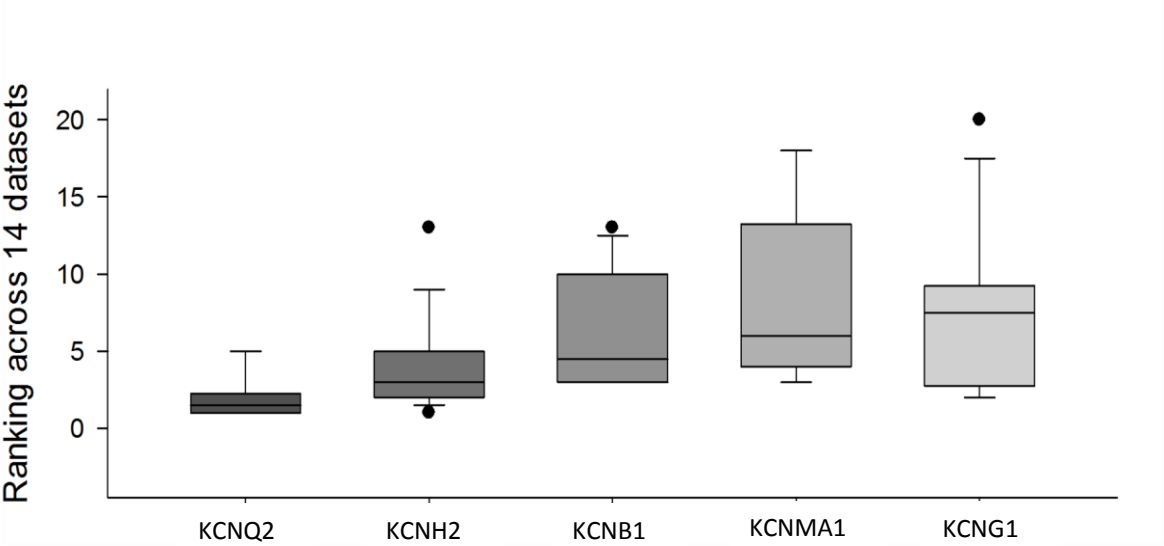

Figure 3.3: Evaluation of voltage-gated and calcium-activated K^+ channel genes across 14 datasets. Box plot representation of the median rank of 5 voltage-gated/calcium activated K^+ channel genes across 14 datasets. Box= 25^{th} and 75^{th} percentiles; bars= minimum and values, dots represent outlying values.

3.1.1 KCNQ2 expression in histological subtypes of peripheral neuroblastic tumours

An additional mode of analysis possible in R2 was to compare gene expression in a dataset with group stratifications. KCNQ2 expression was evaluated in a single dataset (n=28) where data could be stratified by tumour histological subtype i.e. ganglioneuroma, ganglioneuroblastoma and neuroblastoma. Ganglioneuroma and ganglioneuroblastoma are neuroblastic tumours are more histologically mature than neuroblastomas and have a better prognosis [93, 94]

KCNQ2 was differentially expressed between histological subtypes. KCNQ2 is highly expressed in neuroblastomas compared with ganglioneuroma ($p<0.001$) and ganglioneuroblastomas ($p<0.01$). This indicated that increased expression of KCNQ2 may be a genetic marker of undifferentiated tumours, thereby a marker of poor prognosis **(Figure 3.4)**.

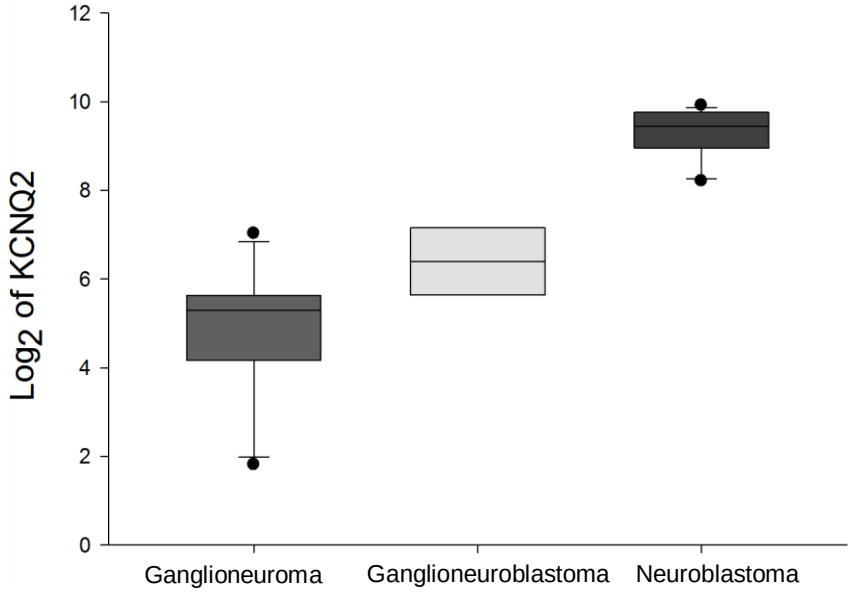

Figure 3.4. KCNQ2 expression in peripheral neuroblastic tumours histologically subtypes tumours. Box plot representation of KCNQ2 expression in all three subtypes of peripheral neuroblastic tumours: neuroblastomas, ganglioneuroblastomas and ganglioneuromas. Box- 25th and 75th percentiles; bars= minimum and maximum values. Dots represent outlying values

3.2 Expression of K^+ channels in neuroblastoma cell lines

Following on from the initial assessment of K^+ channel gene expression in primary neuroblastoma tumours, the next series of experiments aimed to evaluate K^+ channel gene expression in two neuroblastoma cell lines. This was carried out using a combination of gene and protein expression analysis.

Two heterogenous, neuroblastoma-dervied cell lines, BE2C and SKNAS, were selected as they represent two types of high-risk primary neuroblastoma tumours: MYCN-amplified (BE2C) and 11q deletion (SKNAS). All experiments were conducted using BE2C and SKNAS cells to determine if K^+ channel expression was different between the two cell lines.

Initial experiments were designed to determine if the K^+ channel genes identified to be highly expressed in primary neuroblastoma tumours were expressed in BE2C and SKNAS cells and if there were any genes which demonstrate differential expression. The 5 K^+ channel genes which demonstrated relatively high expression in human neuroblastoma tumours were selected for analysis by quantitative PCR: KCNQ2, KCNG1, KCNB1, KCNMA1 and KCNH2 **(Section 3.1)**.

3.2.1 Assessing K^+ channel gene expression by qPCR

3.2.1.1 Primer efficiency

Prior to qPCR experiments, to ensure adequate optimisation, the efficiency of primer pairs was assessed using sample cDNA. Cq values for a 5 point dilution series were plotted against Log2 dilution factor (DF). Linear regression analysis was used to determine the slope of the curve. **Figure 3.5** is an example plot showing how primer efficiency for the KCNQ2 primer pair was determined. KCNQ2 primer efficiency was 95.1%. **Table 3.1** details primer efficiency for all primer pairs used.

A

Dilution factor (DF)	1	0.5	0.25	0.125	0.0625
Log_2 DF	0	-1	-2	-3	-4
Mean Cq value	19.31	20.43	21.47	22.46	23.47

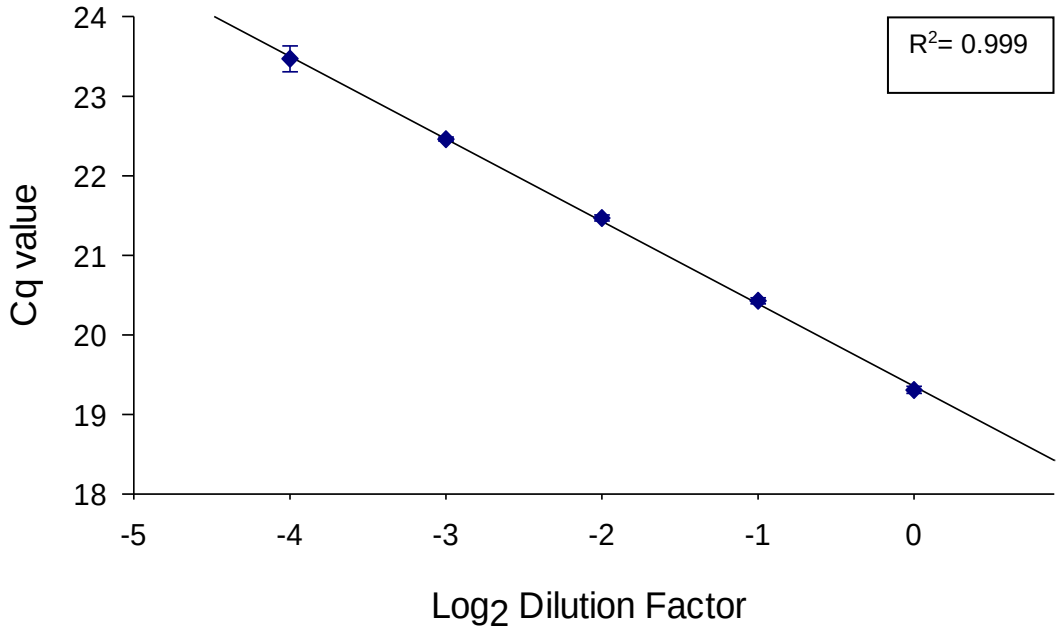

B $$E = 100 \times (10^{-1/m}) - 1$$

Figure 3.5: KCNQ2 primer efficiency. (A) Regression analysis of a 5 point dilutions series produced a linear equation from which the *m* value was used to determine efficiency. Data represents mean Cq ± SEM (n=3). **(B)** Equation used to determine primer efficiency.

Gene	Primer efficiency
UBC	97.5%
HPRT1	94.7%
KCNQ2	95.1%
KCNMA1	91.3%
KCNH2	93.1%
KCNG1	97.9%
KCNB1	112.5%
KLF4	95.8%
STMN4	98.0%
ROBO2	97.4%

Table 3.1: Efficiency of all primers used during qPCR experiments.

3.2.1.2 Expression of K^+ channel genes within cell lines

The 5 most highly expressed K^+ channels in primary neuroblastoma tumours were KCNQ2, KCNH2, KCNB1, KCNMA1 and KCNG1 **(Section 3.1)**. The expression of these genes was evaluated in two neuroblastoma-derived cell lines, BE2C and SKNAS. qPCR was utilised to determine relative quantification values. To compensate for differences in starting quantity of cDNA and reaction kinetics quantification values were normalised to the expression of two reference genes, UBC and HPRT1. In the BE2C cell line, KCNQ2 was the most highly expressed K^+ channel gene, followed by KCNH2. **(Figure 3.6, A)**. In the SKNAS cell line, KCNH2 was the most highly expressed K^+ channel gene **(Figure 3.6, B)**.

A

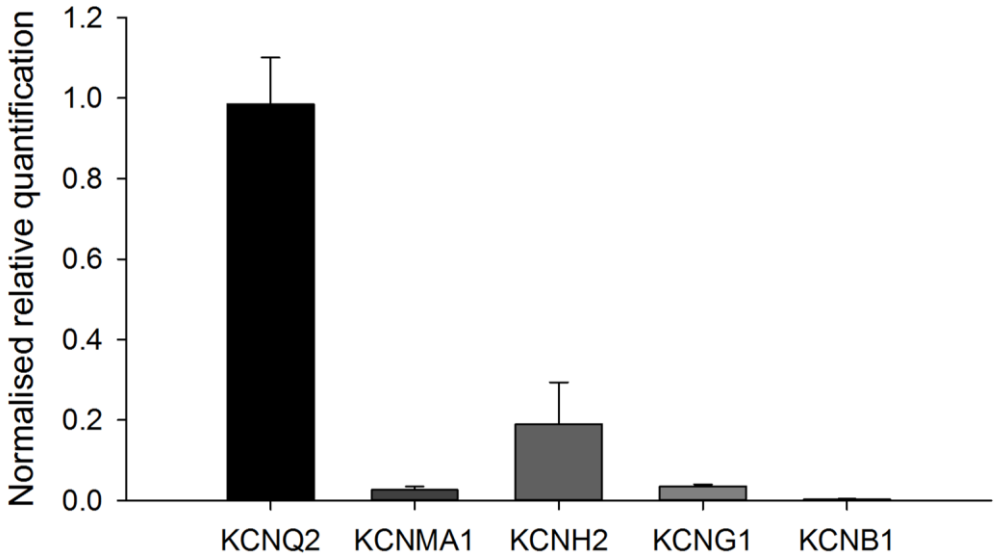

B

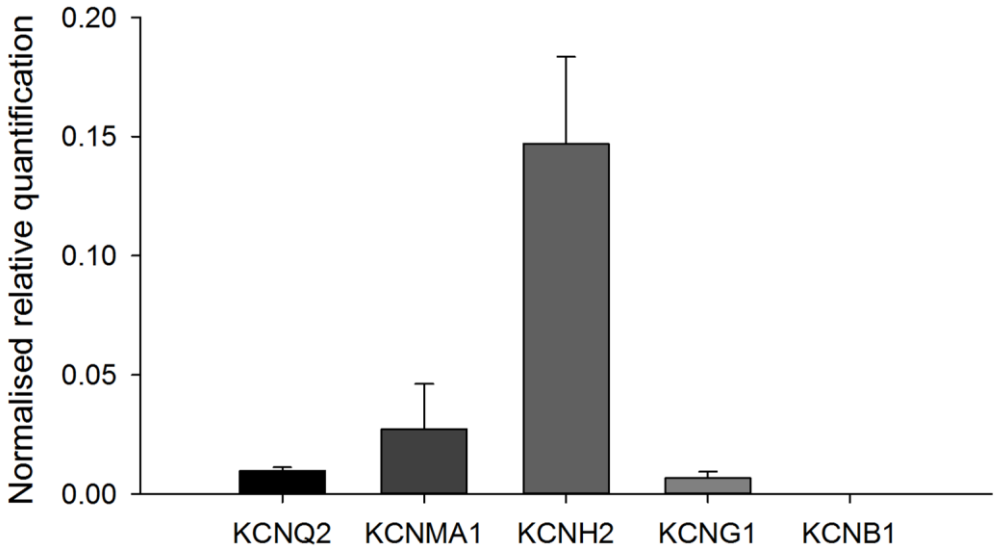

Figure 3.6: K^+ channel gene expression within BE2C and SKNAS cell lines. (A) BE2C cells **(B)** SKNAS cells. Relative quantification values were normalised to UBC and HPRT1 expression. Data represents mean ± SEM (n=3).

3.2.1.3 Differential expression of K^+ channel genes

To determine differential expression of K^+ channel genes between BE2C and SKNAS, relative quantification ratios for each gene was determined for BE2C compared with SKNAS **(Figure 3.7)**. Expression of KCNQ2, KCNB1 and KCNG1 was 101.51 ± 17.52 ($p< 0.001$), 71.91 ± 46.85 ($p< 0.01$) and 5.31 ± 2.41 ($p< 0.05$) fold greater in BE2C cells relative to SKNAS cells, respectively. Expression of KCNMA1 and KCNH2 were not found to be differentially expressed in BE2C cells compared with SKNAS.

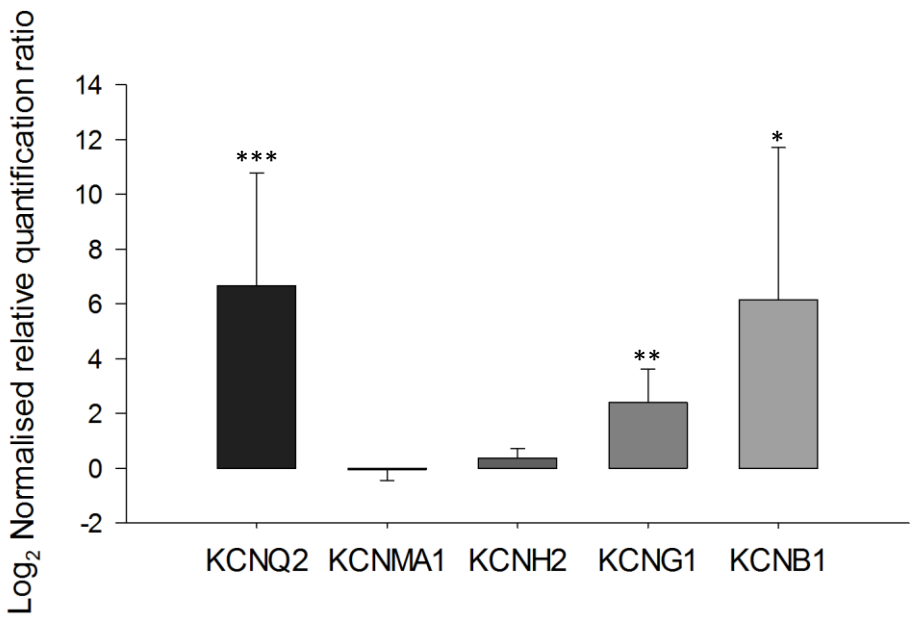

Figure 3.7: Relative expression of K^+ channel genes in BE2C and SKNAS. Normalised relative quantification ratios of K^+ channel genes. Data are displayed for BE2C relative to SKNAS. Data represents mean ± SEM (n=3)

3.3 Western blotting

Western blotting is an important method to identify specific proteins using antibodies. Primary antibodies are designed to target a unique sequence of a target protein. If a single band with predicted size can be detected, then the western blot results can validate the usefulness of a primary antibody.

Assessment of gene expression by qPCR found expression of KCNQ2/Kv7.2 was 100 fold greater in BE2C cells compared with SKNAS. KCNQ2/Kv7.2 expression in BE2C and SKNAS cells was further investigated by western blotting. Several anti-Kv7.2 antibodies were tested **(Section 2.1.2)**. Experiments using two different rabbit anti-Kv7.2 antibodies showed bands at the predicted molecular weight (96 kDa) in BE2C cells **(Figure 3.8 and 3.10, lane A)**, whereas Kv7.2 expression was detected in SKNAS cell lysate by only one of these antibodies **(Figure 3.8 and 3.10**, **lane C)**. A commonly used housekeeping protein is ß-tubulin. Re-blotting with a mouse anti-ß-tubulin antibody after stripping the membrane first blotted against anti-Kv7.2 antibody demonstrated a single band at 50 kDa **(Figure 3.8 and 3.10**, **lanes B and D).** Re-blotting was conducted to ensure any differences detected in Kv7.2 expression were not due to differences in protein loading between the lanes.

3.3.1 Kv7.2 expression (anti-Kv7.2 antibody, Chemicon)

In both BE2C and SKNAS cell lysates the first anti-Kv7.2 antibody (Chemicon) used showed a single band at the predicted molecular weight and a second band just below this **(Figure 3.8)**. The presence of a second band may have been due to the presence of a non-specific band. However, the additional band may represent an isoform of Kv7.2 of which there are known to be 5 [228].

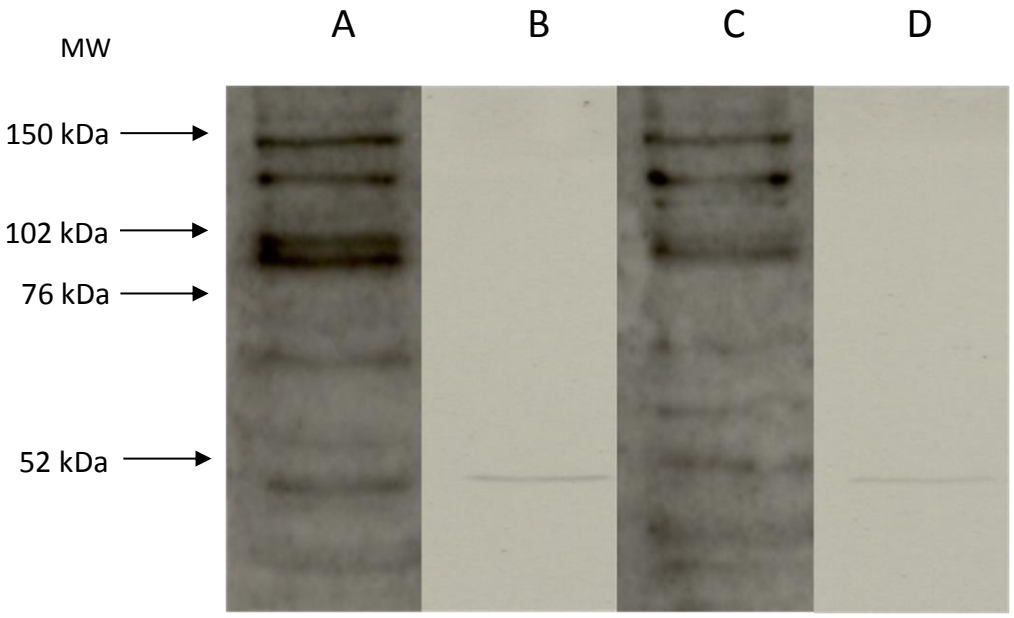

Figure 3.8 Western blot results using anti-Kv7.2 (Chemicon) and ß-tubulin primary antibodies on BE2C and SKNAS cell lysates. Lanes A and B: BE2C cell lysate, **Lanes C and D:** SKNAS cell lysate **Lane A and C:** show two bands of Kv7.2 at 96kDA, two further bands were detected at higher molecular weights, the identities of which were unknown, 1 minute exposure.
Lane B and D: shows a single band of ß-tubulin at 50 kDa after re-blotting the same membrane, 1 minute exposure.

To determine if Kv7.2 is differentially expressed in BE2C and SKNAS densitometric analysis of western blotting data was performed. Membranes were re-blotted with ß-tubulin, a housekeeping protein presumed to demonstrate constant expression between cell lines. Profile plots were drawn for each band of interest and housekeeping protein and the area of each peak was determined. The area of the peak for the Kv7.2 profile plot was divided by the area of the peak for the ß-tubulin profile plot. In BE2C cells expression of Kv7.2 is 5.3 fold greater than ß-tubulin, whereas in SKNAS Kv7.2 expression is 3.5 fold greater than ß-tubulin. Therefore, based on the assumption that ß-tubulin expression is relatively constant expression of Kv7.2 is 1.5 fold greater in BE2C than SKNAS. **(Figure 3.9)**.

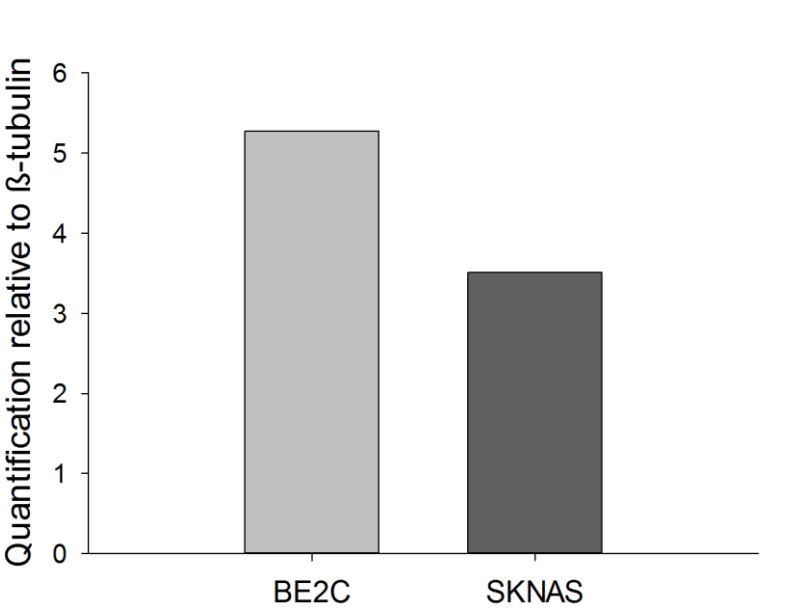

Figure 3.9: Relative quantification of Kv7.2 expression in BE2C and SKNAS. Expression of Kv7.2 was 1.5 fold greater in BE2C than SKNAS (n=1).

3.3.2 Kv.7.2 expression (anti-Kv7.2 antibody, Abcam)

In order to validate the results of western blotting with the first antibody, a second anti-Kv7.2 antibody (Abcam) was used with BE2C and SKNAS protein lysate **(Figure 3.10)**. Unconventionally, the lysate was prepared in non-denaturing conditions i.e. not heated with sample buffer, according to the manufacturer's instructions which stated this was necessary to detect a band at the correct molecular weight. For comparison western blotting was also conducted using denatured lysate (data not shown).

In the BE2C cell lysate a single band at the predicted molecular weight (96 kDa) was detected, but a corresponding band in the SKNAS cell lysate was not detected. The absence of a band in the SKNAS cell lysate supports the results of western blotting with the first antibody **(Section 3.3.1)**.

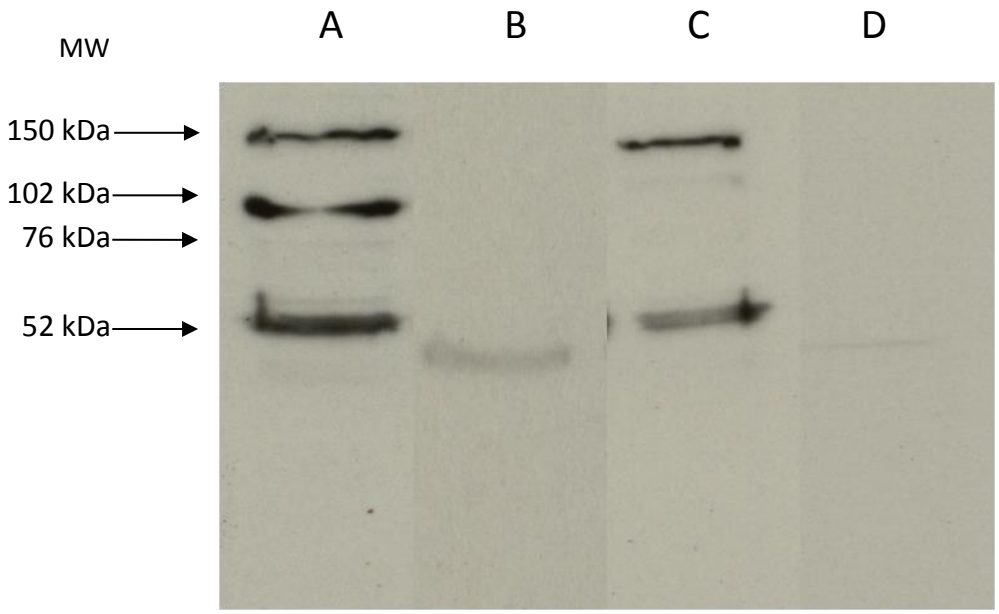

Figure 3.10: Western blot results using anti-Kv7.2 (Abcam) and ß-tubulin primary antibodies on BE2C and SKNAS cell lysates. Lanes A and B: BE2C cell lysate, **Lanes C and D:** SKNAS cell lysate **Lane A and C:** show a single band of Kv7.2 at 96kDA, further bands were detected at lower and higher molecular weights, the identities of which were unknown, 5 minutes exposure. **Lane B and D:** shows a single band ß-tubulin at 50 kDa after re-blotting the same membrane, 5 minutes exposure.

3.4 Immunocytochemistry

Immunocytochemistry was used to investigate NB84 **(Figure 3.11)** and Kv7.2 **(Figure 3.12)** expression in BE2C and SKNAS cells. Cells were stained with primary antibodies, mouse NB84 or goat anti-Kv7.2 and labelled with goat anti-mouse and goat anti-rabbit secondary antibodies respectively. Secondary antibodies were conjugated to Alexa Fluor 488 (green). Slides were viewed using confocal microscopy.

3.4.1 NB84 staining in BE2C and SKNAS cells

NB84 is a monoclonal antibody which recognises an uncharacterised 57 kDa cytoplasmic antigen from human neuroblastoma tissue. It is a highly sensitive marker used in immunohistochemical staining of primary tumours for identifying neuroblastoma cells [229]. NB84 was used a positive control to validate immunocytochemistry technique and confirm detection of neuroblastoma cells. Visual examination of cells stained with NB84 indicated green fluorescence was present throughout the cytoplasm of both BE2C and SKNAS cells **(Figure 3.11)**. Cells were counterstained with DAPI to identify the cell nucleus and no nuclear staining with NB84 was detected. To confirm the positive immunostaining, a negative control was employed; Alexa Fluor 488 was applied without the primary antibody and no green fluorescence was visualised.

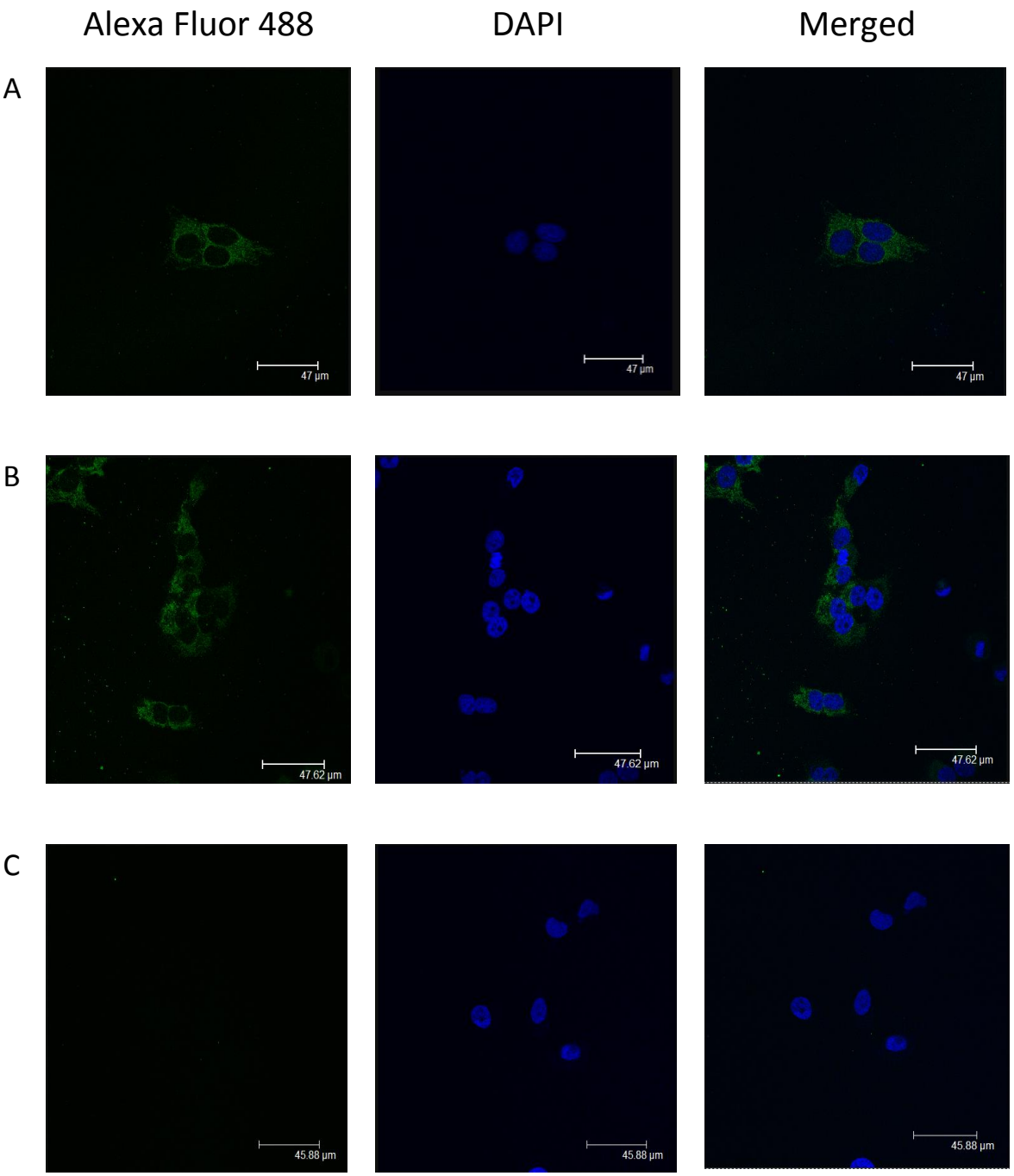

Figure 3.11: Confocal images of BE2C and SKNAS cells stained with mouse NB84 (x200) and labelled with goat anti-mouse secondary antibody conjugated to Alexa-Fluor 488 (x500). (A) BE2C cells demonstrated positive cytoplasmic staining **(B)** SKNAS cells demonstrated positive cytoplasmic staining **(C)** Negative control of BE2C cells stained with Alexa Fluor 488 only.

3.4.2 Expression of Kv7.2 in BE2C and SKNAS cells

Western blotting with an anti-Kv7.2 antibody (Abcam) demonstrated a single band at the predicted molecular weight in BE2C lysate **(Section 3.3)**. To assess the cellular location of Kv7.2 immunocytochemistry with the same antibody was conducted in both cell lines **(Figure 3.12)**. BE2C and SKNAS cells were stained with a rabbit anti-Kv7.2 antibody (Abcam) and labelled with goat anti-rabbit secondary antibody conjugated to Alexa Fluor 488 (green). Examination of both cell lines stained with the anti-Kv7.2 antibody found green fluorescence present throughout the cytoplasm and relatively less nuclear staining.

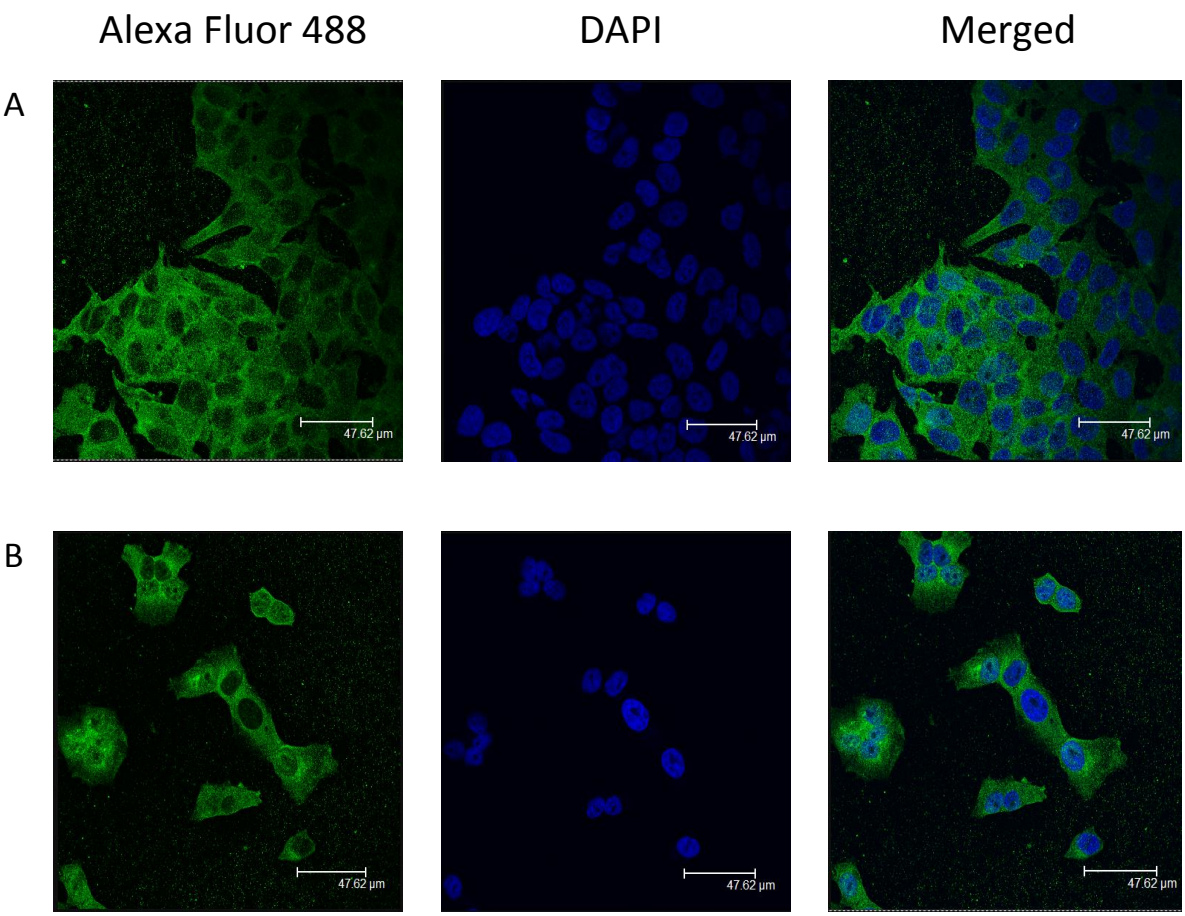

Figure 3.12: Confocal images of BE2C and SKNAS cells stained with rabbit anti-Kv7.2 (x200) and labelled goat anti-rabbit secondary antibody conjugated with Alexa-Fluor 488 (x500). (A) BE2C cells (B) SKNAS cells.

3.5 DiBAC$_4$(3) results

3.5.1 Overview

Bis(1, 3-dibutylbarbituric acid) trimethine oxonol (DiBAC4(3)) belongs to the Oxonol family of slow-response probes. DiBAC$_4$(3) is an anionic, voltage-sensitive fluorescent dye. When present in the intracellular space DiBAC$_4$(3) is adsorbed to intracellular membranes and proteins resulting in fluorescence [230]. As the membrane potential moves to more a positive value DiBAC$_4$(3) accumulates in the intracellular space, according to a Nernst equilibrium distribution. Therefore, cell membrane depolarisation causes DiBAC$_4$(3) to accumulate in the intrac[220]ellular space resulting in a concomitant increase in fluorescence **(Figure 3.12)**. Measuring DiBAC$_4$(3) fluorescence is thereby an indirect method by which changes in membrane potential can be assessed. DiBAC$_4$(3) emits fluorescence at 516 nm in response to an excitation wavelength of 490 nm. Application of a K^+ channel inhibitor would limit the efflux of K^+ and induce membrane potential depolarisation and DiBAC$_4$(3) fluorescence would increase. An activator of K^+ channels would have the converse effect.

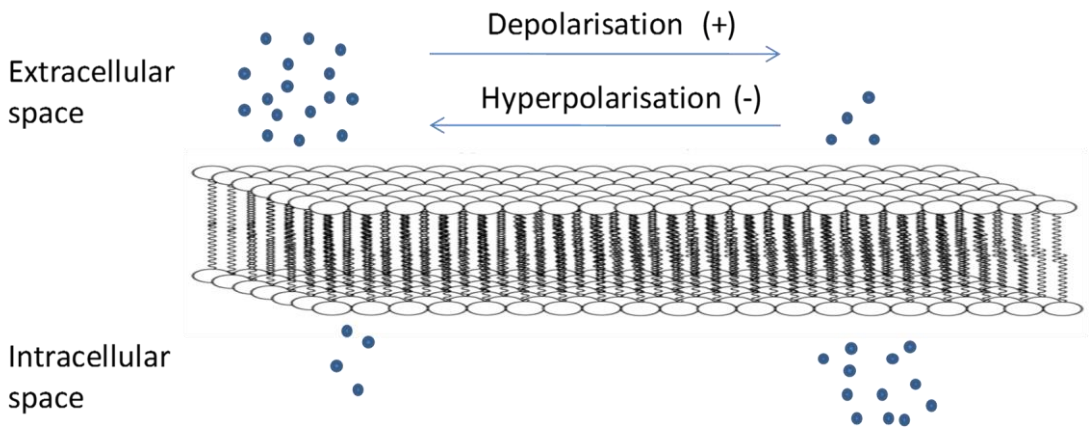

Figure 3.12: Distribution of DiBAC$_4$(3) is determined by membrane potential. Depolarisation of cell membrane potential leads to in intracellular accumulation of dye resulting in increased fluorescence, whereas hyperpolarisation causes a decrease in fluorescence.

3.5.2 Characterising $DiBAC_4(3)$ fluorescence in BE2C and SKNAS cells

Preliminary experiments were undertaken in order to characterise $DiBAC_4(3)$ fluorescence at a series of cell densities. This allowed determination of the cell density at which the fluorescent signal detection was optimal i.e. not too low so that the signal was undetectable or too high such that fluorescence saturated.

In the BE2C cell line there was a linear relationship (R^2=0.996) between cell density and relative fluorescence at cell densities between 1 x 10^4 and 5 x 10^4 cells per well, however fluorescence saturated at higher densities **(Figure 3.13, A)**. The optimal cell density for future experiments with BE2C cells was determined to be 2 x 10^4 cells per well. In the SKNAS cell line, there was a linear relationship (R^2=0.990) between cell density and relative fluorescence. Fluorescence did not saturate at higher cell densities **(Figure 3.13, B)**. The optimal cell density for future experiments with SKNAS cells was determined to be 5 x 10^4 cells per well.

A

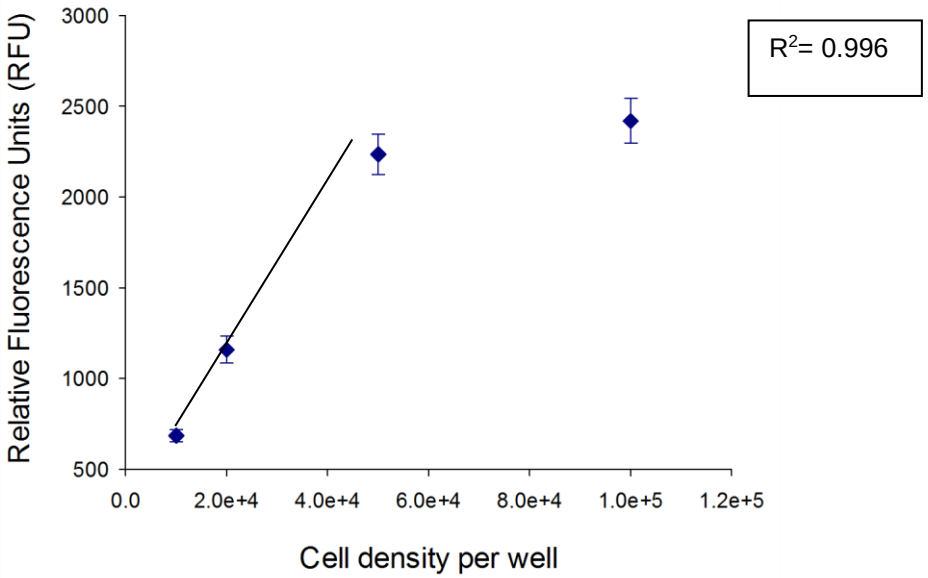

B

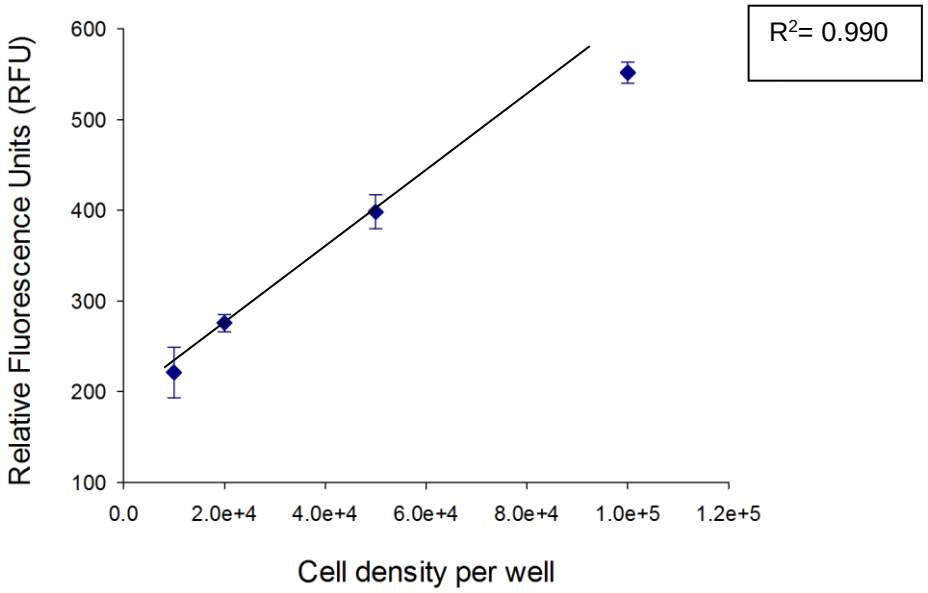

Figure 3.13: Characterisation of DiBAC$_4$(3) fluorescence at a series of cell densities. (A) DiBAC$_4$(3) fluorescence in BE2C cells. Fluorescence saturated at higher cell densities, therefore the data point at 1 x 10^5 was excluded from linear regression analysis. **(B)** DiBAC$_4$(3) fluorescence in SKNAS cells. Data represents the mean ±SEM (n=6).

B

3.5.3 Response to high K^+ solution in BE2C cells

In order to determine the fluorescent signal after inducing sustained depolarisation of the cell membrane potential $DiBAC_4(3)$ solution containing a high K^+ concentration (145 mM) was added to cells pre-incubated in $DiBAC_4(3)$ PSS. An increase in extracellular K^+ concentration abolishes the K^+ concentration gradient across the cell membrane, thus preventing the hyperpolarising outflow of K^+. Resultantly there is predicted to be sustained depolarisation of the cell membrane potential, assuming K^+ channels dominate generation of resting membrane potential.

Addition of $DiBAC_4(3)$ high K^+ solution caused an 11.21 ± 1.92% increase in fluorescent signal, thus demonstrating that $DiBAC_4(3)$ accumulates in BE2C cells upon depolarisation of cell membrane potential **(Figure 3.14)**.

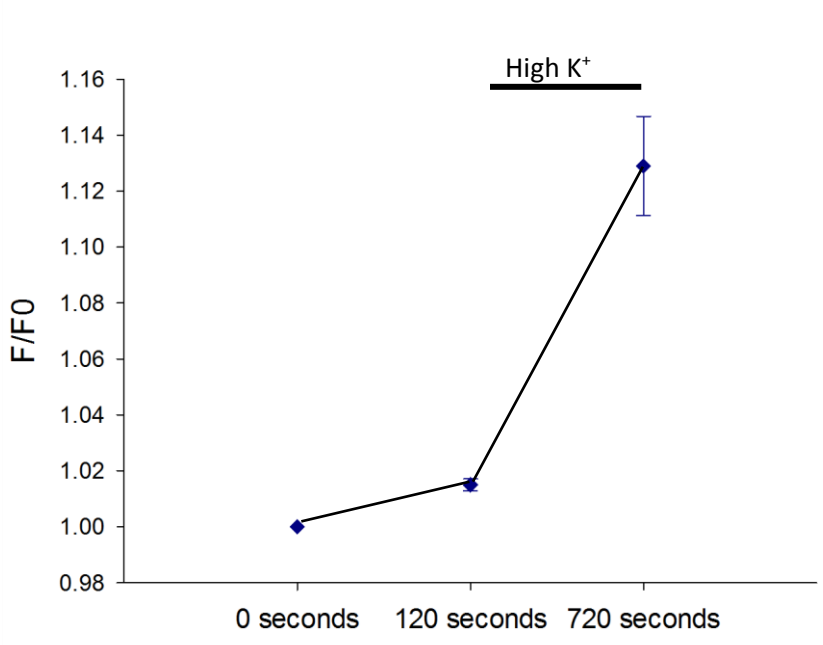

Figure 3.14: Effect of high K^+ solution on $DiBAC_4(3)$ fluorescence. Addition of high K^+ solution at 120 seconds caused a significant increase in $DiBAC_4(3)$ fluorescence. Data are shown as mean ±SEM (n=6), $p<0.001$.

3.5.4 Effect of Kv7 channel modulation in BE2C and SKNAS cells

Molecular expression studies demonstrated that Kv7.2 is expressed in BE2C cells **(Section 3.4)**. The next objective was to determine if Kv7 channels are functional in BE2C and SKNAS cells. The previous experiment **(Section 3.5.3)** with DiBAC4(3) indicated that the cell membrane potential of neuroblastoma cells depolarised in response high K^+ solution. To determine if Kv7 channels are functional, $DiBAC_4(3)$ fluorescence was measured in BE2C and SKNAS cells in response to XE991 and ML213, an inhibitor and activator of Kv7 channels respectively [174].

In BE2C cells, 1 µM $DiBAC_4(3)$ PSS containing DMSO caused a 14.60 ± 3.77% increase in $DiBAC_4(3)$ fluorescence. DMSO is not known to have an effect on membrane potential and the reason for an increase in $DiBAC_4(3)$ fluorescence in response to a DMSO containing solution is unknown. Therefore, the response to Kv7 modulating compounds was calculated relative to $DiBAC_4(3)$ PSS containing DMSO. 10 µM ML213 caused a 5.58 ± 0.70% ($p > 0.05$) decrease in $DiBAC_4(3)$ fluorescence **(Figure 3.15, A)**. Conversely, 10 µM XE991 caused a 5.62 ± 1.76% ($p = 0.035$) increase in $DiBAC_4(3)$ fluorescence **(Figure 3.15, B)**.

In SKNAS cells, 10 µM XE991 caused an 11.82 ± 5.30% ($p > 0.05$) increase and 10 µM ML213 caused a 5.47 ± 2.77% ($p > 0.05$) decrease in DiBAC4(3) fluorescence, respectively **(Figure 3.16)**. The respective changes in $DiBAC_4(3)$ fluorescence in response to both Kv7 channel modulating agents suggests that Kv7 channels are involved in determining membrane potential in both BE2C and SKNAS cells.

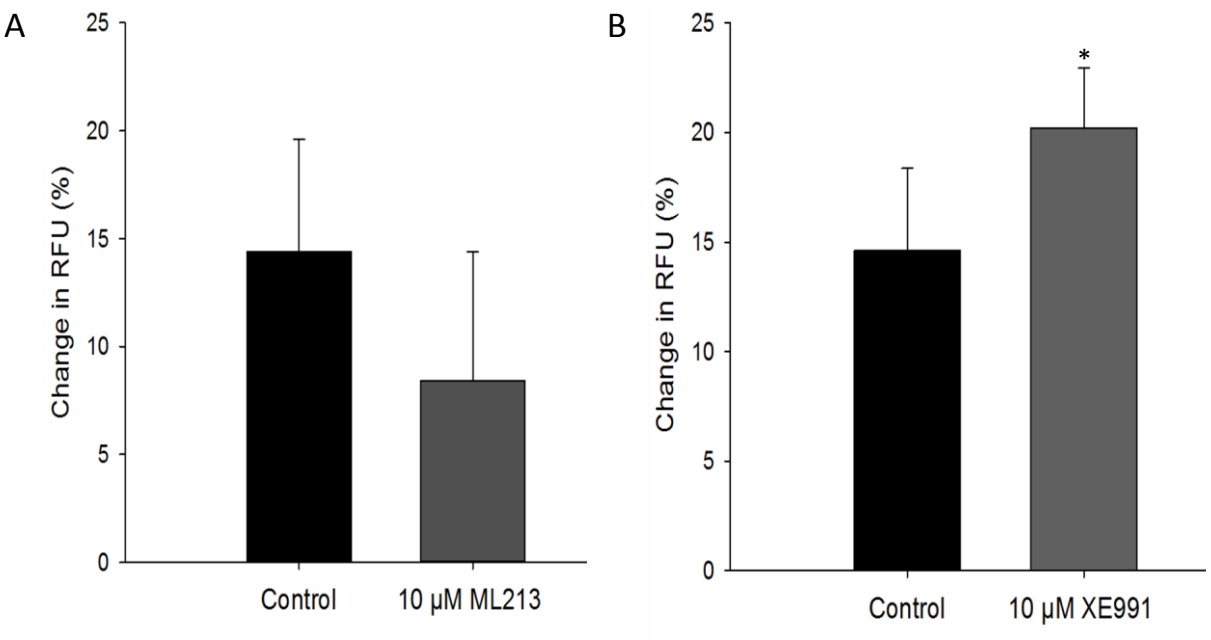

Figure 3.15: Effect of Kv7 channel modulation on DiBAC$_4$(3) fluorescence in BE2C cells. (A) Application of ML213 caused hyperpolarisation of the membrane potential (n= 11, p= 0.067) **(B)** Application of XE991 caused depolarisation of the membrane potential (n= 17, p= 0.035). Data are shown as mean ± SEM.

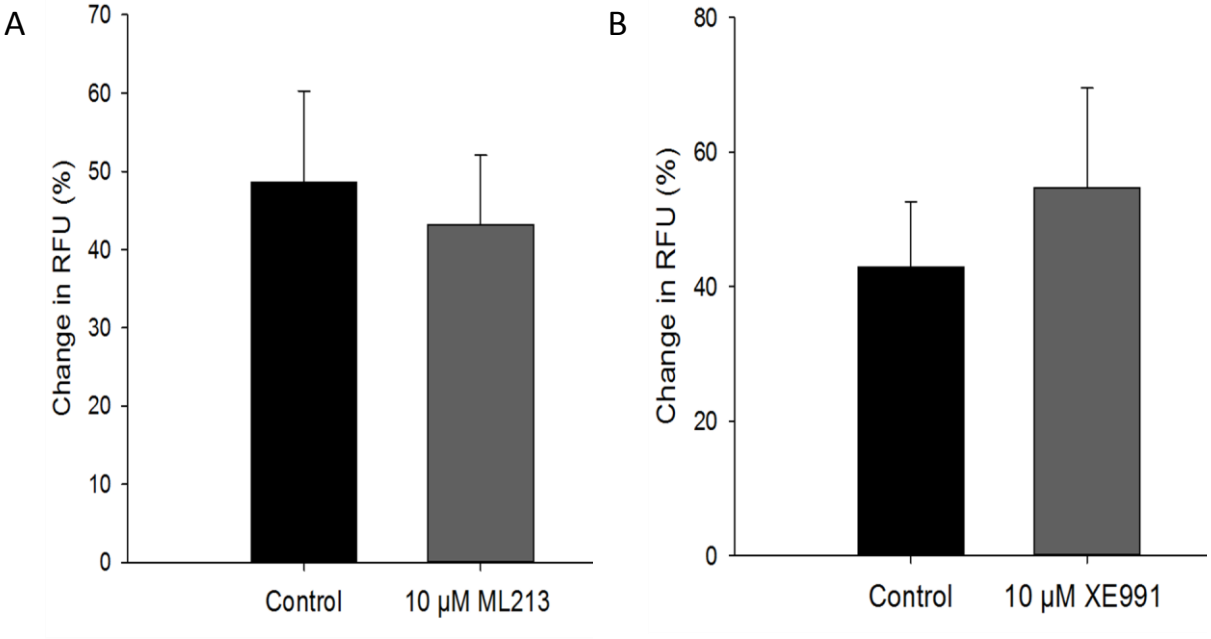

Figure 3.16: Effect of Kv7 channel modulation on DiBAC$_4$(3) fluorescence in SKNAS cells **(A)** Application of XE991 caused depolarisation of the cell membrane (n= 12, p= 0.22). **(B)** Application of ML213 caused hyperpolarisation of the membrane potential (n=12, p= 0.22). Data are shown as mean ± SEM.

3.6 Effect of modulation of Kv7 channels on neuroblastoma cell behaviour *in vitro*

K^+ channel gene expression in neuroblastoma cell lines was evaluated by qPCR **(Section 3.2)**, western blotting **(Section 3.3)**, immunocytochemistry **(Section 3.4)** and DiBAC4(3) fluorescence experiements **(Section 3.5)**. Kv7.2 was demonstrated to be highly expressed and functional in BE2C cells, therefore the next set experiments investigated the effect of pharmacological modulation of Kv7.2 on the behaviour of BE2C and SKNAS cells *in vitro.* The effect of Kv7 modulation on BE2C and SKNAS cell viability was investigated, followed by assessment of cell proliferation and differentiation.

3.6.1 Assessing cell viability

3.6.1.1 Overview

MTT (3-(4,5- dimethyl-2-thiazolyl)-2,5-diphenyl-2H-tetrazolium bromide) assay is a colorimetric-based assessment of cell viability. In metabolically active cells the yellow tetrazolium salt MTT is cleaved to form purple formazan crystals by mitochondrial reductases [231] **(Figure 3.17)**. Spectrophotometric measurement of formazan absorbance is proportional to the metabolic activity of cells in culture, which in turn reflects the number of viable cells. However, metabolic activity is influenced by multiple factors including cell survival, cell proliferation and metabolic rate. Preliminary experiments involved characterising formazan absorbance in both BE2C and SKNAS cells. This was followed by assessing the effect of Kv7 modulation on BE2C and SKNAS cell viability.

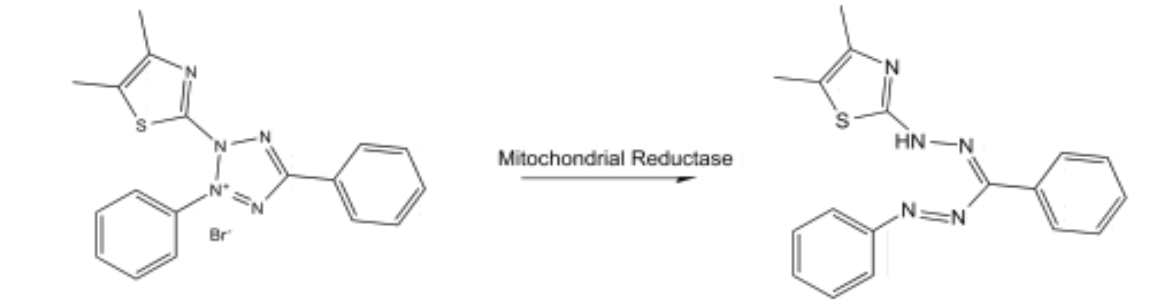

Figure 3.17: MTT reduction reaction. Formazan absorbance is proportional to mitochondrial activity, which in turn reflects the number of viable cells. Therefore, measuring formazan absorbance allows quantitative assessment of the number of viable cells.

3.6.1.2 Characterising formazan absorbance in BE2C and SKNAS cells

Preliminary experiments involved determination of absorbance at a series of cell densities to characterise the optimal cell density for future experiments. The optimal cell density should fall in the linear portion of absorbance; this was necessary to allow determination of both increases and decreases in absorbance.

Plotting absorbance (570 nm) against cell density demonstrated a linear relationship for both cell lines **(Figure 3.18)**, however in both cell lines saturation of the absorbance signal occurred at cell densities above 1×10^5 per well. The optimal cell density for future experiments was determined to be 1×10^4 cells per well for both cell lines. Formazan absorbance was greater in BE2C cells **(Figure 3.18, A)** than SKNAS cells **(Figure 3.18, B)** across all cell densities evaluated. Given that higher absorbance reflects a greater number of viable cells, one interpretation of this finding is that BE2C cells were more rapidly dividing than SKNAS cells.

A

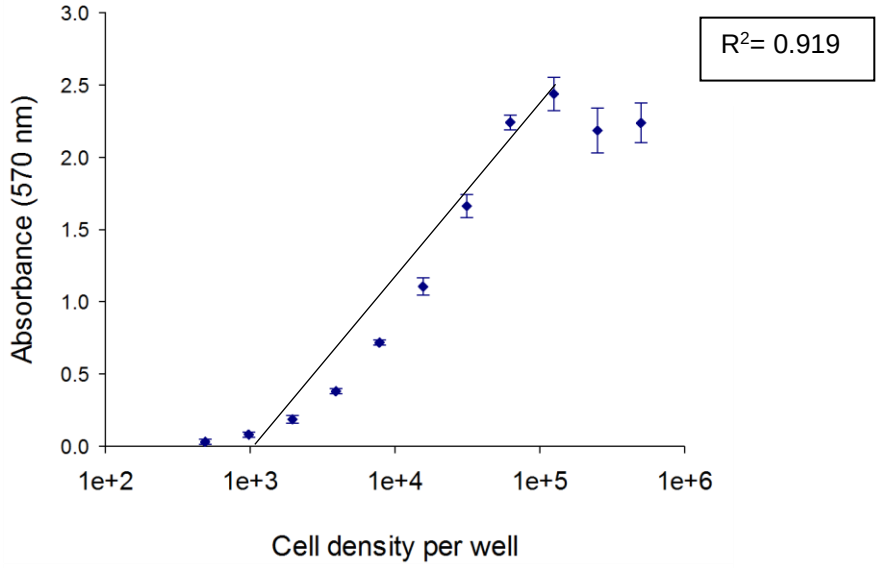

B

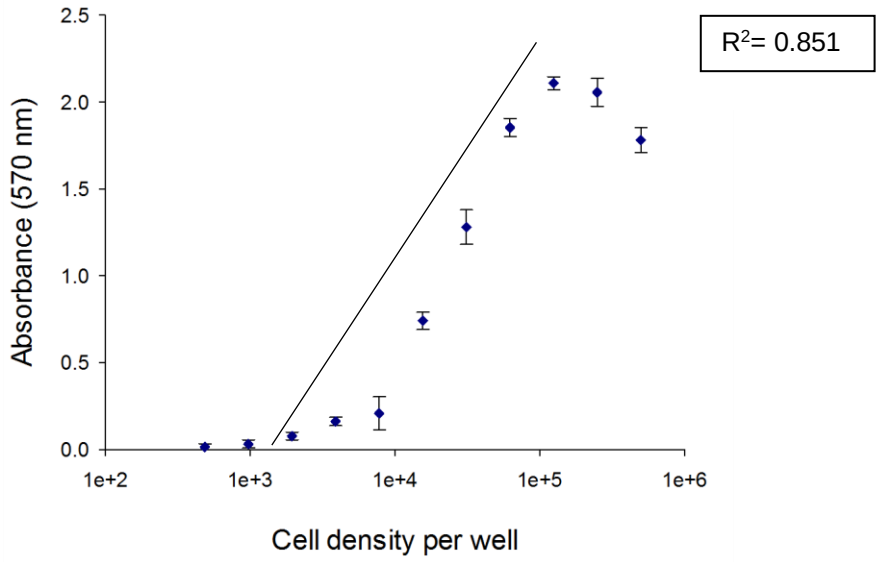

Figure 3.18: Characterisation of absorbance at a series of cell densities over 24 hours. (A) BE2C cells **(B)** SKNAS cells. For both cell lines data for cell densities >1 x 10^5 cells per well were excluded from linear regression analysis due to saturation of absorbance signal. Each data point represents mean ±SEM (n=3).

3.6.1.3 Effect of cycle cell inhibition on cell viability

Palbociclib is a CDK4/6 inhibitor and has been shown to reduce cell proliferation in multiple neuroblastoma cell lines including BE2C [232]. To demonstrate that MTT assay is a viable method to detect changes in the number of viable cells, BE2C cells were cultured with 5 µM Palbociclib for 72 hours. Palbociclib treated BE2C cells demonstrated a 43.83 ± 3.07% reduction in absorbance ($p<0.001$) **(Figure 3.19)**.

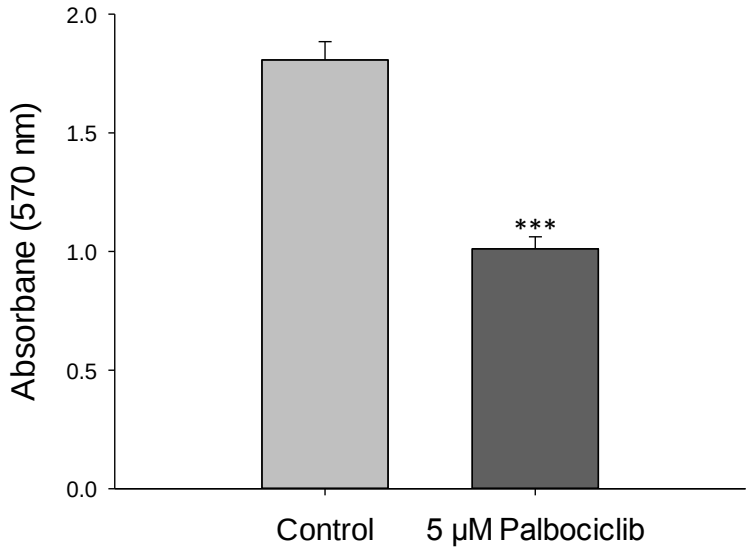

Figure 3.19: Effect of Palbociclib on BE2C cell viability. Cell viability was assessed by MTT assay. Absorbance at 570 nm was corrected for background. Data represents mean ± SEM (n=4).

3.6.1.4 Effect of Kv7 channel modulation on cell viability

Given that Kv7.2 was found to be highly expressed in BE2C cells and relative to SKNAS the effect of Kv7.2 modulation on cell viability was investigated. Both BE2C and SKNAS cells were cultured with two concentrations of XE991 (1 µM and 10 µM) and ML213 (1 µM and 10 µM) for 72 hours. XE991 and ML213 are inhibitor and activator of Kv7 channels, respectively. Two concentrations were tested to determine if a dose response effect could be observed.

BE2C cells treated with 10 µM XE991 demonstrated a 10.10 ± 1.49% reduction in formazan absorbance at 570 nm indicating a reduction in the number of viable cells; however this effect was not significant ($p>0.05$). Application of XE991 at a lower concentration (1 µM) caused the opposite effect and a 10.99 ± 2.19% increase in absorbance was observed ($p>0.05$) **(Figure 3.20, A)**. SKNAS cells treated with XE991 10 µM demonstrated an 11.97 ± 1.06% reduction in the number of viable cells ($p>0.05$). ML213 at 1 µM and 10 µM had no significant effect on absorbance **(Figure 3.20, B).**

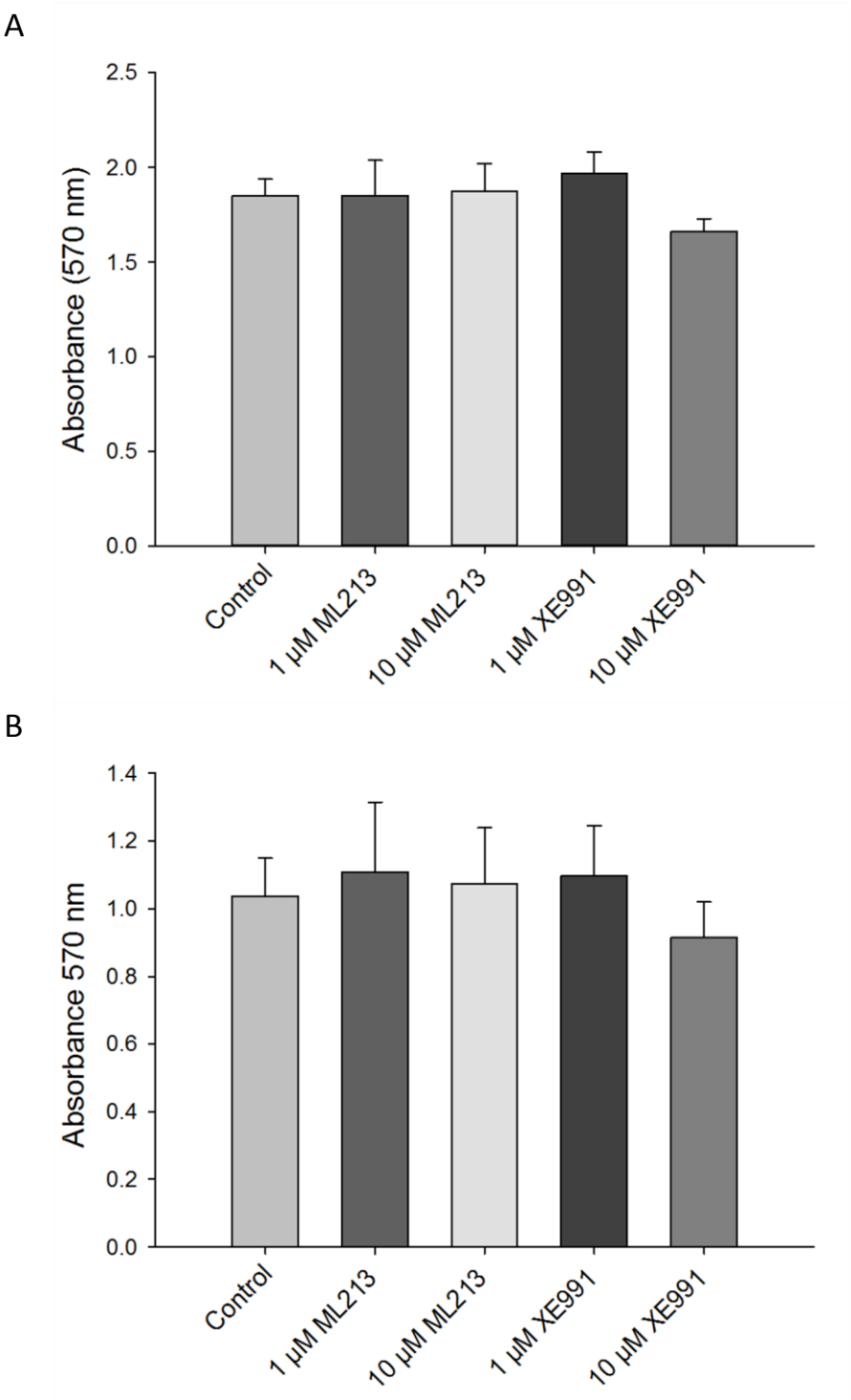

Figure 3.20: Assessment of BE2C and SKNAS cell viability after 72 hours treatment with Kv7 channel modulators. Cell viability was measured using MTT assay. **(A)** BE2C cells (n=4) **(B)** SKNAS cells (n=3). Absorbance at 570 nm was corrected for background. Data represents mean ± SEM.

Overall, despite the lack of statistical significance, the pattern of results suggested that culturing BE2C and SKNAS cells with 10 µM XE991 caused a reduction in the number of viable cells. However, given that the lower concentration of XE991 (1 µM) increased the number of viable BE2C cells and had no effect on SKNAS cells, it was possible that this effect was due to cytotoxicity of the drug at higher concentrations. An alternative rationale for the observed reduction in cell viability may be that XE991 exerted an anti-proliferative effect in both cell lines. This was investigated through an immunofluorescence-based proliferation assay **(Section 3.6.2)**.

3.6.2 Immunofluorescence proliferation assay

Assessment of cell viability by MTT assay demonstrated a reduction in the number of viable cells in response to the 10 µM XE991 in BE2C and SKNAS cell lines **(Figure 3.20)**. To determine if this effect was due to a reduction in cell proliferation, the effect of Kv7 modulating compounds on cell proliferation was assessed using a Ki67 immunofluorescence assay.

3.6.2.1 Overview

Ki67 is preferentially expressed during the G1, S, G2 and M phases of the cell cycle and is absent at the protein level during G0, therefore is regarded as a marker of active cell proliferation [233]. Staining cells with a rabbit anti-Ki67 antibody and labelling with goat anti-rabbit secondary antibody conjugated with Alexa Fluor 594 (red) **(Figure 3.21, A)** enabled identification of proliferating cells whilst counterstaining with DAPI allowed identification of the cell nucleus so the total number of cells present **(Figure 3.21, B)**. The number of Ki67 positive cells were expressed as a percentage of DAPI-stained nuclei to allow determination of the Ki67 proliferation index.

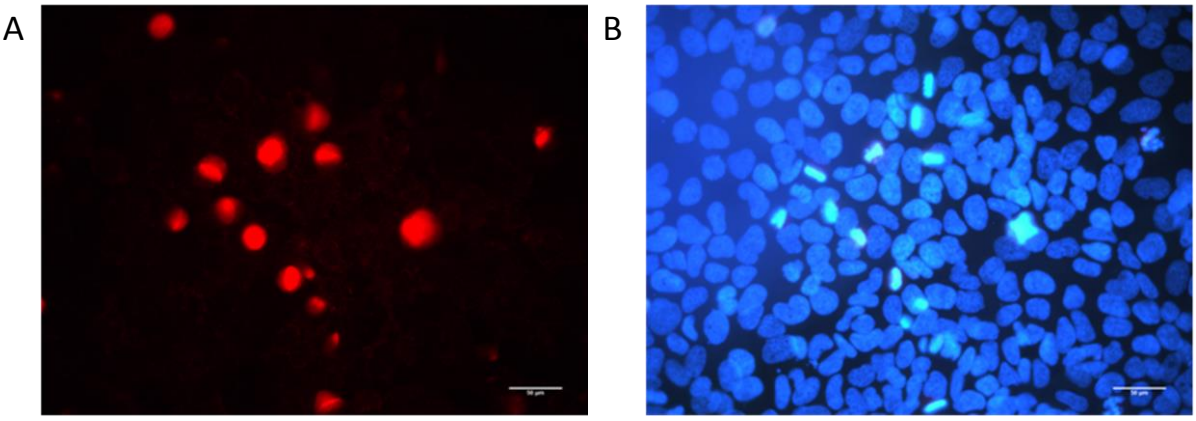

Figure 3.21: Paired images of DAPI and Ki-67 staining. **(A)** Ki67 stained nuclei, multiple red 'hot spots' are visible. **(B)** DAPI-stained nuclei were counted in each field.

3.6.2.2 Effect of Kv7 channel modulation on BE2C and SKNAS cell proliferation

BE2C and SKNAS cells were cultured with 1 µM and 10 µM ML213 and XE991 for 72 hours, after which cells were stained with a mouse anti-Ki67 antibody and a goat anti-mouse secondary antibody conjugated with Alexa Fluor 594. Two concentrations of ML213 and XE991 were tested to determine if a dose response effect could be observed. XE991 and ML213 are inhibitor and activator of Kv7 channels, respectively

Relative to the control, 1µM and 10 µM XE991 caused a 13.33 ± 3.94% ($p > 0.05$) and 32.85 ± 5.87% ($p < 0.05$) reduction in BE2C cell proliferation, respectively **(Figure 3.22)**. 10 µM ML213 caused a 14.61 ± 10.11% increase in BE2C cell proliferation ($p > 0.05$). This suggests that KCNQ2/Kv7.2 has a role in BE2C cell proliferation.

In SKNAS cells, 10 µM ML213 caused a 0.39 ± 2.99% decrease in cell proliferation. 10 µM XE991 caused a 0.95 ± 1.22% reduction in cell proliferation. Therefore, it was concluded that Kv7 modulation had no significant effect on SKNAS cell proliferation **(Figure 3.23)**.

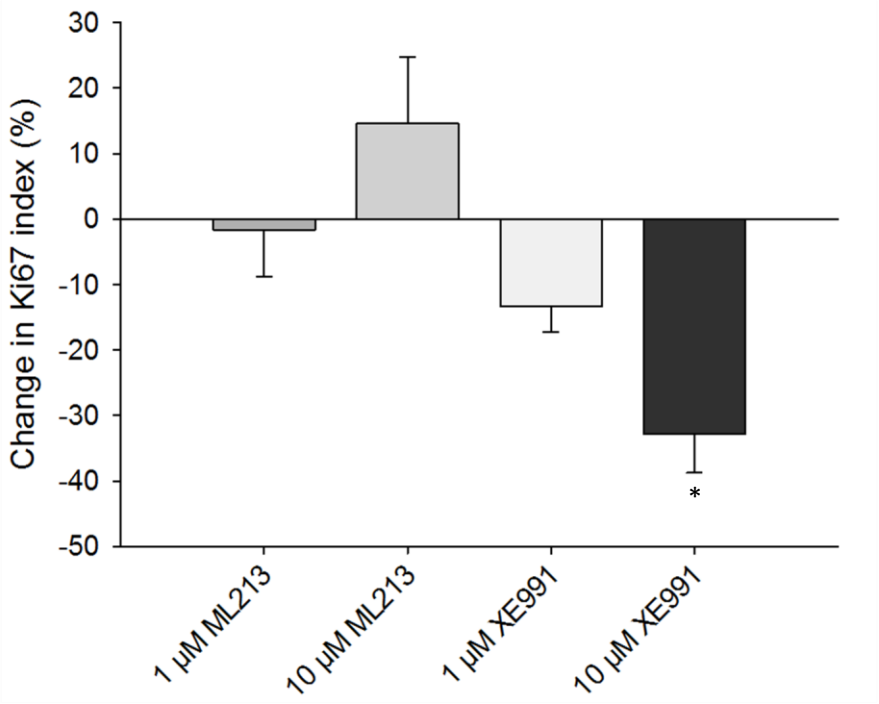

Figure 3.22: Effect of Kv7 modulation on BE2C cell proliferation. Ki67 index= number of Ki67 positive expressed as a percentage of the total number of cells. Data presented relative to control. Data represents mean ± SEM (n=9).

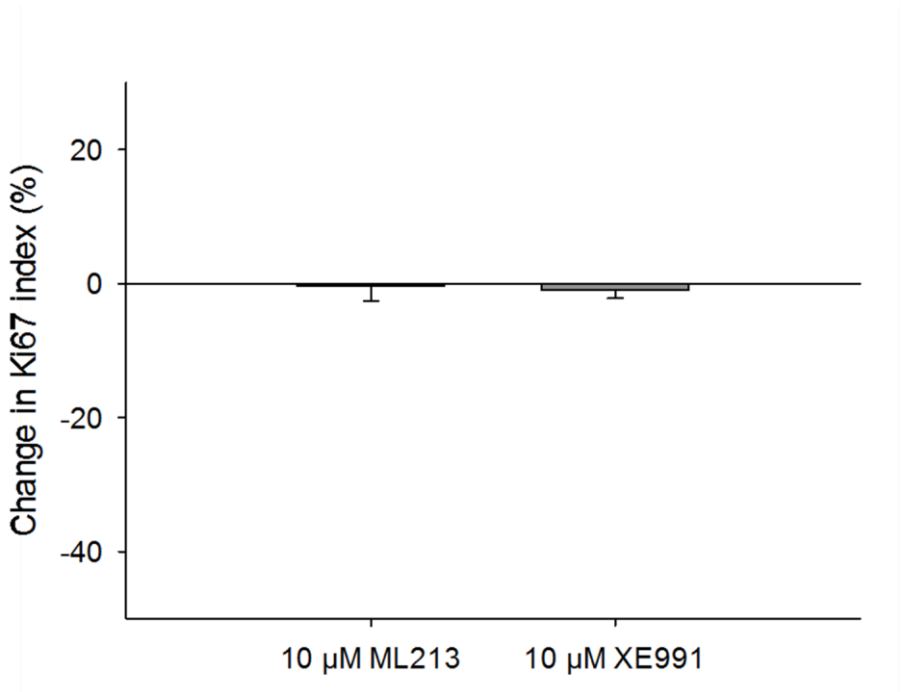

Figure 3.23: Effect of Kv7 modulation on SKNAS cell proliferation. Ki67 index= number of Ki67 positive expressed as a percentage of the total number of cells. Data presented relative to control. Data represents mean ± SEM (n=6).

3.6.3 Cell cycle analysis

Fluorescence activated cell sorting (FACS) was utilised to analyse the cell cycle in BE2C cells. XE991 demonstrated a significant reduction in cell proliferation. ML213 caused an increase in cell proliferation, although this did not reach significance **(Figure 3.22)**. Preliminary experiments involved characterising the cell cycle in BE2C and SKNAS cells and assessing the influence of contact inhibition on BE2C cells. This was followed by determining if Kv7 modulation affected BE2C proliferation through affecting the cell cycle. Kv7 modulating compounds did not demonstrate an effect on SKNAS cell proliferation **(Figure 3.23)**, therefore cell cycle analysis in response to these compounds was not conducted.

3.6.3.1 Overview

FACS is based on the principle of using flow cytometry to sort single cells based on the fluorescent properties of a dye. An application of FACS is cell cycle analysis. This is based on the premise that cells in the Gap 0 (G0) or Gap 1 (G1) phases of the cell cycle possess diploid chromosomal and DNA content, whereas cells in Gap 2 (G2) and just prior to mitosis (M) contain exactly double the DNA content **(Figure 3.25)**. Hoechst 33342 is a dye that binds stoichiometrically to double-stranded DNA, therefore Hoechst labelled cells in the G2/M phase will emit twice the fluorescence.

3.6.3.2 Gating

Analysis of flow cytometry data is fundamentally based on the principle of gating. The parameters used to determine gates are forward scatter (FSC) and side scatter (SSC) and give an estimation of the size and granularity of cells, respectively. Gating is an essential step in analysis to eliminate to cell debris, non-viable cells, doublets or clumps prior to cell cycle analysis. Gates are defined by drawing polygons around a population of cells and only cells within defined gates are carried forward for analysis.

Processed cells labelled with Hoechst 33342 were gated on cell size and granularity by plotting side scatter (SSC) against forward scatter (FSC). Cells with low FSC and SSC were considered to be non-viable or cellular debris and excluded from analysis **(Figure 3.24, A)**.

The next step was to remove doublets and cell clumps from the analysis. Doublets and cell clumps fluoresce at the same wavelength as a cell with truly double DNA content, thereby producing a false-positive result. Single cells truly in G2 will have a smaller width than doublet cells. Plotting forward scatter-height against forward scatter-width allowed identification and exclusion of doublets and cell clumps **(Figure 3.24, B)**.

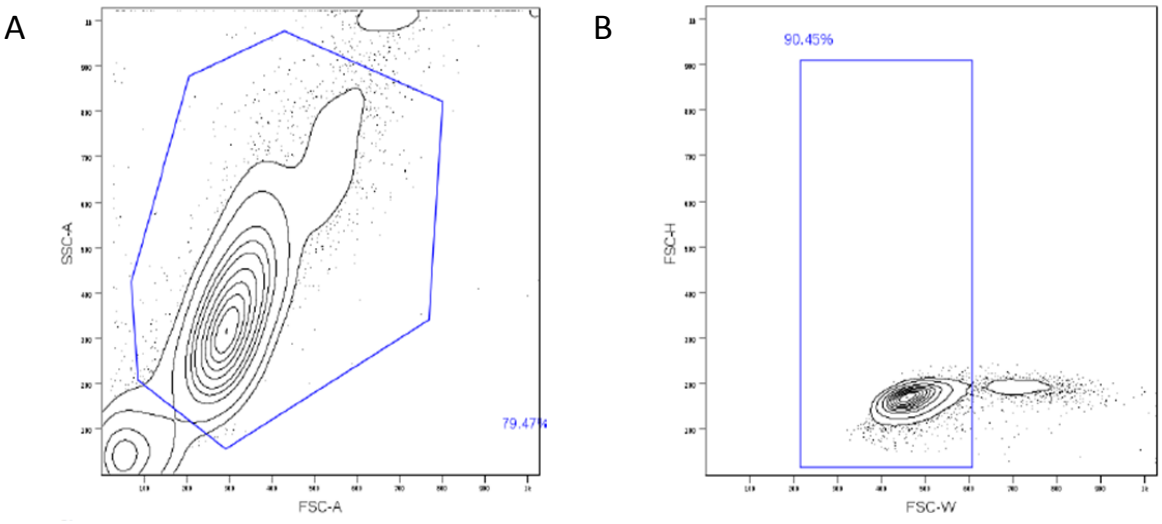

Figure 3.24: BE2C cell population gating scatter plots from one experiment. (A) Scatter plot showing the size and granularity of the BE2C cell population, 20.53% of cells read were excluded from further analysis. **(B)** Scatter plot showing doublet cell and cell clump exclusion, 9.60% cells were excluded from further analysis.

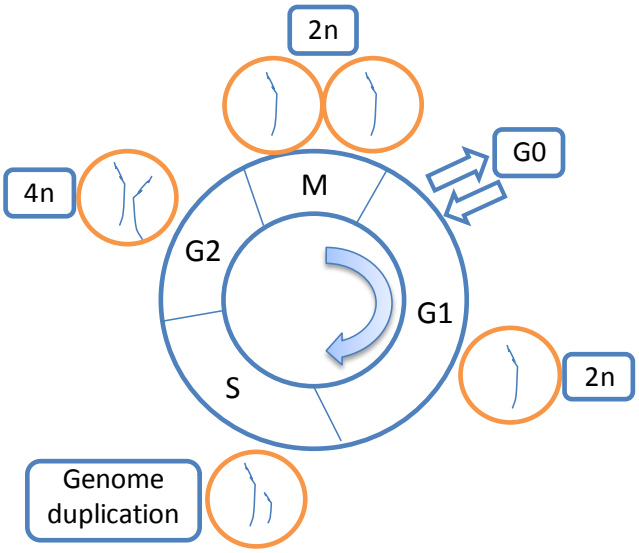

Figure 3.25: Schematic presentation of the cell cycle. The cell cycle is a series of highly regulated steps that govern cell proliferation and has four phases: Gap 1 (G1), Synthesis (S), Gap 2 (G2) and Mitosis (M). During G1 the cell increases the number of its organelles and grows in size, DNA content at this point is diploid (2n). Cells can enter or exit the cycle at G0 if dependent on the presence of mitogenic stimulation. Once a cell passes the restriction point it is committed to progressing to division. The ensuing S phase starts when DNA synthesis commences; when complete DNA content is hyperdiploid (4n). G2 allows replicated to be checked for errors prior to mitosis. The relatively brief M phase is the process by which the cell separates the nuclei, cytoplasm, organelles and cell membrane are divided into two identical daughter cells.

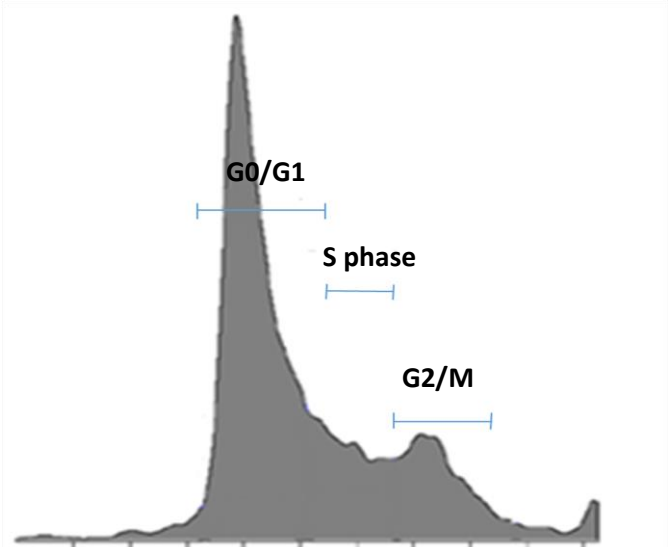

Figure 3.26: Example of labelled cell cycle histogram. The cell cycle histogram generated by FACS is divided into three distinct phases. The DNA content G0/G1 cells is diploid (2n), intermediate during S phase (2n-4n) intermediate DNA content and DNA content is hyperdiploid (4n) at G2/M. Two distinct peaks visible, the first represents the proportion of cell in the G0/G1 phase, these cells have diploid DNA content. The second peak represents the proportion of cells in the G2/M phase, these cells have hyperdiploid DNA content thus emit twice the fluorescence.

3.6.3.3 Characterising the cell cycle in BE2C and SKNAS cells

Preliminary experiments involved comparing the cell cycles of untreated BE2C and SKNAS cells. Cells were labelled with Hoechst 33342 and cell cycle analysis was conducted. A difference in the proportion of cells in each phase of the cell cycle phases was observed between BE2C and SKNAS cells. In BE2C **(Figure 3.27, A)** there were more cells in the S phase, whereas in SKNAS **(Figure 3.27, B)** more a greater proportion of cells were in the G2/M phase. There percentage of cells in the G0/G1 in both cell lines was similar.

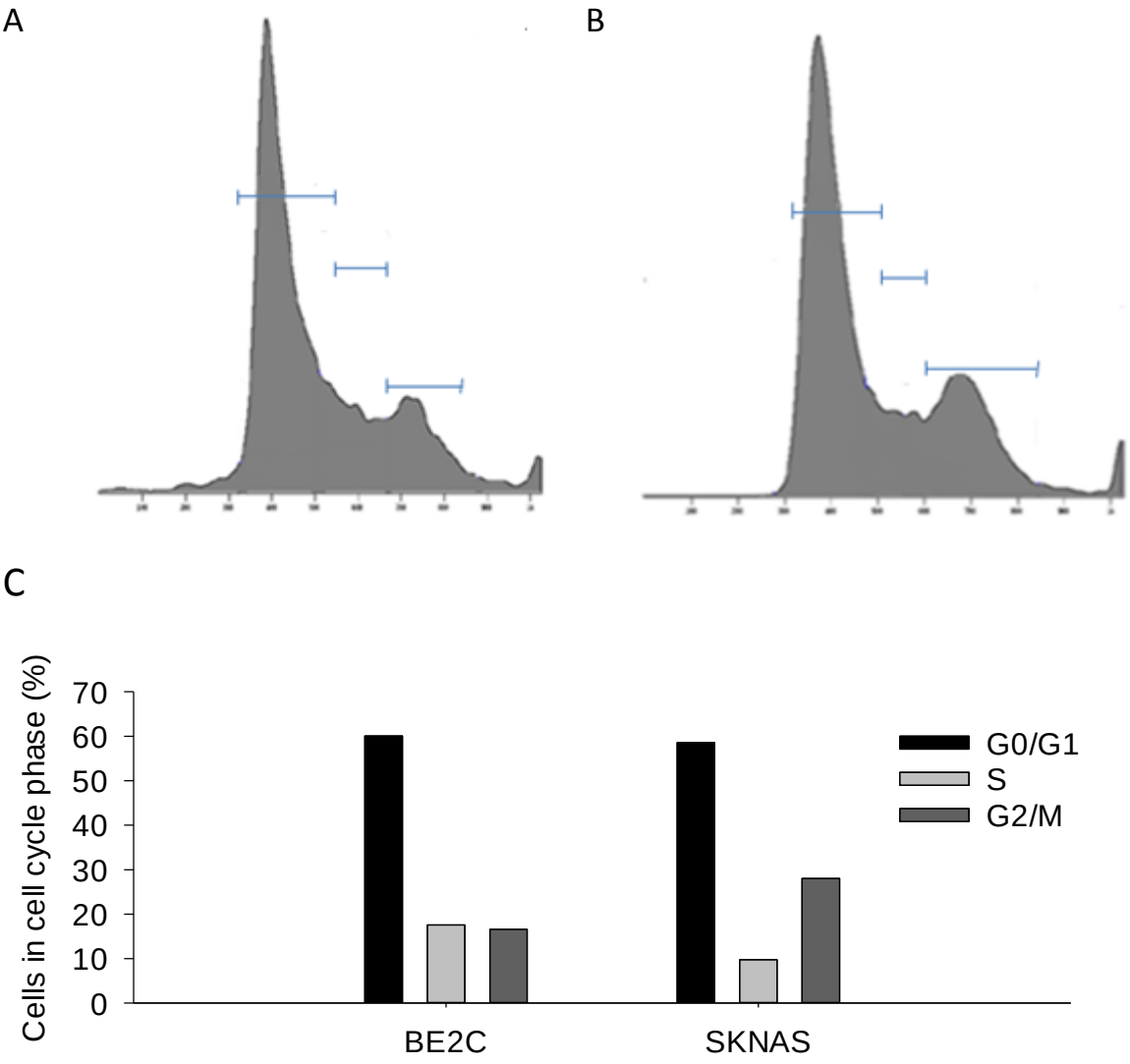

Figure 3.27: Cell cycle analysis of untreated population of BE2C and SKNAS cells. Cell cycle histograms generated by FACS show the distribution of cells in each phase of the cell cycle for untreated **(A)** BE2C cells **(B)** SKNAS cells **(C)** The percentage of cells in each phase of the cell cycle are given (n=1).

3.6.3.4 Effect of cell density on BE2C cell division

Density limitation of cell proliferation, also referred to as contact inhibition, is the process of arresting cell division when cells reach a high density. In culture, the growth of proliferating cells is often arrested once a confluent monolayer is established. This is an important anti-neoplastic mechanism which is often lost in cancer cells [234]. Loss of density limited cell proliferation in BE2C cells was apparent when as cells formed clusters and multiple layers in culture. To quantitatively evaluate this property, BE2C cells were cultured to obtain a highly dense population of cells (100% confluency) and a less dense population of cells (50% confluency). Cell cycle analysis of both populations of cells found similar cell cycle profiles in both populations of cells, indicating BE2C cell growth does not arrest at a high cell density **(Figure 3.28)**.

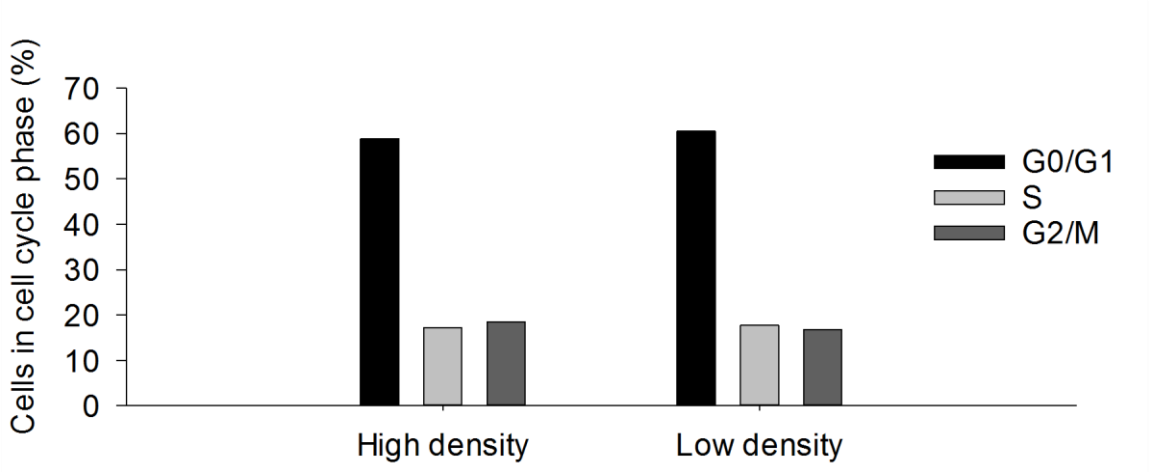

Figure 3.28: Cell cycle analysis of high and low density populations of BE2C cells. The percentage of cells in each phase of the cell cycle are given. **(A)** Cells grown to high density i.e. 100% confluency **(B)** Cells grown to low density i.e. 50% confluency (n=1).

3.6.3.5 Effect of cell cycle inhibition in BE2C cells

Palbociclib is a potent inducer of cell cycle arrest at the G1/S phase of the cell cycle and has been demonstrated to induce G1 arrest in BE2C cells [232, 235]. 5 µM Palbociclib was used as a positive control and significantly reduced the proportion of cells in the G2/M phase of the cell cycle **(Figure 3.29)**. It was concluded Palbociclib mediated cell cycle inhibition leads to fewer actively dividing i.e. cells with hyperdiploid DNA content.

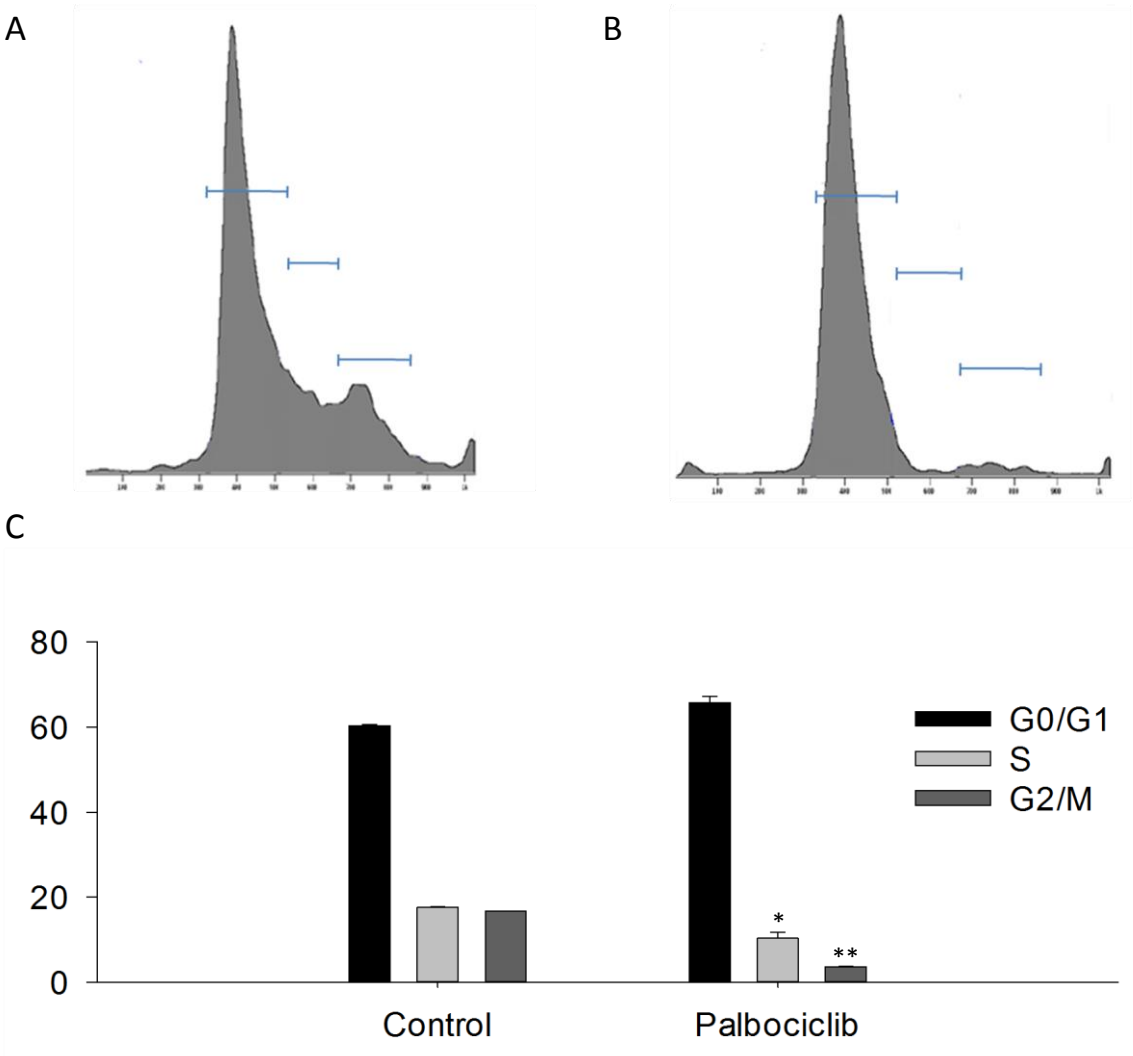

Figure 3.29: Effect of Palbociclib on the cell cycle in BE2C cells. Cell cycle histograms generated by FACS show the distribution of cells in each phase of the cell cycle for **(A)** Control **(B)** 5 µM Palbociclib. **(C)** The percentage of cells in each phase of the cell cycle is given. Data are presented as

3.6.3.6 Effect of Kv7 modulation in BE2C cells

The pattern noticed with ML213 and XE991 was an increase and reduction in BE2C cell proliferation, respectively **(Figure 3.22)**. Therefore, cell cycle analysis was utilised to determine whether Kv7 modulation affected BE2C proliferation through affecting the cell cycle. XE991 and ML213 are inhibitor and activator of Kv7 channels, respectively. Neither 10 µM ML213 nor XE991 demonstrated an effect on the cell cycle **(Figure 3.30)**.

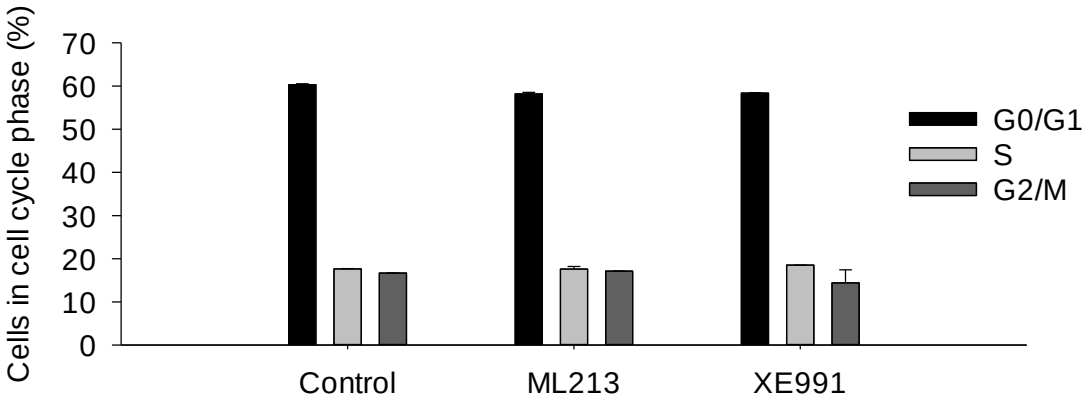

Figure 3.30: Effect of Kv7 channel modulation on BE2C cell cycle. The percentages of cells in each phase of the cell cycle are shown. BE2C cells cultured with 10 µM ML213 and XE991 are compared against the control. Data are presented as mean ± SEM (n=3).

3.7 Assessing the effect of Kv7 inhibition on BE2C cell differentiation

3.7.1 Effect of XE991 on morphology of BE2C cells

Aberrant differentiation is a feature of many cancers, including neuroblastoma. Mutations causing disruption to normal signalling pathways leads to deregulation of proteins required for differentiation. Inducing terminal differentiation of cancer cells reduces their proliferative capacity and promotes apoptosis. In addition, compared with traditional chemotherapy, differentiation therapy causes relatively little damage to normal cells [236]. Therefore, pharmacological agents capable of inducing neuroblast differentiation are important candidates for novel therapeutic compounds. A commonly measured characteristic of neuroblastic differentiation is neurite extension. A neurite refers to any projection from the cell body of a neuron whose length equals or exceeds that of the cell body [237]. To investigate the differentiating properties of XE991 BE2C cells were cultured with 10 μM XE991 for 72 hours. Cells were viewed under fluorescence microscopy and cell surface projections, akin to neurite extensions were observed in some cells **(Figure 3.31, B)**. Morphological changes were compared with cells cultured with DMSO **(Figure 3.31, A)**.

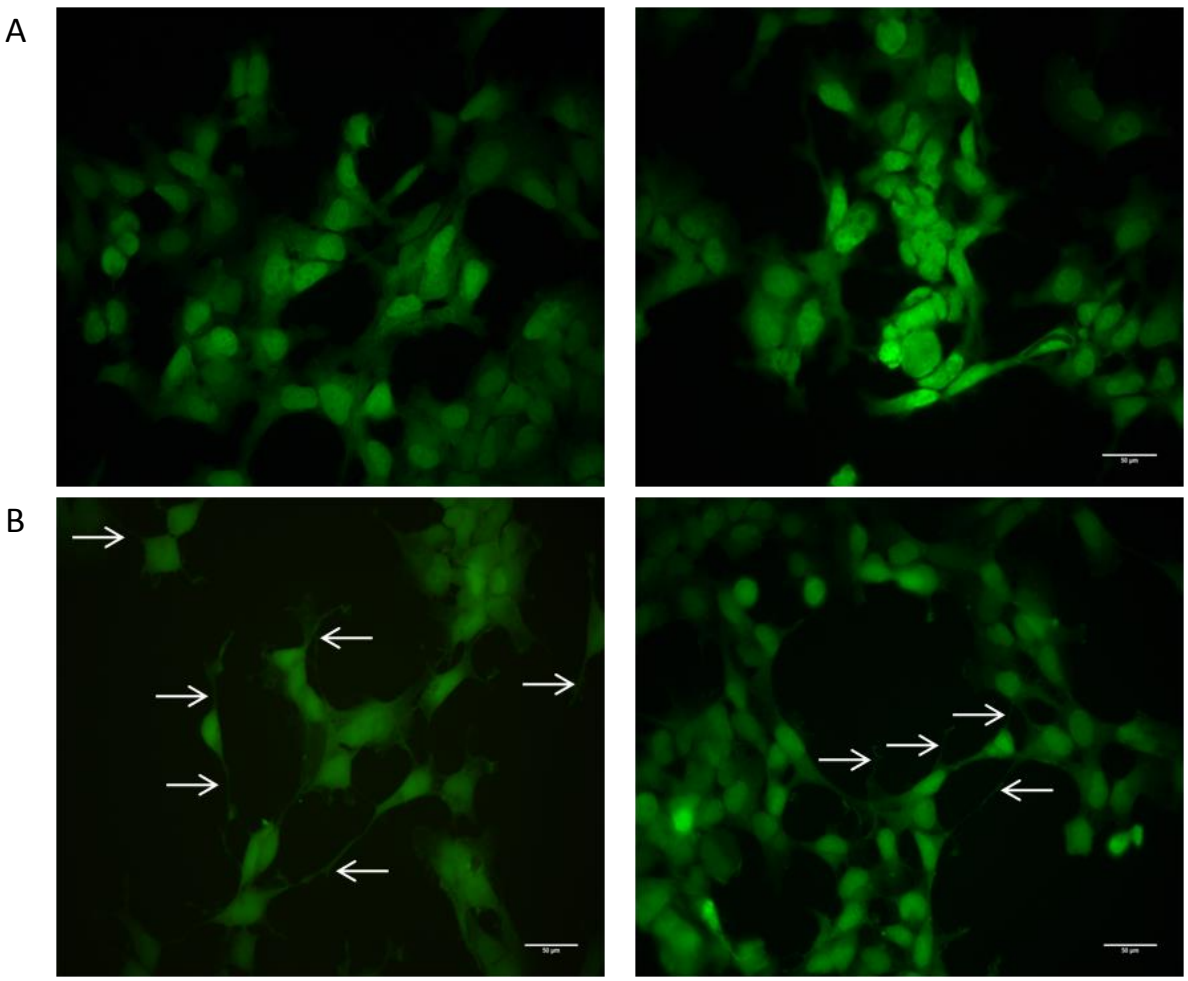

Figure 3.31: Effect of DMSO and XE991 on BE2C cell morphology. (A) BE2C cells treated with DMSO did not demonstrate changes in morphology after 72 hours. **(B)** XE991 treated cells demonstrated cellular processes (white arrows) indicative of neurite extensions (n=3 independent replicates).

3.7.2 Effect of XE991 on differentiation markers in BE2C cells

Based on the evidence of observed morphological changes, XE991 may have had a differentiating effect on BE2C cells **(Section 3.7.1)**. To further investigate this, quantitative assessment of cellular differentiation was undertaken using qPCR. Genes which demonstrate large fold changes upon neuroblastoma cell differentiation were selected: KLF4, STMN4 and ROBO2 [226]. KLF4 is a stem cell marker involved in the regulation of differentiation and its expression would be expected to decrease in differentiated cells [238]. STMN4 and ROBO2 are involved in neuronal differentiation. ROBO2 is also involved in regulation of the actin cytoskeleton and axon development. Expression of both would be expected to increase in differentiated cells [239, 240].

BE2C cells were cultured with 10 µM XE991 for 72 hours after which RNA extraction, cDNA synthesis and qPCR were conducted. In keeping with the low level of morphological changes observed, there was no significant difference in the expression of KLF4, ROBO2 and STMN in XE991 treated cells compared with DMSO treated cells **(Figure 3.32)**.

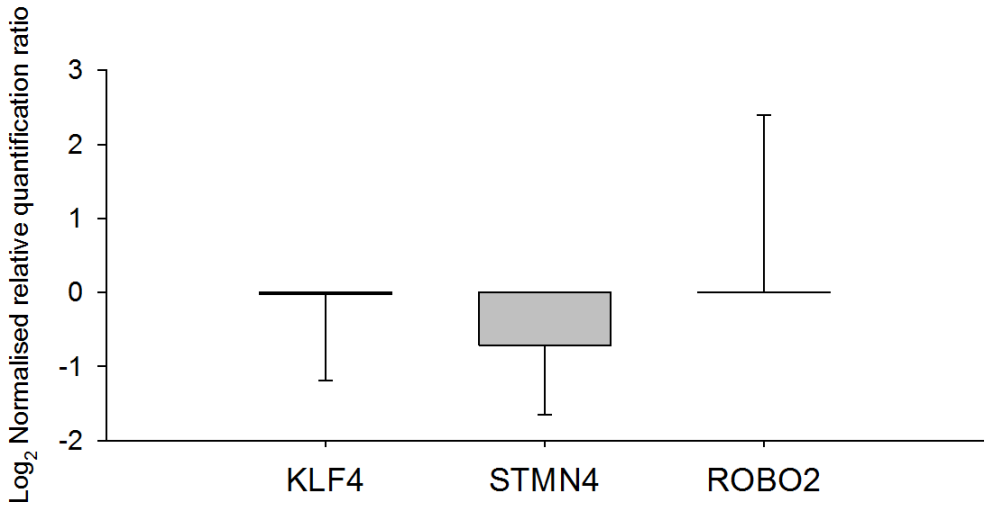

Figure 3.32: Relative expression of differentiation genes in response to 10 µM XE991.
Normalised relative quantification ratio of differentiation genes between XE991 treated BE2C cells and DMSO treated cells. Data represents mean ± SEM (n=3)

3.8 Effect of cellular differentiation on KCNQ2 expression in BE2C cells

Results from bioinformatic database search found KCNQ2 expression was significantly greater in neuroblastoma tumours compared to more histologically mature neuroblastic tumours: ganglioneuromas and ganglioneuroblastomas **(Section 3.1.1)**. This led to the hypothesis that high KCNQ2 expression may be a marker of less differentiated cells. In our laboratory it has been demonstrated that BE2C cell differentiation can be induced by culturing cells with 5 µM Palbociclib (Rasha Swadi, University of Liverpool), an effect that is not seen in SKNAS cells. BE2C cell differentiation was induced by culturing BE2C cells with 5 µM Palbociclib. After 72 hours, significant morphological evidence of differentiation was observed in Palbociclib treated cells **(Figure 3.33)**. RNA was extracted from control (DMSO) and Palbociclib treated cells, followed by cDNA synthesis and qPCR. There was no significant difference in KCNQ2 expression between differentiated and undifferentiated BE2C cells.

A B

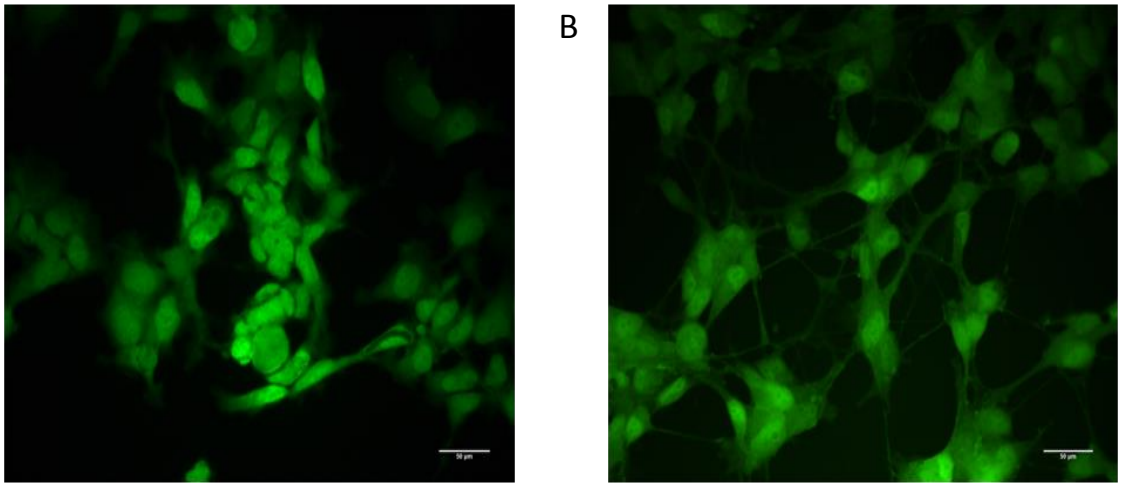

Figure 3.33: Morphological appearance of BE2C cells after 72 hours treatment with Palbociclib. **(A)** BE2C cells cultured with DMSO **(B)** BE2C cultured with 5 µM Palbociclib. Extensive neurite extensions are visible which are indicative of neuroblast differentiation.

3.9 Assessing the effect of XE991 on BE2C cell proliferation *in vivo* using the chick embryo model

It has been previously demonstrated that the BE2C cell line could form tumours using the chick embryo model and the protocol for carrying this out has been optimised within our laboratory.

3.9.1 Tumour formation

XE991 had demonstrated a reduction in BE2C cell proliferation *in vitro*, therefore the same cell line was used to generate tumours in the chick embryo to investigate the anti-proliferative effect of XE991 *in vivo*. Fertilised chick eggs were incubated for a 7 day period (E0 to E7). At E7 GFP-labelled BE2C cells were topically implanted onto the surface of the chorioallantoic membrane (CAM) of the developing chick embryo in order to form tumours. At E11, in eggs where tumours were detectable, XE991 was topically administered to the surface of the CAM. XE991 was dissolved in PBS, therefore control tumours were left untreated. At E14, tumours were visible underneath the surface of the CAM under light microscopy **(Figure 3.34, A)** and were also viewed under fluorescence to detect GFP-labelled cells **(Figure 3.34, B)**. Successful tumour formation was variable and a common outcome of topical implantation of cells was a failure to invade the CAM, with cells remaining on the surface. Where tumours had successfully been formed they were dissected as discrete masses, fixed in PFA and embedded in paraffin prior to Ki67 staining. **Figure 3.35** summarises the survival of embryos and tumour formation.

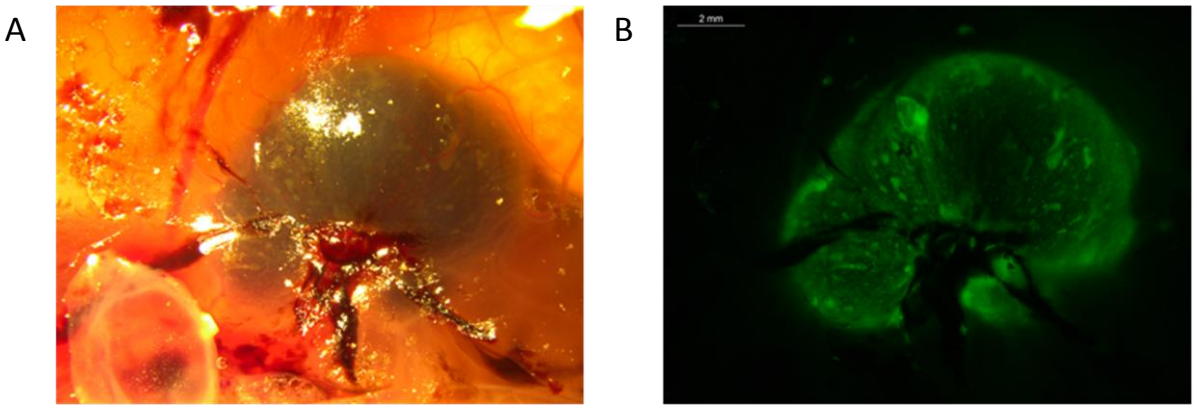

Figure 3.34: Example of a BE2C tumour imaged in vivo. (A) Paired bright-field **(B)** Green fluorescence images of a BE2C tumour in vivo, prior to dissection. Tumours form underneath the surface of the chorioallantoic membrane as a discrete, highly vascularised mass.

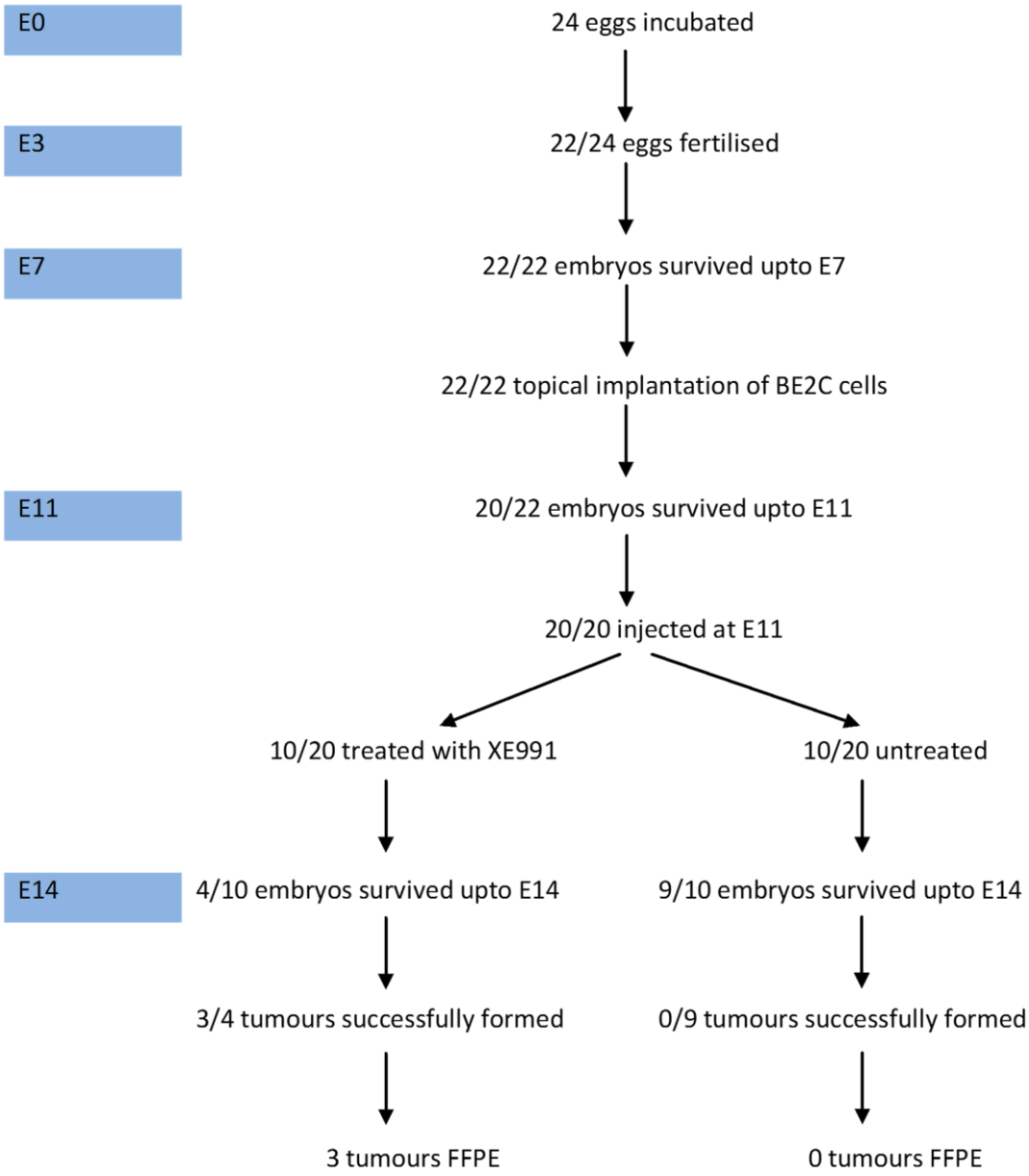

Figure 3.35: Flow chart depicting chick embryo survival and tumour formation. Fertilised eggs were incubated for 3 days prior to windowing. At E3 a window was created in the shell to allow access to the embryo and surrounding membranes and monitor embryo survival. Unfertilised eggs were discarded. At E7 surviving embryos were carried forward and BE2C cells were topically implanted on the surface of the CAM. At E11 XE991 was injected into the allantois of surviving embryos or left untreated. At E14 survival was reassessed and where evident tumours were dissected and stored.

3.9.2 Ki67 immunohistochemical staining of tumour sections

3.9.2.1 Immunohistochemistry controls

To confirm positive immunostaining, tonsillar tissue was utilised as control tissue and a positive and negative control were used. The first control was a positive control, tonsillar tissue is expected to express Ki67 and positive staining was observed on visual examination **(Figure 3.35, A)**. For the second control, an isotype control was used to demonstrate the specificity of the Ki67 antibody and no staining was visible under visual examination **(Figure 3.35, B)**.

3.9.2.2 Ki67 detection in control and XE991 treated tumours

Formalin-fixed, paraffin embedded (FFPE) sections obtained from control **(Figure 3.36, A)** and XE991 treated **(Figure 3.36, B)** tumours were stained for Ki67 to determine proliferative index. Three XE991 tumours were sectioned and stained, however no control tumours were successfully obtained. Two pre-sectioned tumours were provided by Rasha Swadi, University of Liverpool, to conduct Ki67 staining. Immunohistochemical detection of Ki67 in control and XE991 treated tumours was not significantly different, therefore it was determined that XE991 did not reduce BE2C cell proliferation *in vivo*.

A

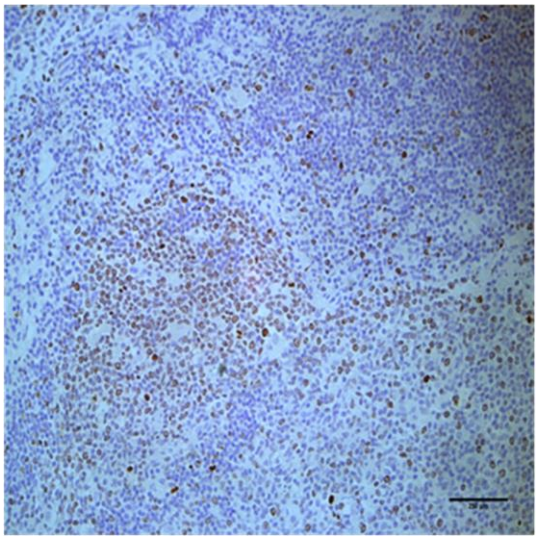

B

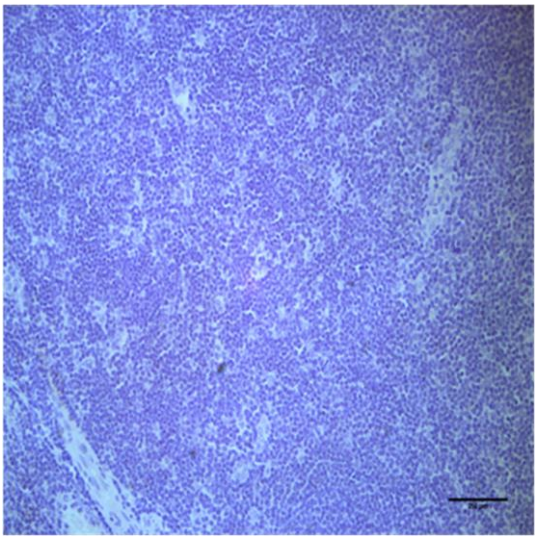

Figure 3.35: Ki67 and Haematoxylin staining of tonsillar tissue. (A) Positive control, brown spots visible throughout tissue represent positive Ki67 staining. **(B)** Negative control, isotype negative control, no brown spots are visible, thus Ki67 staining was not detected.

A

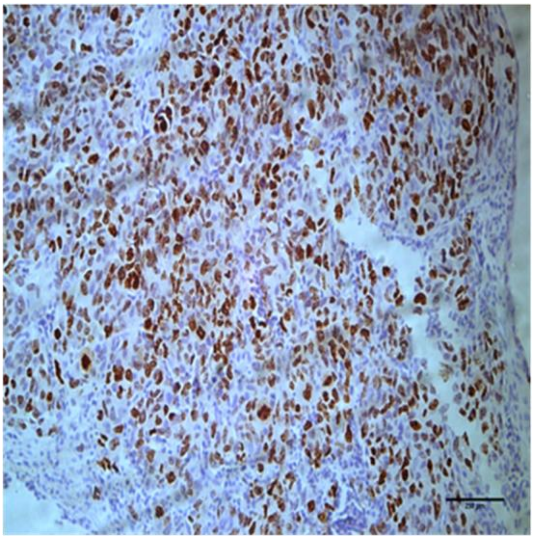

B

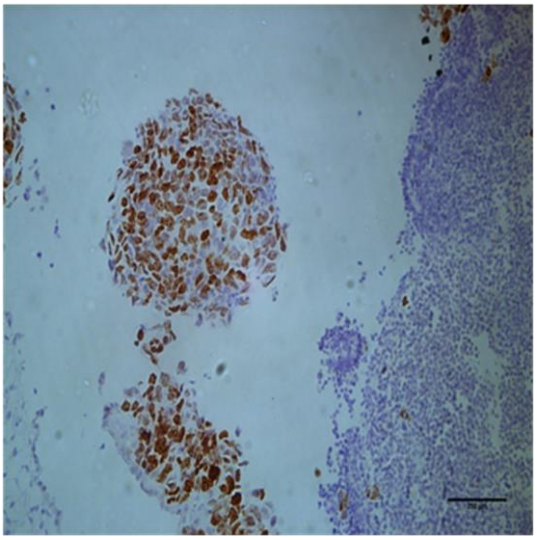

Figure 3.36: Ki67 and Haematoxylin staining of tumour tissue. **(A)** Untreated control **(B)** XE991 treated tumour. Ki67 staining is visible in both tissues. BE2C cells have relatively large nuclei compared with chick tissue which allows the two to be distinguished.

Chapter 4: Discussion

4.1 Rationale

Seminal work by DeCoursey et al. demonstrated that voltage-gated K^+ channels are the predominant channel in proliferative lymphocytes and application of K^+ channel blockers inhibited DNA synthesis [241]. This discovery led to further research which has firmly established the role of K^+ channels in the regulation of the cell cycle and cell proliferation. Furthermore, there is increasing evidence that demonstrates K^+ channels are involved in the regulation of multiple oncological processes including apoptosis, cell migration, metastasis and angiogenesis [144, 145]. The EAG subfamily of voltage-gated K^+ channels has been extensively studied in a number of cancer types. With regards to neuroblastoma, most studies evaluating the expression and influence on cell behaviour of K^+ channels in neuroblastoma have focused on a single member of the EAG family, the hERG channel [214-220]. The aim of this study was to build upon the existing knowledge of the role of K^+ channels in neuroblastoma and investigate whether K^+ channels contribute to neuroblastoma tumour development and progression. This was carried out by evaluating K^+ channel expression and function in primary neuroblastoma tumours and cell lines. Following this, the next set of experiments aimed to evaluate the effect of K^+ channel modulation on cell behaviour was then assessed *in vitro* and *in vivo*.

4.2 K^+ expression in primary neuroblastoma tumours and cell lines

An initial bioinformatic screen identified the 5 K^+ channel genes with the highest relative expression in primary neuroblastoma tumours: KCNQ2, KCNMA1, KCNH2, KCNG1 and KCNB1. These 5 channels were selected for *in vitro* assessment. 4 of these channels (KCNQ2, KNH2, KCNG1 and KCNB1) belong to the voltage-gated K^+ channel superfamily (Kv) and there is substantial evidence to support the oncogenic potential of Kv channels [193, 207]. KCNQ2 has been comprehensively studied in the context of neurological disorders [175]; however its role in cancer has yet to be extensively explored. KNCQ2 was shown to be expressed in certain breast cancer cell lines and pharmacological inhibition led to reduced cell proliferation [242]. KCNMA1 (BKCa, big conductance calcium-activated potassium channel) has been strongly implicated in human cancers and has been shown to be overexpressed in human prostate cancer [243] and breast cancer [244, 245]. However, one study demonstrated KCNMA1 acts as a tumour suppressor in gastric cancer [246]. The role of KCNH2 (Kv11.1/hERG) in cancer has been widely studied and has been demonstrated to be overexpressed in a multitude of human cancers including endometrial cancer, leukaemia, colorectal cancer, glioblastoma multiforme [196]. KCNB1 (Kv2.1) was found to be expressed in endometrial cancer cells and channel inhibition reduces cell proliferation [247]. There is no existing evidence implicating KCNG1 (Kv6.1) in cancer.

Following the bioinformatic screen K^+ channel gene expression in two neuroblastoma cell lines was assessed by qPCR. Clinically, the presence of MYCN amplification and chromosome 11q deletion are two features of primary neuroblastoma tumours which confer high risk [37]. Therefore, two neuroblastoma derived cell lines representative of these features, BE2C and SKNAS, were selected for *in vitro* studies. BE2C is a MYCN amplified neuroblastoma cell lines, whereas SKNAS cells possess chromosome 11q deletion.

KCNQ2 was found to be highly expressed in BE2C cells and expression of KCNQ2 was 101 fold greater in BE2C relative to SKNAS cells **(Figure 3.7)**. A previous study has demonstrated KCNQ2 is expressed in IMR-32 neuroblastoma cells, which share similar characteristics to BE2C cells e.g. MYCN amplification [248]. Neuroblastic cells represent neoplastic proliferation of the precursor cells to sympathetic ganglion neurons and characterisation of marker genes demonstrates that neuroblastoma cells have sympathetic neuronal properties [249, 250]. It is known that in sympathetic ganglion neurons Kv7.2 homomers and Kv7.2/3 heteromers coassemble to form M-channels [172]. Therefore, high expression of KCNQ2 in BE2C cells may reflect the expected acquisition of normal neuronal properties in developing sympathetic ganglion cells, prior to their malignant transformation. Conversely, it is plausible that high expression of KCNQ2 observed in BE2C cells contributes to its aggressive phenotype.

With regards to other K^+ channel genes investigated this study, KCNH2/hERG demonstrated low expression in both cell lines. This was surprising given previous investigations have demonstrated a significant role for KCNH2 expression in the SH-SY5Y neuroblastoma cell lines [214-220]. However, this may be reflective of the heterogeneity of K^+ channel expression in neuroblastoma cell lines. Overexpression of KCNMA1 has been implicated to have oncogenic potential in other cancers [243-245], however in this study relatively low expression was observed in both cell lines. Despite demonstrating relatively high expression in primary neuroblastoma tumours, expression of KCNB1 was low in BE2C and SKNAS cells; however this must be interpreted with consideration for inadequate primer efficiency.

In this study protein expression of Kv7.2 was initially investigated by western blotting. The Kv7.2 protein has an estimated molecular weight of 96 kDa and a band at this molecular weight was detected in both BE2C and SKNAS cell lysate using two different anti-Kv7.2 antibodies. However, additional bands were also detected at higher and lower molecular weights. The appearance of multiple bands suggested possible non-specific binding of the primary antibody which limited the interpretation of western blotting results in this study. Consequently the band of interest identified at 96 kDa may have also be non-specific. An alternative explanation for the presence of multiple

bands is the concentration of primary antibody used may have been too high. This may have been amended by using a lower concentration or using a series of dilutions to optimise the concentration. Nevertheless, there are alternative explanations for the presence of multiple bands unrelated to the specificity or concentration of the antibody. Bands at higher molecular weights may have been due to unresolved protein multimers or post-translational protein modifications e.g. phosphorylation, glycosylation, ubiquitination. Conversely, bands at a lower molecular weight may have been due to detection of a degraded/cleaved form or a splice variant of the protein of interest.

There are multiple methods by which the specificity of a primary antibody may have been investigated. A common method is the use of a positive control i.e. a lysate in which the protein of interest is known to be expressed. For example, Kv7.2 is known to be expressed in rat sympathetic neurons [180], thus lysate derived from this source could have been used to assess antibody specificity. A positive result would have indicated the antibody is identifying Kv7.2. In addition, where available, application of a controlled peptide is an alternative method of validating the primary antibody. The primary antibody would be pre-incubated with the controlled peptide, a peptide which corresponds with the antibody epitope, thus preventing the antibody-epitope interaction and band detection. Furthermore, genetic knockdown of Kv7.2 expression, for example by RNA interference, in BE2C and SKNAS cells would have been a robust method by which antibody specificity could have been demonstrated. Through inhibition of mRNA translation, Kv7.2 expression would have been inhibited, the primary antibody would not have detected the epitope and a lack of band detection in the knockdown cell lysate would have demonstrated that the anti-Kv7.2 antibody is correctly binding to Kv7.2. With regards to the secondary antibody, non-specific binding of the secondary antibody may have also caused the detection of multiple bands; a no primary antibody control i.e. omitting addition of the primary antibody would have been a method to assess secondary antibody specificity.

In this study the first anti-Kv7.2 antibody detected possible Kv7.2 expression in both BE2C and SKNAS cells. The second anti-Kv7.2 antibody tested showed possible expression of Kv7.2 in BE2C cells and no detectable expression of Kv7.2 in SKNAS cells. Overall, the results of western blotting were consistent with the results of qPCR. Both methods demonstrated that KCNQ2/Kv7.2 expression is greater in BE2C cells compared with SKNAS cells. The observed fold difference in KCNQ2/Kv7.2 expression determined by western blotting was significantly lower than the fold difference in expression identified by qPCR, although this was only based on a single replicate. Nevertheless, the degree of correlation between gene and protein correlation is notoriously low as there are multiple

processes between gene transcription and translation [251]. In addition, protein degradation may also explain why a high protein to gene to protein expression ratio was observed.

In this study assessment of Kv7.2 expression by immunocytochemistry was relatively inconclusive. Fluorescence was observed throughout the cytoplasm of both BE2C and SKNAS cells which suggests Kv7.2 is expressed in the cytoplasm. However Kv7.2 is a transmembrane protein and fluorescence would be expected to be limited to the plasma membrane. This picture may have been distorted as the biogenesis of most transmembrane proteins involves synthesis in the endoplasmic reticulum, modification in the Golgi apparatus and transport across the cytoplasm, therefore the localisation of Kv7.2 may not be strictly to the plasma membrane. An alternative explanation may have been that fluorescence was detected throughout the cytoplasm due to non-specific antibody binding of the primary antibody; this would correlate with the pattern of multiple bands observed by western blotting. In addition, there are limitations of immunocytochemistry to be considered; fluorescence is not permanent, as the samples were examined they underwent photobleaching and fluorescence faded. In addition, cells required fixation and permeabilisation, both of these procedures could have introduced unwanted artifacts.

Furthermore, as mentioned for western blotting, to validate the use of anti-Kv7.2 antibodies for immunocytochemistry both primary and secondary antibody controls could have been employed. There are multiple methods by which the primary antibody may have been validated. Firstly, immunocytochemistry may have been undertaken with a positive control i.e. a cell type known to express Kv7.2 e.g. rat sympathetic ganglion neuron [180]. A negative control, a cell type known not to express Kv7.2, could have been employed and a negative result i.e. no fluorescence detection would have helped to validate the primary antibody. Similarly to western blotting, during immunocytochemistry the primary antibody could have been incubated with a controlled peptide, thus preventing epitope recognition and a negative result would have been expected. An additional method by which the specificity of the primary antibody may have been demonstrated would have been to use the genetic approach and conduct knockdown of KCNQ2 in both BE2C and SKNAS cells. A negative result in knockdown cells would have significantly helped to demonstrate the specificity of the primary antibody. An additional cause of non-specific fluorescence may be non-specific binding of the secondary antibody; employing a no primary antibody control i.e. only incubating cells with the secondary antibody should produce no fluorescent labelling, thereby demonstrating specific binding of the secondary antibody.

Following on from assessing the expression of KCNQ2/Kv7.2 in BE2C and SKNAS cells, the next set of experiments in this study aimed to determine whether the channel was involved in governing

membrane potential. An indirect measure of membrane potential, $DiBAC_4(3)$ fluorescence, was used to determine whether Kv7.2 is functional in BE2C and SKNAS cells. XE991 caused depolarisation of BE2C cell membrane potential. Conversely, ML213 caused hyperpolarisation of BE2C cell membrane potential, although this result did not reach significance. This data indicates that KCNQ2/Kv7.2 is present in the BE2C cell membrane and has a role in regulating membrane potential. Despite qPCR and western blot data suggesting absent or low KCNQ2/Kv7.2 expression a similar pattern was observed in SKNAS cells. XE991 and ML213 caused depolarisation and hyperpolarisation of SKNAS cell membrane potential; however these results did not attain statistical significance. To directly measure ion channel activity patch clamp recordings would have been required.

Given that neither XE991 nor ML213 can be regarded as specific for Kv7.2 channels the results obtained in this study should be interpreted with caution. At the concentration used XE991 inhibits homomeric Kv7.2 and Kv7.1 channels and Kv7.2/3 heteromeric channels and ML213 activates Kv7.2 and Kv7.4 homomeric channels. Previous studies have shown that XE991 is a potent inhibitor of channels formed by Kv7.2 homomeric subunits (IC_{50}= 0.7 μM), Kv7.1 homomeric subunits (IC_{50}= 0.8 μM) and coassembly of Kv7.2/Kv7.3 heteromers (IC_{50}= 0.6 μM) [252]. KCNQ1/Kv7.1 expression has not been previously demonstrated in native sympathetic neurons or neuroblastoma cells. Previous studies have suggested that in early sympathetic ganglion neurons and brain development Kv7.2 subunits are the dominant component of the native M-channel and acquisition of KCNQ3/Kv7.3 expression occurs at a later stage during embryonic development [253, 254]. Given that neuroblastic cells are derived from the precursor cell of sympathetic ganglion neurons, it can be hypothesised that KCNQ2/Kv7.2 homomeric channels predominate in neuroblastoma cells. This would suggest that the effect of XE991 on membrane potential in neuroblastoma cells is through inhibition of KNCQ2/Kv7.2 homomeric channels.

4.3 Role of KCNQ2/Kv7.2 in neuroblastoma cell viability and proliferation

Does expression of KCNQ2/Kv7.2 in neuroblastoma cells drive its malignant phenotype or have no functional significance? To address this question the role of KCNQ2/Kv7.2 in cell viability and proliferation was assessed in both cell lines.

MTT assay was utilised as an initial screen in this study to assess changes in cell viability in response to culturing cells with Kv7 modulating compounds. 10 μM XE991 caused a reduction in cell viability in both BE2C and SKNAS cells, however these results did not attain statistical significance. Previous investigations have shown application of Kv7.2/3 channel openers, N-ethylamide and flupirtine caused cell death in hippocampal neuronal cultures [255, 256].

Cell proliferation was assessed by determining the Ki67 proliferative index. This was achieved by fluorescence microscopy and manual counting. Manual quantification of the Ki67 index is subject to uncertainty caused by unclear immunostaining and human error [257]. In addition, manual methods of quantification may also suffer from bias by deliberate selection of areas of low/high proliferation [258]. To eliminate this potential source of bias, counting was performed blind i.e. the treatment condition was unknown when counting.

10 µM XE991 caused a 33% reduction BE2C cell proliferation. 10 µM ML213 caused a 15% increase in the number of proliferating cells, although this did not attain statistical significance. Opposing effects by the KCNQ2/Kv7.2 activator and inhibitor support the hypothesis that KCNQ2/Kv7.2 is implicated in the regulation of neuroblastoma cell proliferation. There is very limited evidence to suggest that Kv7 channels play a role in cancer cell proliferation [259]. Kv7 channels have been demonstrated to regulate skeletal muscle cell proliferation and differentiation [260, 261].

By what mechanism could inhibition of Kv7 channels inhibit BE2C cell proliferation? It has been demonstrated that membrane potential undergoes rhythmic oscillations during cell cycle progression [145, 146, 196]. During the G1-S transition phase of the cell cycle proliferating cells demonstrate a hyperpolarised membrane potential, as the cell cycle progresses to mitosis membrane potential undergoes depolarisation [198, 262]. This phenomenon has been observed in neuroblastoma cells [262]. Cell-cycle dependent changes in membrane potential are mediated by ion conductance and hyperpolarisation of membrane potential at the G1-S transition point is facilitated by K^+ channel opening. Therefore, outward K^+ currents contribute to cell cycle progression. Further to this, cell proliferation requires an accurate control of cell volume which is governed by cellular osmolality [145, 146]. At the G2-M transition point of the cell cycle, water molecules follow the flux of K^+ and Cl- creating a reduction in cell volume referred to as pre-mitotic condensation (PMC) and impairment of PMC can delay progression of the cell cycle. K^+ efflux appears to contribute to progression of the cell cycle at the G2-M transition phase, thus inhibition of K^+ channels at the G2-M phase may limit cell cycle progression and cell proliferation. To achieve hyperpolarisation of membrane potential and PMC at the G1-S and G2-M transition points of the cell cycle, respectively cancer cells may require increased expression of K^+ channels. Based on our findings KCNQ2/Kv7.2 is highly expressed in BE2C cells. Indeed, rapidly dividing cells are known to have a relatively depolarised membrane potential and in BE2C cells resting membrane potential is -55 ± 3 mV [263]. Resultantly, to achieve membrane potential hyperpolarisation at G1-S and PMC at G2-M BE2C cells may require increased expression of KCNQ2/Kv7.2. Therefore, the anti-proliferative effect of XE991 in BE2C cells may be due to interference with the transient hyperpolarisation

necessary for cells to progress from G1 -S phase and impaired PMC at the G2-M transition. This hypothesis is consistent with the lack of effect of XE991 on cell proliferation in SKNAS cells which demonstrated significantly lower KCNQ2/Kv7.2 expression compared with BE2C cells **(Figure 3.7)**.

Overall modulation of KCNQ2/Kv7.2 seems to affect cell viability and proliferation, however this effect was not observed during cell cycle analysis. If proliferation was arrested an increase in the proportion of cells in the G0/G1 and decrease in S and G2/M phases of the cell cycle would be expected. This may be attributable to an overall small effect size on cell proliferation which was not significant enough to be detected by cell cycle analysis.

4.4 Role of KCNQ2/Kv7.2 in BE2C cell differentiation

Neuroblastoma tumours are capable of spontaneous differentiation to a benign phenotype [99]. Based on this observation many agents which induce differentiation have been tested *in vitro* as an experimental model for *in vivo* maturation of tumours [264, 265]. Differentiation therapy offers an alternative mechanism of action in treating neuroblastoma tumours as inducing differentiation also promotes growth arrest [265]. One of the most potent inducers of differentiation is retinoic acid (RA), an isomer of which, 13-cis RA, is used clinically and results in significantly improved overall survival [103, 130].

The effect of Kv7.2 inhibition on BE2C cell differentiation was initially investigated by assessing cell morphology in response to culturing cells with XE991. BE2C cells demonstrated morphological changes reflective of cellular differentiation i.e. outgrowth of cell surface projections akin to neurite development **(Figure 3.31, B).** These changes were noted across 3 independent replicates, but were only notice in a limited number of cells in each field examined. Also, it must be noted that in comparison with other agents which are capable of inducing BE2C cell differentiation e.g. Palbociclib **(Figure 3.33, B)** these changes were significantly less pronounced.

As cell differentiation is coupled with growth arrest it is possible that XE991 mediated morphological changes BE2C cells are linked to the observed reduction in cell proliferation. Indeed, voltage-gated K^+ channels have been previously implicated in neural, cancer and stem cell differentiation [266-268]. By what mechanism could inhibition of Kv7.2 channels induce BE2C cell differentiation? In this study it was demonstrated that application of XE991 caused depolarisation of BE2C cell membrane potential **(Figure 3.16, B)**. Depolarisation of the membrane potential activates T- type Ca^{2+} channels; Ca^{2+} influx through T-type channels has been shown to promote neurite outgrowth in spinal and hippocampal neurons [268-270]. Furthermore, previous investigations have demonstrated genetic knockdown of KCNQ2 in PC12 cells, which share a common progenitor with neuroblastoma cells,

induced neurite outgrowth and cellular differentiation [271]. Conversely, previous investigations in BE2C cells documented that continuous Ca^{2+} influx allowed maintenance of BE2C cells in an undifferentiated state [272].

Following on from assessing cell morphology, the expression of the differentiation markers, KLF4, STMN4 and ROBO2 in XE991 treated BE2C cells was assessed. Sung et al. demonstrated that retinoic acid induces significant morphological changes and large fold changes in KLF4, STMN4 and ROBO2 expression in neuroblastoma cells [226]. In keeping with the relatively low level of morphological changes seen in XE991 treated BE2C cells, there was no significant change in the expression of KLF4, STMN4 and ROBO2. Overall the data suggests that XE991 may induce mild morphological changes in BE2C cells akin to characteristic features of differentiation, but did not induce changes in the expression of differentiation markers.

Another aspect of this study was to evaluate KNCQ2 expression in differentiated and undifferentiated BE2C cells, as evaluation of a bioinformatic database found KCNQ2 expression is higher in histologically mature tumours. There was no difference in expression of KCNQ2 between undifferentiated and differentiated BE2C cells. Previous investigations have demonstrated the IMR-32 neuroblastoma cell line expresses two splice variants of KCNQ2, Q2 long transcript (Q2L) and Q2 short transcript (Q2S). Q2L is predominantly expressed in differentiated cells, whereas Q2S is expressed mainly in undifferentiated cells [248]. The coding DNA sequence (CDS) of Q2L is 2565 base pairs, in comparison the CDS of Q2S is truncated and is 1182 base pairs. The KCNQ2 primer pair used in this study was designed to recognise both Q2L and Q2S. This suggests, in contrast to IMR-32 cells, that in response to differentiation the expressed KCNQ2 transcript does not change in BE2C cells.

4.5 Role of KCNQ2/Kv7.2 in BE2C tumours *in vivo*

The chick embryo model is an established model to determine the response of solid tumours to therapeutic compounds *in vivo*. There were multiple advantages of using the chick embryo model in this study. The rapid development, accessibility and visibility of the CAM allowed experimental manipulation and regular monitoring. In addition, the naturally immunodeficient nature of the chick embryo allowed the implantation of human neuroblastoma BE2C cells without genomic manipulation, whereas using a murine xenograft model would have necessitated the acquisition of immunodeficient mice strains. Furthermore, once BE2C cells were implanted onto the CAM, tumour xenografts were visible by E7; in murine models tumour formation takes 3-6 weeks [273]. Additionally, there were several practical benefits of using the chick embryo model. A home office license was not required for this study as the law permits working with eggs upto day 14 of incubation without obtaining a licensce; eggs were readily available from a local supplier and the

cost of obtaining and maintaining eggs was significantly lower in comparison with obtaining mice [140-142].

Despite the aforementioned strengths of the chick embryo model all *in vivo* models have a common limitation in that species-related differences need to be taken into account when interpreting results from animal experiments. With specific regard to use of the chick embryo model, a limitation in this study was that tumour development was dependent on initial fertilisation and subsequent survival of the embryo. The survival of the embryo may have been compromised at multiple stages; egg windowing, tumour cell transplantation and drug delivery. Handling and removal of the eggs from the incubator at various time points also increased the risk of dehydration and infections. This risk was minimised by maintaining an aseptic technique, careful handling of the egg and delicate manipulation of the embryo. Nevertheless, the number of tumours available for immunohistochemical analysis was reflected by poor survival of the embryos. In particular in the treatment group 6/10 embryos did not survive upto E14.

Furthermore, using the chick embryo model involved implantation of human neuroblastoma cells onto the chorioallantoic membrane which posed two main problems. Firstly, although the immunodeficient nature of the chick embryo aided in xenografting BE2C cells, it is established that the host immune response is a vital aspect of neuroblastoma tumour development and progression and human neuroblastoma most often arises in an immunocompetent host [50, 84-90]. Therefore the xenograft tumours developed in the CAM model may not have truly recapitulated human tumours. Secondly, implanting human neuroblastoma cells onto the CAM failed to replicate the human tumour microenvironment which may have influenced tumour behaviour.

In this study i*n vivo* assessment found XE991 had no significant on BE2C cell proliferation. However, it must be noted that *in vivo* assessment was limited by the very low number of tumours available for immunohistochemistry in both control (n=2) and treatment (n=3) groups. Given that XE991 inhibited BE2C cell proliferation *in vitro* it was unclear as to why there may have been a dissociation between *in vitro* and preliminary *in vivo* results. One possible explanation may be that the expression and/or function of KCNQ2 in xenografted tumours may differ to cultured cells, therefore the response of xenograft tumours to XE991 may also vary. Alternatively, it is plausible that the effect of XE991 on BE2C cell proliferation observed *in vitro* may not translate to an *in vivo* model.

4.6 Limitations

XE991 significantly influenced BE2C cell membrane potential and cell proliferation. Previous investigations have shown XE991 inhibits Kv7.2/7.3 heterodimers, Kv7.2 and Kv7.1 homomers with similar potency. Without characterising the expression and function of all Kv7 channels expressed by neuroblastoma cells there is uncertainty as to which channel is mediating the observed effect. For example, it is known that KCNQ3/5/Kv7.3/5 subunits can form heteromers with KCNQ2/Kv7.2 to form functional M-channels in sympathetic neurons; however gene/protein expression of these channels wasn't investigated. Characterising the expression levels of these channels would help to determine stoichiometry of the M-channel in neuroblastoma cells. Nevertheless, as mentioned above, existing evidence suggests that Kv7.2 homomeric channels are the predominant Kv7 channel in neuroblastoma cells. Furthermore, with regards to pharmacological agents, Kv7 channels display significant structural homology; resultantly there is a difficulty in synthesising subtype selective agents [274].

There are 79 K^+ channel genes and targeting a single channel or subfamily of channels doesn't account for the presence of multiple other types of K^+ channels present and functional in the cell membrane. Any conclusions drawn based on experiments with a single channel do not account for the dynamic nature of ion channel conductance and membrane potential. For example, a channel modulating compound may induce a change in membrane potential, however ion channels work in concert and the activity of one type of channel can determine changes in ion flux in another channel.

Furthermore, there are comparatively few studies investigating K^+ channel physiology beyond K^+ permeation. Kv7.2 has a large cytoplasmic domain capable of interacting with secondary messengers and other proteins in the cell [173]. It is plausible that channel-protein interactions influence cell proliferation independent of K^+ permeation. Performing genetic knockdown studies would remove the transmembrane and cytoplasmic components of the protein; this would significantly contribute to determining the function of the intracellular domains of Kv7.2.

4.7 Future direction

Preliminary i*n vivo* experiments using the chick embryo model were undertaken in this study. However, immunohistochemical detection of Ki67 staining was carried out only once due to an insufficient number of replicates of xenograft tumours. This limited the determination of the effect of XE991 on BE2C cell tumours *in vivo*. Further validation of the results may be obtained by increasing the number of xenograft tumours in both the XE991 treated and control group, followed

by immunohistochemical detection of Ki67 staining to assess the effect on BE2C cell proliferation *in vivo*.

All experiments were carried out using the BE2C and SKNAS cell lines. There are many other neuroblastoma cell lines, thus it would be useful to extend the investigation of the expression and function of KCNQ2 in more cell lines to represent a wider spectrum of disease and other cancer types. In addition, there may be discrepancies in the results obtained in neuroblastoma cell lines, xenografted tumours and primary human tumours. Expression of KCNQ2/Kv7.2 in xenografted tumours and primary tumours from patient samples could be assessed by qPCR, western blotting and immunohistochemistry to further characterise the expression of KCNQ2/Kv7.2 neuroblastoma.

In this study the aim was to assess the effect of KCNQ2/Kv7.2 modulation on cell viability, proliferation and differentiation. K^+ channels have been implicated in a number of additional oncological processes including cell migration, invasion and angiogenesis [144, 145]. Future studies could assess the role of this channel in these processes *in vitro* and *in vivo*.

With regards to other K^+ channels, KCNH2 and KCNMA1 have been implicated in many other human cancers, although in this study it was found that they do not demonstrate high expression in BE2C and SKNAS cells. However, low expression does not preclude a significant function. The role of these channels and other K^+ channels implicated in the development and progression of cancer should be assessed.

4.8 Conclusion

Neuroblastoma is a malignant condition that demonstrates significant clinical and biological heterogeneity. Further understanding of the biology of neuroblastoma may contribute significantly to developing novel therapeutic approaches. K^+ channels are expressed ubiquitously in normal and malignant tissue and there is significant evidence implicating their role in oncogenesis.

In this study we have established that K^+ channels are indeed expressed by neuroblastoma cells and differential expression exists between two neuroblastoma cell lines. KCNQ2/Kv7.2 expression may contribute to the biological heterogeneity observed in neuroblastoma cell lines and primary tumours. Furthermore, it is evident that modulation of KCNQ2/Kv7.2 has some impact on cell behaviour *in vitro*. We hope that further work to establish the role of KNCQ2/Kv7.2 and other K^+ channels in neuroblastoma is undertaken to ultimately gain a better understanding of the biology of neuroblastoma and provide a target for therapeutic compounds.

Bibliography

1. Mullassery D, Dominici C, Jesudason EC, McDowell HP, Losty PD. Neuroblastoma: contemporary management. *Arch Dis Child Educ Pract Ed* 2009;94(6):177-85.
2. Cancer Research UK. *Embryonal Tumours: 1996-2005 Incidene Rates per Million Population, Children (0-14), Great Britain*. 2011. (accessed 04/05 2017).
3. Cancer Research UK. *Great Britain Cancer Incidence (1996-2005) Summary - Children 2014*. 2014. (accessed 04/05 2017).
4. CancerResearchUK. *Great Britain Cancer Mortality (1995-2004) Summary - Children, 2014*. 2014. (accessed 04/05 2017).
5. Mullassery D, Losty PD. Neuroblastoma. *Paediatrics and Child Health* 2016;26(2):68-72.
6. Chen Y, Takita J, Choi YL, Kato M, Ohira M, Sanada M, et al. Oncogenic mutations of ALK kinase in neuroblastoma. *Nature* 2008;455(7215):971-4.
7. Trochet D, Bourdeaut F, Janoueix-Lerosey I, Deville A, de Pontual L, Schleiermacher G, et al. Germline mutations of the paired-like homeobox 2B (PHOX2B) gene in neuroblastoma. *Am J Hum Genet* 2004;74(4):761-4.
8. Bluhm E, McNeil DE, Cnattingius S, Gridley G, El Ghormli L, Fraumeni JF, Jr. Prenatal and perinatal risk factors for neuroblastoma. *Int J Cancer* 2008;123(12):2885-90.
9. Ferris i Tortajada J, Ortega Garcia JA, Garcia i Castell J, Lopez Andreu JA, Berbel Tornero O, Crehua Gaudiza E. Risk factors for neuroblastoma. *An Pediatr (Barc)* 2005;63(1):50-60.
10. Jiang M, Stanke J, Lahti JM. The connections between neural crest development and neuroblastoma. *Curr Top Dev Biol* 2011;94:77-127.
11. Huber K. The sympathoadrenal cell lineage: specification, diversification, and new perspectives. *Dev Biol* 2006;298(2):335-43.
12. Heukamp LC, Thor T, Schramm A, De Preter K, Kumps C, De Wilde B, et al. Targeted expression of mutated ALK induces neuroblastoma in transgenic mice. *Sci Transl Med* 2012;4(141):141ra91.
13. Weiss WA, Aldape K, Mohapatra G, Feuerstein BG, Bishop JM. Targeted expression of MYCN causes neuroblastoma in transgenic mice. *EMBO J* 1997;16(11):2985-95.
14. Gammill LS, Bronner-Fraser M. Neural crest specification: migrating into genomics. *Nat Rev Neurosci* 2003;4(10):795-805.
15. Jessen KR, Mirsky R. The origin and development of glial cells in peripheral nerves. *Nat Rev Neurosci* 2005;6(9):671-82.

16. Prasad MS, Sauka-Spengler T, LaBonne C. Induction of the neural crest state: control of stem cell attributes by gene regulatory, post-transcriptional and epigenetic interactions. *Dev Biol* 2012;366(1):10-21.
17. Mayor R, Theveneau E. The neural crest. *Development* 2013;140(11):2247-51.
18. Shyamala K, Yanduri S, Girish HC, Murgod S. Neural crest: The fourth germ layer. *J Oral Maxillofac Pathol* 2015;19(2):221-9.
19. Taneyhill LA. To adhere or not to adhere: the role of Cadherins in neural crest development. *Cell Adh Migr* 2008;2(4):223-30.
20. Kim J, Lo L, Dormand E, Anderson DJ. SOX10 maintains multipotency and inhibits neuronal differentiation of neural crest stem cells. *Neuron* 2003;38(1):17-31.
21. Stewart RA, Arduini BL, Berghmans S, George RE, Kanki JP, Henion PD, et al. Zebrafish foxd3 is selectively required for neural crest specification, migration and survival. *Dev Biol* 2006;292(1):174-88.
22. Zimmerman KA, Yancopoulos GD, Collum RG, Smith RK, Kohl NE, Denis KA, et al. Differential expression of myc family genes during murine development. *Nature* 1986;319(6056):780-3.
23. Kuo BR, Erickson CA. Regional differences in neural crest morphogenesis. *Cell Adh Migr* 2010;4(4):567-85.
24. Gammill LS, Roffers-Agarwal J. Division of labor during trunk neural crest development. *Dev Biol* 2010;344(2):555-65.
25. Theveneau E, Mayor R. Neural crest delamination and migration: from epithelium-to-mesenchyme transition to collective cell migration. *Dev Biol* 2012;366(1):34-54.
26. Kasemeier-Kulesa JC, Bradley R, Pasquale EB, Lefcort F, Kulesa PM. Eph/ephrins and N-cadherin coordinate to control the pattern of sympathetic ganglia. *Development* 2006;133(24):4839-47.
27. Kasemeier-Kulesa JC, McLennan R, Romine MH, Kulesa PM, Lefcort F. CXCR4 controls ventral migration of sympathetic precursor cells. *J Neurosci* 2010;30(39):13078-88.
28. Mohlin SA, Wigerup C, Pahlman S. Neuroblastoma aggressiveness in relation to sympathetic neuronal differentiation stage. *Semin Cancer Biol* 2011;21(4):276-82.
29. Schneider C, Wicht H, Enderich J, Wegner M, Rohrer H. Bone morphogenetic proteins are required *in vivo* for the generation of sympathetic neurons. *Neuron* 1999;24(4):861-70.
30. Ernsberger U, Reissmann E, Mason I, Rohrer H. The expression of dopamine beta-hydroxylase, tyrosine hydroxylase, and Phox2 transcription factors in sympathetic neurons: evidence for common regulation during noradrenergic induction and diverging regulation later in development. *Mech Dev* 2000;92(2):169-77.

31. Pattyn A, Morin X, Cremer H, Goridis C, Brunet JF. The homeobox gene Phox2b is essential for the development of autonomic neural crest derivatives. *Nature* 1999;399(6734):366-70.
32. Schmidt M, Lin S, Pape M, Ernsberger U, Stanke M, Kobayashi K, et al. The bHLH transcription factor Hand2 is essential for the maintenance of noradrenergic properties in differentiated sympathetic neurons. *Dev Biol* 2009;329(2):191-200.
33. Cheung NK, Dyer MA. Neuroblastoma: developmental biology, cancer genomics and immunotherapy. *Nat Rev Cancer* 2013;13(6):397-411.
34. Pugh TJ, Morozova O, Attiyeh EF, Asgharzadeh S, Wei JS, Auclair D, et al. The genetic landscape of high-risk neuroblastoma. *Nat Genet* 2013;45(3):279-84.
35. Rajagopalan H, Lengauer C. Aneuploidy and cancer. *Nature* 2004;432(7015):338-41.
36. Kaneko Y, Kanda N, Maseki N, Sakurai M, Tsuchida Y, Takeda T, et al. Different karyotypic patterns in early and advanced stage neuroblastomas. *Cancer Res* 1987;47(1):311-8.
37. Cohn SL, Pearson ADJ, London WB, Monclair T, Ambros PF, Brodeur GM, et al. The International Neuroblastoma Risk Group (INRG) Classification System: An INRG Task Force Report. *Journal of Clinical Oncology* 2009;27(2):289-97.
38. Thorner PS. The molecular genetic profile of neuroblastoma. *Diagnostic Histopathology* 2014;20(2):76-83.
39. Bown N, Cotterill S, Lastowska M, O'Neill S, Pearson AD, Plantaz D, et al. Gain of chromosome arm 17q and adverse outcome in patients with neuroblastoma. *N Engl J Med* 1999;340(25):1954-61.
40. Ambros PF, Ambros IM, Brodeur GM, Haber M, Khan J, Nakagawara A, et al. International consensus for neuroblastoma molecular diagnostics: report from the International Neuroblastoma Risk Group (INRG) Biology Committee. *British Journal of Cancer* 2009;100(9):1471-82.
41. Guo C, White PS, Weiss MJ, Hogarty MD, Thompson PM, Stram DO, et al. Allelic deletion at 11q23 is common in MYCN single copy neuroblastomas. *Oncogene* 1999;18(35):4948-57.
42. Attiyeh EF, London WB, Mosse YP, Wang Q, Winter C, Khazi D, et al. Chromosome 1p and 11q deletions and outcome in neuroblastoma. *N Engl J Med* 2005;353(21):2243-53.
43. Moreau LA, McGrady P, London WB, Shimada H, Cohn SL, Maris JM, et al. Does MYCN amplification manifested as homogeneously staining regions at diagnosis predict a worse outcome in children with neuroblastoma? A Children's Oncology Group study. *Clin Cancer Res* 2006;12(19):5693-7.

44. Knoepfler PS, Cheng PF, Eisenman RN. N-myc is essential during neurogenesis for the rapid expansion of progenitor cell populations and the inhibition of neuronal differentiation. *Genes Dev* 2002;16(20):2699-712.
45. Grandori C, Cowley SM, James LP, Eisenman RN. The Myc/Max/Mad network and the transcriptional control of cell behavior. *Annu Rev Cell Dev Biol* 2000;16:653-99.
46. Huang M, Weiss WA. Neuroblastoma and MYCN. *Cold Spring Harb Perspect Med* 2013;3(10):a014415.
47. Chesler L, Weiss WA. Genetically engineered murine models--contribution to our understanding of the genetics, molecular pathology and therapeutic targeting of neuroblastoma. *Semin Cancer Biol* 2011;21(4):245-55.
48. Marshall GM, Carter DR, Cheung BB, Liu T, Mateos MK, Meyerowitz JG, et al. The prenatal origins of cancer. *Nat Rev Cancer* 2014;14(4):277-89.
49. Thompson D, Vo KT, London WB, Fischer M, Ambros PF, Nakagawara A, et al. Identification of patient subgroups with markedly disparate rates of MYCN amplification in neuroblastoma: A report from the International Neuroblastoma Risk Group project. *Cancer* 2016;122(6):935-45.
50. Hanahan D, Weinberg RA. Hallmarks of cancer: the next generation. *Cell* 2011;144(5):646-74.
51. Kumar V, Abbas AK, Fausto N, Robbins SL, Cotran RS. *Robbins and Cotran pathologic basis of disease*. Philadelphia: Elsevier Saunders., 2005.
52. Borriello L, Seeger RC, Asgharzadeh S, DeClerck YA. More than the genes, the tumor microenvironment in neuroblastoma. *Cancer Lett* 2016;380(1):304-14.
53. Carpenter EL, Mosse YP. Targeting ALK in neuroblastoma--preclinical and clinical advancements. *Nat Rev Clin Oncol* 2012;9(7):391-9.
54. Holla VR, Elamin YY, Bailey AM, Johnson AM, Litzenburger BC, Khotskaya YB, et al. ALK: a tyrosine kinase target for cancer therapy. *Cold Spring Harb Mol Case Stud* 2017;3(1):a001115.
55. Brodeur GM, Minturn JE, Ho R, Simpson AM, Iyer R, Varela CR, et al. Trk receptor expression and inhibition in neuroblastomas. *Clin Cancer Res* 2009;15(10):3244-50.
56. Gogolin S, Ehemann V, Becker G, Brueckner LM, Dreidax D, Bannert S, et al. CDK4 inhibition restores G(1)-S arrest in MYCN-amplified neuroblastoma cells in the context of doxorubicin-induced DNA damage. *Cell Cycle* 2013;12(7):1091-104.

57. Westermann F, Muth D, Benner A, Bauer T, Henrich KO, Oberthuer A, et al. Distinct transcriptional MYCN/c-MYC activities are associated with spontaneous regression or malignant progression in neuroblastomas. *Genome Biol* 2008;9(10):R150.
58. Olivier M, Hollstein M, Hainaut P. TP53 mutations in human cancers: origins, consequences, and clinical use. *Cold Spring Harb Perspect Biol* 2010;2(1):a001008.
59. Chen L, Iraci N, Gherardi S, Gamble LD, Wood KM, Perini G, et al. p53 is a direct transcriptional target of MYCN in neuroblastoma. *Cancer Res* 2010;70(4):1377-88.
60. Van Maerken T, Vandesompele J, Rihani A, De Paepe A, Speleman F. Escape from p53-mediated tumor surveillance in neuroblastoma: switching off the p14(ARF)-MDM2-p53 axis. *Cell Death Differ* 2009;16(12):1563-72.
61. Tweddle DA, Pearson AD, Haber M, Norris MD, Xue C, Flemming C, et al. The p53 pathway and its inactivation in neuroblastoma. *Cancer Lett* 2003;197(1-2):93-8.
62. Knudson AG, Jr. Mutation and cancer: statistical study of retinoblastoma. *Proc Natl Acad Sci U S A* 1971;68(4):820-3.
63. Knudson A, Strong L. Mutation and cancer: neuroblastoma and pheochromocytoma. *Am J Hum Genet* 1972;24:514-32.
64. Henrich KO, Schwab M, Westermann F. 1p36 tumor suppression--a matter of dosage? *Cancer Res* 2012;72(23):6079-88.
65. Molenaar JJ, Koster J, Zwijnenburg DA, van Sluis P, Valentijn LJ, van der Ploeg I, et al. Sequencing of neuroblastoma identifies chromothripsis and defects in neuritogenesis genes. *Nature* 2012;483(7391):589-93.
66. Evan GI, Vousden KH. Proliferation, cell cycle and apoptosis in cancer. *Nature* 2001;411(6835):342-8.
67. Dole MG, Jasty R, Cooper MJ, Thompson CB, Nunez G, Castle VP. Bcl-xL is expressed in neuroblastoma cells and modulates chemotherapy-induced apoptosis. *Cancer Res* 1995;55(12):2576-82.
68. Castle VP, Heidelberger KP, Bromberg J, Ou X, Dole M, Nunez G. Expression of the apoptosis-suppressing protein bcl-2, in neuroblastoma is associated with unfavorable histology and N-myc amplification. *Am J Pathol* 1993;143(6):1543-50.
69. Abel F, Sjoberg RM, Nilsson S, Kogner P, Martinsson T. Imbalance of the mitochondrial pro- and anti-apoptotic mediators in neuroblastoma tumours with unfavourable biology. *Eur J Cancer* 2005;41(4):635-46.
70. Casciano I, Banelli B, Croce M, De Ambrosis A, di Vinci A, Gelvi I, et al. Caspase-8 gene expression in neuroblastoma. *Ann N Y Acad Sci* 2004;1028:157-67.

71. Teitz T, Wei T, Valentine MB, Vanin EF, Grenet J, Valentine VA, et al. Caspase 8 is deleted or silenced preferentially in childhood neuroblastomas with amplification of MYCN. *Nat Med* 2000;6(5):529-35.
72. Hiyama E, Hiyama K, Yokoyama T, Matsuura Y, Piatyszek MA, Shay JW. Correlating telomerase activity levels with human neuroblastoma outcomes. *Nat Med* 1995;1(3):249-55.
73. Peifer M, Hertwig F, Roels F, Dreidax D, Gartlgruber M, Menon R, et al. Telomerase activation by genomic rearrangements in high-risk neuroblastoma. *Nature* 2015;526(7575):700-4.
74. Cesare AJ, Reddel RR. Alternative lengthening of telomeres: models, mechanisms and implications. *Nat Rev Genet* 2010;11(5):319-30.
75. Napier CE, Huschtscha LI, Harvey A, Bower K, Noble JR, Hendrickson EA, et al. ATRX represses alternative lengthening of telomeres. *Oncotarget* 2015;6(18):16543-58.
76. Chlenski A, Liu S, Cohn SL. The regulation of angiogenesis in neuroblastoma. *Cancer Lett* 2003;197(1-2):47-52.
77. Meitar D, Crawford SE, Rademaker AW, Cohn SL. Tumor angiogenesis correlates with metastatic disease, N-myc amplification, and poor outcome in human neuroblastoma. *J Clin Oncol* 1996;14(2):405-14.
78. Chlenski A, Liu S, Crawford SE, Volpert OV, DeVries GH, Evangelista A, et al. SPARC is a key Schwannian-derived inhibitor controlling neuroblastoma tumor angiogenesis. *Cancer Res* 2002;62(24):7357-63.
79. Sugiura Y, Shimada H, Seeger RC, Laug WE, DeClerck YA. Matrix metalloproteinases-2 and -9 are expressed in human neuroblastoma: contribution of stromal cells to their production and correlation with metastasis. *Cancer Res* 1998;58(10):2209-16.
80. Klymkowsky MW, Savagner P. Epithelial-mesenchymal transition: a cancer researcher's conceptual friend and foe. *Am J Pathol* 2009;174(5):1588-93.
81. Valsesia-Wittmann S, Magdeleine M, Dupasquier S, Garin E, Jallas AC, Combaret V, et al. Oncogenic cooperation between H-Twist and N-Myc overrides failsafe programs in cancer cells. *Cancer Cell* 2004;6(6):625-30.
82. Kushner BH, Yeung HW, Larson SM, Kramer K, Cheung NK. Extending positron emission tomography scan utility to high-risk neuroblastoma: fluorine-18 fluorodeoxyglucose positron emission tomography as sole imaging modality in follow-up of patients. *J Clin Oncol* 2001;19(14):3397-405.
83. Aminzadeh S, Vidali S, Sperl W, Kofler B, Feichtinger RG. Energy metabolism in neuroblastoma and Wilms tumor. *Transl Pediatr* 2015;4(1):20-32.

84. Bottino C, Dondero A, Bellora F, Moretta L, Locatelli F, Pistoia V, et al. Natural killer cells and neuroblastoma: tumor recognition, escape mechanisms, and possible novel immunotherapeutic approaches. *Front Immunol* 2014;5:56.
85. Lampson LA, Fisher CA, Whelan JP. Striking paucity of HLA-A, B, C and beta 2-microglobulin on human neuroblastoma cell lines. *J Immunol* 1983;130(5):2471-8.
86. Bernards R, Dessain SK, Weinberg RA. N-myc amplification causes down-modulation of MHC class I antigen expression in neuroblastoma. *Cell* 1986;47(5):667-74.
87. Liu D, Song L, Wei J, Courtney AN, Gao X, Marinova E, et al. IL-15 protects NKT cells from inhibition by tumor-associated macrophages and enhances antimetastatic activity. *J Clin Invest* 2012;122(6):2221-33.
88. Shurin GV, Shurin MR, Bykovskaia S, Shogan J, Lotze MT, Barksdale EM, Jr. Neuroblastoma-derived gangliosides inhibit dendritic cell generation and function. *Cancer Res* 2001;61(1):363-9.
89. Shen Z. Genomic instability and cancer: an introduction. *J Mol Cell Biol* 2011;3(1):1-3.
90. Greaves M, Maley CC. Clonal evolution in cancer. *Nature* 2012;481(7381):306-13.
91. Pistoia V, Morandi F, Bianchi G, Pezzolo A, Prigione I, Raffaghello L. Immunosuppressive microenvironment in neuroblastoma. *Front Oncol* 2013;3:167.
92. Ara T, Nakata R, Sheard MA, Shimada H, Buettner R, Groshen SG, et al. Critical role of STAT3 in IL-6-mediated drug resistance in human neuroblastoma. *Cancer Res* 2013;73(13):3852-64.
93. Joshi VV. Peripheral neuroblastic tumors: pathologic classification based on recommendations of international neuroblastoma pathology committee (Modification of shimada classification). *Pediatr Dev Pathol* 2000;3(2):184-99.
94. Shimada H. The International Neuroblastoma Pathology Classification. *Pathologica* 2003;95(5):240-1.
95. Shimada H, Chatten J, Newton WA, Jr., Sachs N, Hamoudi AB, Chiba T, et al. Histopathologic prognostic factors in neuroblastic tumors: definition of subtypes of ganglioneuroblastoma and an age-linked classification of neuroblastomas. *J Natl Cancer Inst* 1984;73(2):405-16.
96. Carachi R. Perspectives on neuroblastoma. *Pediatr Surg Int* 2002;18(5-6):299-305.
97. Lonergan G, Schwab C, Suarez E, Carlson C. Anatomic distribution of sympathetic ganglia: Neuroblastoma, Ganglioneuroblastoma, and Ganglioneuroma: Radiologic-Pathologic Correlation. *RadioGraphics* 2002;22(4):911-34.
98. Geoerger B, Hero B, Harms D, Grebe J, Scheidhauer K, Berthold F. Metabolic activity and clinical features of primary ganglioneuromas. *Cancer* 2001;91(10):1905-13.

99. Brodeur GM, Bagatell R. Mechanisms of neuroblastoma regression. *Nat Rev Clin Oncol* 2014;11(12):704-13.
100. Hann HW, Evans AE, Siegel SE, Wong KY, Sather H, Dalton A, et al. Prognostic importance of serum ferritin in patients with Stages III and IV neuroblastoma: the Childrens Cancer Study Group experience. *Cancer Res* 1985;45(6):2843-8.
101. Simon T, Hero B, Hunneman DH, Berthold F. Tumour markers are poor predictors for relapse or progression in neuroblastoma. *Eur J Cancer* 2003;39(13):1899-903.
102. Strenger V, Kerbl R, Dornbusch HJ, Ladenstein R, Ambros PF, Ambros IM, et al. Diagnostic and prognostic impact of urinary catecholamines in neuroblastoma patients. *Pediatr Blood Cancer* 2007;48(5):504-9.
103. Matthay KK, Maris JM, Schleiermacher G, Nakagawara A, Mackall CL, Diller L, et al. Neuroblastoma. *Nat Rev Dis Primers* 2016;2:16078.
104. Kembhavi SA, Shah S, Rangarajan V, Qureshi S, Popat P, Kurkure P. Imaging in neuroblastoma: An update. *Indian J Radiol Imaging* 2015;25(2):129-36.
105. Papaioannou G, McHugh K. Neuroblastoma in childhood: review and radiological findings. *Cancer Imaging* 2005;5:116-27.
106. Gelfand MJ. Meta-iodobenzylguanidine in children. *Semin Nucl Med* 1993;23(3):231-42.
107. Sharp SE, Shulkin BL, Gelfand MJ, Salisbury S, Furman WL. 123I-MIBG scintigraphy and 18F-FDG PET in neuroblastoma. *J Nucl Med* 2009;50(8):1237-43.
108. Mullassery D, Sharma V, Salim A, Jawaid WB, Pizer BL, Abernethy LJ, et al. Open versus needle biopsy in diagnosing neuroblastoma. J Pediatr Surg. 2014;49(10):1505-7
109. Beiske K, Burchill SA, Cheung IY, Hiyama E, Seeger RC, Cohn SL, et al. Consensus criteria for sensitive detection of minimal neuroblastoma cells in bone marrow, blood and stem cell preparations by immunocytology and QRT-PCR: recommendations by the International Neuroblastoma Risk Group Task Force. *Br J Cancer* 2009;100(10):1627-37.
110. Yamamoto K, Ohta S, Ito E, Hayashi Y, Asami T, Mabuchi O, et al. Marginal decrease in mortality and marked increase in incidence as a result of neuroblastoma screening at 6 months of age: cohort study in seven prefectures in Japan. *J Clin Oncol* 2002;20(5):1209-14.
111. Woods WG, Gao RN, Shuster JJ, Robison LL, Bernstein M, Weitzman S, et al. Screening of infants and mortality due to neuroblastoma. *N Engl J Med* 2002;346(14):1041-6.
112. Vo KT, Matthay KK, Neuhaus J, London WB, Hero B, Ambros PF, et al. Clinical, biologic, and prognostic differences on the basis of primary tumor site in neuroblastoma: a report from the international neuroblastoma risk group project. *J Clin Oncol* 2014;32(28):3169-76.

113. Zafeiriou DI, Economou M, Koliouskas D, Triantafyllou P, Kardaras P, Gombakis N. Congenital Horner's syndrome associated with cervical neuroblastoma. *Eur J Paediatr Neurol* 2006;10(2):90-2.
114. Rudolf JW, Thapa M. Thoracic neuroblastoma. *Radiol Case Rep* 2011;6(2):440.
115. Fawzy M, El-Beltagy M, Shafei ME, Zaghloul MS, Kinaai NA, Refaat A, et al. Intraspinal neuroblastoma: Treatment options and neurological outcome of spinal cord compression. *Oncol Lett* 2015;9(2):907-11.
116. De Bernardi B, Quaglietta L, Haupt R, Castellano A, Tirtei E, Luksch R, et al. Neuroblastoma with symptomatic epidural compression in the infant: the AIEOP experience. *Pediatr Blood Cancer* 2014;61(8):1369-75.
117. DuBois SG, Kalika Y, Lukens JN, Brodeur GM, Seeger RC, Atkinson JB, et al. Metastatic sites in stage IV and IVS neuroblastoma correlate with age, tumor biology, and survival. *J Pediatr Hematol Oncol* 1999;21(3):181-9.
118. Raffaghello L, Conte M, De Grandis E, Pistoia V. Immunological mechanisms in opsoclonus-myoclonus associated neuroblastoma. *Eur J Paediatr Neurol* 2009;13(3):219-23.
119. Matthay KK, Blaes F, Hero B, Plantaz D, De Alarcon P, Mitchell WG, et al. Opsoclonus myoclonus syndrome in neuroblastoma a report from a workshop on the dancing eyes syndrome at the advances in neuroblastoma meeting in Genoa, Italy, 2004. *Cancer Lett* 2005;228(1-2):275-82.
120. Bourdeaut F, de Carli E, Timsit S, Coze C, Chastagner P, Sarnacki S, et al. VIP hypersecretion as primary or secondary syndrome in neuroblastoma: A retrospective study by the Societe Francaise des Cancers de l'Enfant (SFCE). *Pediatr Blood Cancer* 2009;52(5):585-90.
121. Schleiermacher G, Rubie H, Hartmann O, Bergeron C, Chastagner P, Mechinaud F, et al. Treatment of stage 4s neuroblastoma--report of 10 years' experience of the French Society of Paediatric Oncology (SFOP). *Br J Cancer* 2003;89(3):470-6.
122. Mehta V, Balachandran C, Lonikar V. Blueberry muffin baby: a pictoral differential diagnosis. *Dermatol Online J* 2008;14(2):8.
123. Luksch R, Castellani MR, Collini P, De Bernardi B, Conte M, Gambini C, et al. Neuroblastoma (Peripheral neuroblastic tumours). *Crit Rev Oncol Hematol* 2016;107:163-81.
124. Brisse HJ, McCarville MB, Granata C, Krug KB, Wootton-Gorges SL, Kanegawa K, et al. Guidelines for imaging and staging of neuroblastic tumors: consensus report from the International Neuroblastoma Risk Group Project. *Radiology* 2011;261(1):243-57.

125. Rich BS, La Quaglia MP. Chapter 31 - Neuroblastoma A2 - Coran, Arnold G. In: *Pediatric Surgery (Seventh Edition).* Philadelphia: Mosby, 2012:441-58. http://www.sciencedirect.com/science/article/pii/B9780323072557000313.

126. Leclair MD, de Lagausie P, Becmeur F, Varlet F, Thomas C, Valla JS, et al. Laparoscopic resection of abdominal neuroblastoma. *Ann Surg Oncol* 2008;15(1):117-24.

127. Laverdiere C, Liu Q, Yasui Y, Nathan PC, Gurney JG, Stovall M, et al. Long-term outcomes in survivors of neuroblastoma: a report from the Childhood Cancer Survivor Study. *J Natl Cancer Inst* 2009;101(16):1131-40.

128. Strother DR, London WB, Schmidt ML, Brodeur GM, Shimada H, Thorner P, et al. Outcome after surgery alone or with restricted use of chemotherapy for patients with low-risk neuroblastoma: results of Children's Oncology Group study P9641. *J Clin Oncol* 2012;30(15):1842-8.

129. Baker DL, Schmidt ML, Cohn SL, Maris JM, London WB, Buxton A, et al. Outcome after reduced chemotherapy for intermediate-risk neuroblastoma. *N Engl J Med* 2010;363(14):1313-23.

130. Matthay KK, Villablanca JG, Seeger RC, Stram DO, Harris RE, Ramsay NK, et al. Treatment of high-risk neuroblastoma with intensive chemotherapy, radiotherapy, autologous bone marrow transplantation, and 13-cis-retinoic acid. Children's Cancer Group. *N Engl J Med* 1999;341(16):1165-73.

131. Reynolds CP. Detection and treatment of minimal residual disease in high-risk neuroblastoma. *Pediatr Transplant* 2004;8 Suppl 5:56-66.

132. Yu AL, Gilman AL, Ozkaynak MF, London WB, Kreissman SG, Chen HX, et al. Anti-GD2 antibody with GM-CSF, interleukin-2, and isotretinoin for neuroblastoma. *N Engl J Med* 2010;363(14):1324-34.

133 Pinto NR, Applebaum MA, Volchenboum SL, Matthay KK, London WB, Ambros PF, et al. Advances in Risk Classification and Treatment Strategies for Neuroblastoma. *J Clin Oncol* 2015;33(27):3008-17.

134. Moreno L, Chesler L, Hargrave D, Eccles SA, Pearson AD. Preclinical drug development for childhood cancer. Expert Opin Drug Discov. 2011;6(1):49-64

135. Teitz T, Stanke JJ, Federico S, Bradley CL, Brennan R, Zhang J, et al. Preclinical models for neuroblastoma: establishing a baseline for treatment. PLoS One. 2011;6(4):e19133

136. Rubin H. The early history of tumor virology: Rous, RIF, and RAV. Proc Natl Acad Sci U S A. 2011;108(35):14389-96

137. Kobayashi T, Koshida K, Endo Y, Imao T, Uchibayashi T, Sasaki T, et al. A chick embryo model for metastatic human prostate cancer. Eur Urol. 1998;34(2):154-60
138. Strojnik T, Kavalar R, Barone TA, Plunkett RJ. Experimental model and immunohistochemical comparison of U87 human glioblastoma cell xenografts on the chicken chorioallantoic membrane and in rat brains. Anticancer Res. 2010;30(12):4851-60
139. Taizi M, Deutsch VR, Leitner A, Ohana A, Goldstein RS. A novel and rapid in vivo system for testing therapeutics on human leukemias. Exp Hematol. 2006;34(12):1698-708
140. Kain KH, Miller JW, Jones-Paris CR, Thomason RT, Lewis JD, Bader DM, et al. The chick embryo as an expanding experimental model for cancer and cardiovascular research. Dev Dyn. 2014;243(2):216-28
141. Gabrielli MG, Accili D. The chick chorioallantoic membrane: a model of molecular, structural, and functional adaptation to transepithelial ion transport and barrier function during embryonic development. J Biomed Biotechnol. 2010;2010:940741
142. Nowak-Sliwinska P, Segura T, Iruela-Arispe ML. The chicken chorioallantoic membrane model in biology, medicine and bioengineering. Angiogenesis. 2014;17(4):779-804
143. Alberts B JA, Lewis J. *Molecular Biology of the Cell*. 4th ed. New York: Garland Science, 2002. (The Lipid Bilayer).
144. Pardo LA, Stuhmer W. The roles of K+ channels in cancer. *Nat Rev Cancer* 2014;14(1):39-48.
145. Huang X, Jan LY. Targeting potassium channels in cancer. *J Cell Biol* 2014;206(2):151-62.
146. Choe S. Potassium channel structures. *Nat Rev Neurosci* 2002;3(2):115-21.
147. Tian C, Zhu R, Zhu L, Qiu T, Cao Z, Kang T. Potassium Channels: Structures, Diseases, and Modulators. *Chemical Biology & Drug Design* 2014;83(1):1-26.
148. Sansom MS, Shrivastava IH, Bright JN, Tate J, Capener CE, Biggin PC. Potassium channels: structures, models, simulations. *Biochim Biophys Acta* 2002;1565(2):294-307.
149. MacKinnon R, Cohen SL, Kuo A, Lee A, Chait BT. Structural conservation in prokaryotic and eukaryotic potassium channels. *Science* 1998;280(5360):106-9.
150. Doyle DA, Morais Cabral J, Pfuetzner RA, Kuo A, Gulbis JM, Cohen SL, et al. The structure of the potassium channel: molecular basis of K+ conduction and selectivity. *Science* 1998;280(5360):69-77.
151. Yellen G. The voltage-gated potassium channels and their relatives. *Nature* 2002;419(6902):35-42.
152. Berneche S, Roux B. Energetics of ion conduction through the K+ channel. *Nature* 2001;414(6859):73-7.

153. Papazian DM, Schwarz TL, Tempel BL, Jan YN, Jan LY. Cloning of genomic and complementary DNA from Shaker, a putative potassium channel gene from Drosophila. *Science* 1987;237(4816):749-53.
154. Abbott GW, Sesti F, Splawski I, Buck ME, Lehmann MH, Timothy KW, et al. MiRP1 forms IKr potassium channels with HERG and is associated with cardiac arrhythmia. *Cell* 1999;97(2):175-87.
155. Bezanilla F. The voltage sensor in voltage-dependent ion channels. *Physiol Rev* 2000;80(2):555-92.
156. Tombola F, Pathak MM, Isacoff EY. How does voltage open an ion channel? *Annu Rev Cell Dev Biol* 2006;22:23-52.
157. Long SB, Campbell EB, Mackinnon R. Voltage sensor of Kv1.2: structural basis of electromechanical coupling. *Science* 2005;309(5736):903-8.
158. Antz C, Fakler B. Fast Inactivation of Voltage-Gated K(+) Channels: From Cartoon to Structure. *News Physiol Sci* 1998;13:177-82.
159. Hoshi T, Armstrong CM. C-type inactivation of voltage-gated K+ channels: pore constriction or dilation? *J Gen Physiol* 2013;141(2):151-60.
160. Kaczmarek LK, Aldrich RW, Chandy KG, Grissmer S, Wei AD, Wulff H. International Union of Basic and Clinical Pharmacology. C. Nomenclature and Properties of Calcium-Activated and Sodium-Activated Potassium Channels. *Pharmacol Rev* 2017;69(1):1-11.
161. Weiger TM, Hermann A, Levitan IB. Modulation of calcium-activated potassium channels. *J Comp Physiol A Neuroethol Sens Neural Behav Physiol* 2002;188(2):79-87.
162. Ledoux J, Werner ME, Brayden JE, Nelson MT. Calcium-activated potassium channels and the regulation of vascular tone. *Physiology (Bethesda)* 2006;21:69-78.
163. Kubo Y, Adelman JP, Clapham DE, Jan LY, Karschin A, Kurachi Y, et al. International Union of Pharmacology. LIV. Nomenclature and molecular relationships of inwardly rectifying potassium channels. *Pharmacol Rev* 2005;57(4):509-26.
164. Hibino H, Inanobe A, Furutani K, Murakami S, Findlay I, Kurachi Y. Inwardly rectifying potassium channels: their structure, function, and physiological roles. *Physiol Rev* 2010;90(1):291-366.
165. Cook DL, Hales CN. Intracellular ATP directly blocks K+ channels in pancreatic B-cells. *Nature* 1984;311(5983):271-3.
166. Andelfinger G, Tapper AR, Welch RC, Vanoye CG, George AL, Jr., Benson DW. KCNJ2 mutation results in Andersen syndrome with sex-specific cardiac and skeletal muscle phenotypes. *Am J Hum Genet* 2002;71(3):663-8.

167. Goonetilleke L, Quayle J. TREK-1 K(+) channels in the cardiovascular system: their significance and potential as a therapeutic target. *Cardiovasc Ther* 2012;30(1):e23-9.
168. Goldstein SA, Bayliss DA, Kim D, Lesage F, Plant LD, Rajan S. International Union of Pharmacology. LV. Nomenclature and molecular relationships of two-P potassium channels. *Pharmacol Rev* 2005;57(4):527-40.
169. Kuang Q, Purhonen P, Hebert H. Structure of potassium channels. *Cell Mol Life Sci* 2015;72(19):3677-93.
170. Kim JB. Channelopathies. *Korean J Pediatr* 2014;57(1):1-18.
171. Gutman GA, Chandy KG, Grissmer S, Lazdunski M, McKinnon D, Pardo LA, et al. International Union of Pharmacology. LIII. Nomenclature and molecular relationships of voltage-gated potassium channels. *Pharmacol Rev* 2005;57(4):473-508.
172. Brown DA, Passmore GM. Neural KCNQ (Kv7) channels. *Br J Pharmacol* 2009;156(8):1185-95.
173. Soldovieri MV, Miceli F, Taglialatela M. Driving with no brakes: molecular pathophysiology of Kv7 potassium channels. *Physiology (Bethesda)* 2011;26(5):365-76.
174. Robbins J. KCNQ potassium channels: physiology, pathophysiology, and pharmacology. *Pharmacol Ther* 2001;90(1):1-19.
175. Howard RJ, Clark KA, Holton JM, Minor DL, Jr. Structural insight into KCNQ (Kv7) channel assembly and channelopathy. *Neuron* 2007;53(5):663-75.
176. Barhanin J, Lesage F, Guillemare E, Fink M, Lazdunski M, Romey G. K(V)LQT1 and lsK (minK) proteins associate to form the I(Ks) cardiac potassium current. *Nature* 1996;384(6604):78-80.
177. Halliwell JV, Adams PR. Voltage-clamp analysis of muscarinic excitation in hippocampal neurons. *Brain Res* 1982;250(1):71-92.
178. Suh BC, Inoue T, Meyer T, Hille B. Rapid chemically induced changes of PtdIns(4,5)P2 gate KCNQ ion channels. *Science* 2006;314(5804):1454-7.
179. Wang HS, Pan Z, Shi W, Brown BS, Wymore RS, Cohen IS, et al. KCNQ2 and KCNQ3 potassium channel subunits: molecular correlates of the M-channel. *Science* 1998;282(5395):1890-3.
180. Hadley JK, Passmore GM, Tatulian L, Al-Qatari M, Ye F, Wickenden AD, et al. Stoichiometry of expressed KCNQ2/KCNQ3 potassium channels and subunit composition of native ganglionic M channels deduced from block by tetraethylammonium. *J Neurosci* 2003;23(12):5012-9.
181. Schroeder BC, Hechenberger M, Weinreich F, Kubisch C, Jentsch TJ. KCNQ5, a novel potassium channel broadly expressed in brain, mediates M-type currents. *J Biol Chem* 2000;275(31):24089-95.

182. Delmas P, Brown DA. Pathways modulating neural KCNQ/M (Kv7) potassium channels. *Nat Rev Neurosci* 2005;6(11):850-62.

183. Miceli F, Soldovieri MV, Martire M, Taglialatela M. Molecular pharmacology and therapeutic potential of neuronal Kv7-modulating drugs. *Curr Opin Pharmacol* 2008;8(1):65-74.

184. Main MJ, Cryan JE, Dupere JR, Cox B, Clare JJ, Burbidge SA. Modulation of KCNQ2/3 potassium channels by the novel anticonvulsant retigabine. *Mol Pharmacol* 2000;58(2):253-62.

185. Yu H, Wu M, Townsend SD, Zou B, Long S, Daniels JS, et al. Discovery, Synthesis, and Structure Activity Relationship of a Series of N-Aryl- bicyclo[2.2.1]heptane-2-carboxamides: Characterization of ML213 as a Novel KCNQ2 and KCNQ4 Potassium Channel Opener. *ACS Chem Neurosci* 2011;2(10):572-7.

186. Zaczek R, Chorvat RJ, Saye JA, Pierdomenico ME, Maciag CM, Logue AR, et al. Two new potent neurotransmitter release enhancers, 10,10-bis(4-pyridinylmethyl)-9(10H)-anthracenone and 10,10-bis(2-fluoro-4-pyridinylmethyl)-9(10H)-anthracenone: comparison to linopirdine. *J Pharmacol Exp Ther* 1998;285(2):724-30.

187. Maljevic S, Wuttke TV, Seebohm G, Lerche H. KV7 channelopathies. *Pflugers Arch* 2010;460(2):277-88.

188. Maljevic S, Wuttke TV, Lerche H. Nervous system KV7 disorders: breakdown of a subthreshold brake. *J Physiol* 2008;586(7):1791-801.

189. Jentsch TJ. Neuronal KCNQ potassium channels: physiology and role in disease. *Nat Rev Neurosci* 2000;1(1):21-30.

190. Dedek K, Kunath B, Kananura C, Reuner U, Jentsch TJ, Steinlein OK. Myokymia and neonatal epilepsy caused by a mutation in the voltage sensor of the KCNQ2 K+ channel. *Proc Natl Acad Sci U S A* 2001;98(21):12272-7.

191. Seebohm G, Strutz-Seebohm N, Ureche ON, Henrion U, Baltaev R, Mack AF, et al. Long QT syndrome-associated mutations in KCNQ1 and KCNE1 subunits disrupt normal endosomal recycling of IKs channels. *Circ Res* 2008;103(12):1451-7.

192. Coucke PJ, Van Hauwe P, Kelley PM, Kunst H, Schatteman I, Van Velzen D, et al. Mutations in the KCNQ4 gene are responsible for autosomal dominant deafness in four DFNA2 families. *Hum Mol Genet* 1999;8(7):1321-8.

193. Urrego D, Tomczak AP, Zahed F, Stuhmer W, Pardo LA. Potassium channels in cell cycle and cell proliferation. *Philos Trans R Soc Lond B Biol Sci* 2014;369(1638):20130094.

194. Mu D, Chen L, Zhang X, See LH, Koch CM, Yen C, et al. Genomic amplification and oncogenic properties of the KCNK9 potassium channel gene. *Cancer Cell* 2003;3(3):297-302.

195. Pardo LA, del Camino D, Sanchez A, Alves F, Bruggemann A, Beckh S, et al. Oncogenic potential of EAG K(+) channels. *EMBO J* 1999;18(20):5540-7.
196. Yang M, Brackenbury WJ. Membrane potential and cancer progression. *Front Physiol* 2013;4:185.
197. Pardo LA, Contreras-Jurado C, Zientkowska M, Alves F, Stuhmer W. Role of voltage-gated potassium channels in cancer. *J Membr Biol* 2005;205(3):115-24.
198. Rao VR, Perez-Neut M, Kaja S, Gentile S. Voltage-gated ion channels in cancer cell proliferation. *Cancers (Basel)* 2015;7(2):849-75.
199. Habela CW, Sontheimer H. Cytoplasmic volume condensation is an integral part of mitosis. *Cell Cycle* 2007;6(13):1613-20.
200. Huang X, Dubuc AM, Hashizume R, Berg J, He Y, Wang J, et al. Voltage-gated potassium channel EAG2 controls mitotic entry and tumor growth in medulloblastoma via regulating cell volume dynamics. *Genes Dev* 2012;26(16):1780-96.
201. Hanada T, Lin L, Chandy KG, Oh SS, Chishti AH. Human homologue of the Drosophila discs 1large tumor suppressor binds to p56lck tyrosine kinase and Shaker type Kv1.3 potassium channel in T lymphocytes. *J Biol Chem* 1997;272(43):26899-904.
202. Szabo I, Gulbins E, Apfel H, Zhang X, Barth P, Busch AE, et al. Tyrosine phosphorylation-dependent suppression of a voltage-gated K+ channel in T lymphocytes upon Fas stimulation. *J Biol Chem* 1996;271(34):20465-9.
203. Pillozzi S, Brizzi MF, Bernabei PA, Bartolozzi B, Caporale R, Basile V, et al. VEGFR-1 (FLT-1), beta1 integrin, and hERG K+ channel for a macromolecular signaling complex in acute myeloid leukemia: role in cell migration and clinical outcome. *Blood* 2007;110(4):1238-50.
204. Wang Z. Roles of K+ channels in regulating tumour cell proliferation and apoptosis. *Pflugers Arch* 2004;448(3):274-86.
205. Szabo I, Bock J, Grassme H, Soddemann M, Wilker B, Lang F, et al. Mitochondrial potassium channel Kv1.3 mediates Bax-induced apoptosis in lymphocytes. *Proc Natl Acad Sci U S A* 2008;105(39):14861-6.
206. Leanza L, Zoratti M, Gulbins E, Szabo I. Induction of apoptosis in macrophages via Kv1.3 and Kv1.5 potassium channels. *Curr Med Chem* 2012;19(31):5394-404.
207. Leanza L, Henry B, Sassi N, Zoratti M, Chandy KG, Gulbins E, et al. Inhibitors of mitochondrial Kv1.3 channels induce Bax/Bak-independent death of cancer cells. *EMBO Mol Med* 2012;4(7):577-93.
208. Wulff H, Castle NA, Pardo LA. Voltage-gated Potassium Channels as Therapeutic Drug Targets. *Nature reviews. Drug discovery* 2009;8(12):982-1001.

209. Garcia-Ferreiro RE, Kerschensteiner D, Major F, Monje F, Stuhmer W, Pardo LA. Mechanism of block of hEag1 K+ channels by imipramine and astemizole. *J Gen Physiol* 2004;124(4):301-17.

210. Rouzaire-Dubois B, Gerard V, Dubois JM. Involvement of K+ channels in the quercetin-induced inhibition of neuroblastoma cell growth. *Pflugers Arch* 1993;423(3-4):202-5.

211. Rouzaire-Dubois B, Dubois JM. Tamoxifen blocks both proliferation and voltage-dependent K+ channels of neuroblastoma cells. *Cell Signal* 1990;2(4):387-93.

212. Vandenberg JI, Perry MD, Perrin MJ, Mann SA, Ke Y, Hill AP. hERG K(+) channels: structure, function, and clinical significance. *Physiol Rev* 2012;92(3):1393-478.

213. Arcangeli A. Expression and role of hERG channels in cancer cells. *Novartis Found Symp* 2005;266:225-32; discussion 32-4.

214. Arcangeli A, Rosati B, Cherubini A, Crociani O, Fontana L, Ziller C, et al. HERG- and IRK-like inward rectifier currents are sequentially expressed during neuronal development of neural crest cells and their derivatives. *Eur J Neurosci* 1997;9(12):2596-604.

215. Arcangeli A, Rosati B, Cherubini A, Crociani O, Fontana L, Passani B, et al. Long-term exposure to retinoic acid induces the expression of IRK1 channels in HERG channel-endowed neuroblastoma cells. *Biochem Biophys Res Commun* 1998;244(3):706-11.

216. Arcangeli A, Bianchi L, Becchetti A, Faravelli L, Coronnello M, Mini E, et al. A novel inward-rectifying K+ current with a cell-cycle dependence governs the resting potential of mammalian neuroblastoma cells. *J Physiol* 1995;489 (Pt 2):455-71.

217. Crociani O, Guasti L, Balzi M, Becchetti A, Wanke E, Olivotto M, et al. Cell cycle-dependent expression of HERG1 and HERG1B isoforms in tumor cells. *J Biol Chem* 2003;278(5):2947-55.

218. Guasti L, Crociani O, Redaelli E, Pillozzi S, Polvani S, Masselli M, et al. Identification of a posttranslational mechanism for the regulation of hERG1 K+ channel expression and hERG1 current density in tumor cells. *Mol Cell Biol* 2008;28(16):5043-60.

219. Zhao J, Wei XL, Jia YS, Zheng JQ. Silencing of herg gene by shRNA inhibits SH-SY5Y cell growth in vitro and in vivo. *Eur J Pharmacol* 2008;579(1-3):50-7.

220. Wei X, Sun H, Yan H, Zhang C, Zhang S, Liu X, et al. ZC88, a novel 4-amino piperidine analog, inhibits the growth of neuroblastoma cells through blocking hERG potassium channel. *Cancer Biology & Therapy* 2013;14(5):450-7.

221. Curci A, Mele A, Camerino GM, Dinardo MM, Tricarico D. The large conductance Ca(2+) -activated K(+) (BKCa) channel regulates cell proliferation in SH-SY5Y neuroblastoma cells by activating the staurosporine-sensitive protein kinases. *Front Physiol* 2014;5:476.

222. Leung YM, Huang CF, Chao CC, Lu DY, Kuo CS, Cheng TH, et al. Voltage-gated K+ channels play a role in cAMP-stimulated neuritogenesis in mouse neuroblastoma N2A cells. *J Cell Physiol* 2011;226(4):1090-8.

223. Li X, Hu X, Li X, Hao X. Overexpression of tau downregulated the mRNA levels of Kv channels and improved proliferation in N2A cells. *PLoS One* 2015;10(1):e0116628.

224. Hu XM, Li XQ, Li XT. The Tau-Induced Reduction of mRNA Levels of Kv Channels in Human Neuroblastoma SK-N-SH Cells. *J Mol Neurosci* 2016;58(2):306-11.

225. Vandesompele J, De Preter K, Pattyn F, Poppe B, Van Roy N, De Paepe A, et al. Accurate normalization of real-time quantitative RT-PCR data by geometric averaging of multiple internal control genes. *Genome Biology* 2002;3(7).

226. Sung PJ, Boulos N, Tilby MJ, Andrews WD, Newbold RF, Tweddle DA, et al. Identification and characterisation of STMN4 and ROBO2 gene involvement in neuroblastoma cell differentiation. *Cancer Lett* 2013;328(1):168-75.

227. Rieu I, Powers SJ. Real-time quantitative RT-PCR: design, calculations, and statistics. *Plant Cell* 2009;21(4):1031-3.

228. NCBI. *KCNQ2 potassium voltage-gated channel subfamily Q member 2* 2017. (accessed 27/06 2017).

229. Thomas JO, Nijjar J, Turley H, Micklem K, Gatter KC. NB84: a new monoclonal antibody for the recognition of neuroblastoma in routinely processed material. *J Pathol* 1991;163(1):69-75.

230. Apell HJ, Bersch B. Oxonol VI as an optical indicator for membrane potentials in lipid vesicles. Biochim Biophys Acta. 1987;903(3):480-94

231. Berridge MV, Herst PM, Tan AS. Tetrazolium dyes as tools in cell biology: new insights into their cellular reduction. Biotechnol Annu Rev. 2005;11:127-52.

232. Rihani A, Vandesompele J, Speleman F, Van Maerken T. Inhibition of CDK4/6 as a novel therapeutic option for neuroblastoma. Cancer Cell Int. 2015;15:76

233. Gerdes J, Lemke H, Baisch H, Wacker HH, Schwab U, Stein H. Cell cycle analysis of a cell proliferation-associated human nuclear antigen defined by the monoclonal antibody Ki-67. J Immunol. 1984;133(4):1710-5

234. Seluanov A, Hine C, Azpurua J, Feigenson M, Bozzella M, Mao Z, et al. Hypersensitivity to contact inhibition provides a clue to cancer resistance of naked mole-rat. Proc Natl Acad Sci U S A. 2009;106(46):19352-7

235. Fry DW, Harvey PJ, Keller PR, Elliott WL, Meade M, Trachet E, et al. Specific inhibition of cyclin-dependent kinase 4/6 by PD 0332991 and associated antitumor activity in human tumor xenografts. Mol Cancer Ther. 2004;3(11):1427-38

236. Schenk T, Stengel S, Zelent A. Unlocking the potential of retinoic acid in anticancer therapy. Br J Cancer. 2014;111(11):2039-45

237. Dwane S, Durack E, Kiely PA. Optimising parameters for the differentiation of SH-SY5Y cells to study cell adhesion and cell migration. BMC Res Notes. 2013;6:366

238. Kruppel-like factor 4 (Klf4) prevents embryonic stem (ES) cell differentiation by regulating Nanog gene expression. J Biol Chem. 2010;285(12):9180-9

239. Beilharz EJ, Zhukovsky E, Lanahan AA, Worley PF, Nikolich K, Goodman LJ. Neuronal activity induction of the stathmin-like gene RB3 in the rat hippocampus: possible role in neuronal plasticity. J Neurosci. 1998;18(23):9780-9

240. Andrews W, Barber M, Hernadez-Miranda LR, Xian J, Rakic S, Sundaresan V, et al. The role of Slit-Robo signaling in the generation, migration and morphological differentiation of cortical interneurons. Dev Biol. 2008;313(2):648-58.

241. DeCoursey TE, Chandy KG, Gupta S, Cahalan MD. Voltage-gated K+ channels in human T lymphocytes: a role in mitogenesis? Nature. 1984;307(5950):465-8

242. Salyer SA, Olberding JR, Distler AA, Lederer ED, Clark BJ, Delamere NA, et al. Vacuolar ATPase driven potassium transport in highly metastatic breast cancer cells. Biochim Biophys Acta. 2013;1832(10):1734-43

243. Bloch M, Ousingsawat J, Simon R, Schraml P, Gasser TC, Mihatsch MJ, et al. KCNMA1 gene amplification promotes tumor cell proliferation in human prostate cancer. Oncogene. 2007;26(17):2525-34

244. Oeggerli M, Tian Y, Ruiz C, Wijker B, Sauter G, Obermann E, et al. Role of KCNMA1 in breast cancer. PLoS One. 2012;7(8):e41664

245. Khaitan D, Sankpal UT, Weksler B, Meister EA, Romero IA, Couraud PO, et al. Role of KCNMA1 gene in breast cancer invasion and metastasis to brain. BMC Cancer. 2009;9:258

246. Ma G, Liu H, Hua Q, Wang M, Du M, Lin Y, et al. KCNMA1 cooperating with PTK2 is a novel tumor suppressor in gastric cancer and is associated with disease outcome. Mol Cancer. 2017;16(1):46

247. Suzuki T, Takimoto K. Selective expression of HERG and Kv2 channels influences proliferation of uterine cancer cells. Int J Oncol. 2004;25(1):153-9

248. Smith JS, Iannotti CA, Dargis P, Christian EP, Aiyar J. Differential expression of kcnq2 splice variants: implications to m current function during neuronal development. J Neurosci. 2001;21(4):1096-103

249. Edsjo A, Holmquist L, Pahlman S. Neuroblastoma as an experimental model for neuronal differentiation and hypoxia-induced tumor cell dedifferentiation. Semin Cancer Biol. 2007;17(3):248-56

250. Mohlin SA, Wigerup C, Pahlman S. Neuroblastoma aggressiveness in relation to sympathetic neuronal differentiation stage. Semin Cancer Biol. 2011;21(4):276-82

251. de Sousa Abreu R, Penalva LO, Marcotte EM, Vogel C. Global signatures of protein and mRNA expression levels. Mol Biosyst. 2009;5(12):1512-26

252. Miceli F, Soldovieri MV, Martire M, Taglialatela M. Molecular pharmacology and therapeutic potential of neuronal Kv7-modulating drugs. Curr Opin Pharmacol. 2008;8(1):65-74

253. Tinel N, Lauritzen I, Chouabe C, Lazdunski M, Borsotto M. The KCNQ2 potassium channel: splice variants, functional and developmental expression. Brain localization and comparison with KCNQ3. FEBS Lett. 1998;438(3):171-6

254. Hadley JK, Passmore GM, Tatulian L, Al-Qatari M, Ye F, Wickenden AD, et al. Stoichiometry of expressed KCNQ2/KCNQ3 potassium channels and subunit composition of native ganglionic M channels deduced from block by tetraethylammonium. J Neurosci. 2003;23(12):5012-9

255. Zhou X, Wei J, Song M, Francis K, Yu SP. Novel role of KCNQ2/3 channels in regulating neuronal cell viability. Cell Death Differ. 2011;18(3):493-505

256. Xia S, Lampe PA, Deshmukh M, Yang A, Brown BS, Rothman SM, et al. Multiple channel interactions explain the protection of sympathetic neurons from apoptosis induced by nerve growth factor deprivation. J Neurosci. 2002;22(1):114-22

257. Gonzalez-Gonzalez R, Molina-Frechero N, Carreon-Burciaga RG, Lopez-Verdin S, Robles-Bonilla C, Pereira-Prado V, et al. Comparison between Manual and Automated Methods for Ki-67 Immunoexpression Quantification in Ameloblastomas. Anal Cell Pathol (Amst). 2016;2016:7486989.

258. Chabot-Richards DS, Martin DR, Myers OB, Czuchlewski DR, Hunt KE. Quantitative image analysis in the assessment of diffuse large B-cell lymphoma. Mod Pathol. 2011;24(12):1598-605

259. Iannotti FA, Panza E, Barrese V, Viggiano D, Soldovieri MV, Taglialatela M. Expression, localization, and pharmacological role of Kv7 potassium channels in skeletal muscle proliferation, differentiation, and survival after myotoxic insults. J Pharmacol Exp Ther. 2010;332(3):811-20

260. Roura-Ferrer M, Sole L, Martinez-Marmol R, Villalonga N, Felipe A. Skeletal muscle Kv7 (KCNQ) channels in myoblast differentiation and proliferation. Biochem Biophys Res Commun. 2008;369(4):1094-7

261. Wonderlin WF, Woodfork KA, Strobl JS. Changes in membrane potential during the progression of MCF-7 human mammary tumor cells through the cell cycle. J Cell Physiol. 1995;165(1):177-85

262. Boonstra J, Mummery CL, Tertoolen LG, Van Der Saag PT, De Laat SW. Cation transport and growth regulation in neuroblastoma cells. Modulations of K+ transport and electrical membrane properties during the cell cycle. J Cell Physiol. 1981;107(1):75-83

263. Yamamori E, Asai M, Yoshida M, Takano K, Itoi K, Oiso Y, et al. Calcium/calmodulin kinase IV pathway is involved in the transcriptional regulation of the corticotropin-releasing hormone gene promoter in neuronal cells. J Mol Endocrinol. 2004;33(3):639-49c

264. Pahlman S, Odelstad L, Larsson E, Grotte G, Nilsson K. Phenotypic changes of human neuroblastoma cells in culture induced by 12-O-tetradecanoyl-phorbol-13-acetate. Int J Cancer. 1981;28(5):583-9

265. Voigt A, Zintl F. Effects of retinoic acid on proliferation, apoptosis, cytotoxicity, migration, and invasion of neuroblastoma cells. Med Pediatr Oncol. 2003;40(4):205-13

266. Hocking JC, Pollock NS, Johnston J, Wilson RJ, Shankar A, McFarlane S. Neural activity and branching of embryonic retinal ganglion cell dendrites. Mech Dev. 2012;129(5-8):125-35

267. Yasuda T, Cuny H, Adams DJ. Kv3.1 channels stimulate adult neural precursor cell proliferation and neuronal differentiation. J Physiol. 2013;591(10):2579-91

268. Zhang YY, Yue J, Che H, Sun HY, Tse HF, Li GR. BKCa and hEag1 channels regulate cell proliferation and differentiation in human bone marrow-derived mesenchymal stem cells. J Cell Physiol. 2014;229(2):202-12

269. Zhang YY, Yue J, Che H, Sun HY, Tse HF, Li GR. BKCa and hEag1 channels regulate cell proliferation and differentiation in human bone marrow-derived mesenchymal stem cells. J Cell Physiol. 2014;229(2):202-12

270. Schmidt-Hieber C, Jonas P, Bischofberger J. Enhanced synaptic plasticity in newly generated granule cells of the adult hippocampus. Nature. 2004;429(6988):184-7
271. Zhou N, Huang S, Li L, Huang D, Yan Y, Du X, et al. Suppression of KV7/KCNQ potassium channel enhances neuronal differentiation of PC12 cells. Neuroscience. 2016;333:356-67
272. Feliciano DM, Edelman AM. Repression of Ca2+/calmodulin-dependent protein kinase IV signaling accelerates retinoic acid-induced differentiation of human neuroblastoma cells. J Biol Chem. 2009;284(39):26466-81.
273. Ribatti D. The chick embryo chorioallantoic membrane as a model for tumor biology. Exp Cell Res. 2014;328(2):314-24
274. Wulff H, Christophersen P. Recent developments in ion channel pharmacology. Channels (Austin). 2015;9(6):335